Prediction of Time-Dependent Stresses and Deflections in Prestressed, Concrete Girders: From Start of Fabrication to End of Service Life

Bill Davison

A thesis
Submitted in partial fulfillment of the
requirements of the degree of

Master of Science in Civil Engineering

University of Washington
2014

Committee:

John F. Stanton
Marc O. Eberhard

Program Authorized to Offer Degree:
Civil and Environmental Engineering

ABSTRACT

Fabricators and contractors need accurate prediction of the camber in precast, prestressed, concrete girders. Large differences in the camber between adjacent girders lead to significant construction difficulties that often have financial and/or legal ramifications. Many factors affect the time-dependent deflections of these girders including; creep and shrinkage of concrete, prestressing relaxation, temperature variations and numerous fabrication conditions. The current models used to predict the deflection history are largely empirical and, although they account approximately for some of the important effects, they do not explicitly consider the interactions among these factors.

The goal of this research was to generate a camber prediction algorithm that links the time-dependent constitutive models and explicitly considers the fabrication conditions. This was done by using classical structural analysis techniques and combining them with explicit, time-dependent material models.

The analysis was divided into four time phases that encompass a girder's life-span, from fabrication through it service life. These phases are:

- Strand jacking: The phase during which the prestressing strands are brought up to their specified jacking stress,
- Pre-bonding: The phase during which the prestressing strands are anchored to the abutments in the casting bed, but the strands have not yet bonded to the surrounding concrete,

- Post-bonding: The phase during which the concrete has bonded to the strands, but the girder is still resting in the casting bed, and the strands are still restrained by the abutments.
- Post-release: The phase during which the prestressing strands have been released from the abutments and the girder is removed from the casting bed. This phase includes the entire service life.

In each of these four phases, the boundary conditions are different and the system is analyzed to determine the stresses, deformations and deflected shape. The calculations are necessarily iterative because the constitutive laws for the strand and concrete are time-dependent. The foundation of this analysis method is the proper time-dependent constitutive models.

A time-dependent constitutive model was developed for concrete creep using basic Kelvin-Voigt rheological models, modified to include time-dependent parameters. This new model was then calibrated against currently accepted creep models in order to optimize model parameters for a specific girder concrete.

For the time-dependent strand relaxation model, the model proposed by Bazant and Yu (2012) was used. Unlike the commonly used Magura model (1964) this model is capable of addressing variable stress loading. It also accounts for the key factors that affect relaxation, including temperature and variations in strain. This model was calibrated against relaxation data.

Using these calibrated material constitutive models, the camber prediction algorithm was used to predict the pre-release material stresses as well as the camber history for a girder. The resulting predictions were compared with measured cambers at release and up to ten hours after release. The resulting predictions were reasonable and resulted in expected trends. The predictions also compared favorably with the AASHTO (2012) model for long-term predictions.

TABLE OF CONTENTS

LIST OF FIGURES

LIST OF TABLES

CHAPTER 1 INTRODUCTION

The development of prestressing has greatly increased the range of capabilities of concrete as a structural engineering solution. One of its most common applications is for bridge girders. Prestressed, precast, concrete girders are used throughout the world because of their economy and speed of construction. Because these girders can be manufactured off-site and delivered when requested by the contractor, they are an economical and rapid construction material for bridges. Structural members that are similar in principle but smaller are also used in building structural systems.

Prestressing compensates for the concrete's poor tension behavior. Prestressing introduces pre-compression stresses in the regions of a member likely to experience tension to ensure that the stress in the concrete does not exceed the tensile capacity during service. Although this is a successful and widely used method for improving the behavior of concrete, the prestressing has significant ramifications for the long-term performance of the member.

Concrete suffers both elastic and time-dependent deformations. Deformations that occur without the presence of loads (or changes in temperature) are referred to as shrinkage. Additional deformations that occur under sustained loading are referred to as creep deformations. Prestressing a girder introduces a sustained compression stress in the concrete, which inhibits cracking but also leads to additional creep deflections.

The prestressing force in precast girders is commonly applied with prestressing strands. These strands are made from high-strength steel, and they are stressed very highly before release after the girder concrete has hardened. The strands lose stress over time, both due to relaxation (the loss of stress in a material subjected to a constant strain) and due to the shortening of the

concrete in compression. The combined time-dependent effects of concrete creep and strand relaxation cause the time-dependent changes in girder camber.

The demand for ever-longer girder spans has led to an increasing need for accurate predictions of these time-dependent deflections. Accurate prediction is necessary to avoid construction problems. A girder that cambers upwards too much at the time of construction may interfere with the slab reinforcing bars. On the other hand, a girder that has insufficient camber requires additional concrete to fill the space beneath the deck slab. This results in additional concrete being added to the top of the girder, which is expensive and increases the vertical deflections of the girder. Both of these conditions have economic and possibly legal ramifications.

The analysis of these time-dependent phenomena is difficult because of the simultaneous occurrence of concrete creep and strand relaxation. It is further complicated by a variety of factors including:

- The fabrication process used by the manufacturer to make the girder. Some plants use a one-day turnaround time for girders while others use longer processes. Some plants manufacture components out of doors and others manufacture components within a building. These differences impact the material behavior after release, and therefore, the camber.
- Shrinkage and creep deformations vary with environmental factors, such as relative humidity and temperature.
- The geometry of the member.
- Variations in concrete chemistry.

In previous approaches, the inter-dependence of concrete shrinkage, concrete creep, strand relaxation and temperature variations have not been linked explicitly. For example, the reduction in stress due to relaxation would need to change the creep behavior of the concrete and visa-versa.

In this research, a new approach was applied to the problem of predicting time-dependent camber. This research applies the standard methods of structural analysis to solve this problem in terms of constitutive models and kinematic and equilibrium relationships.

In this research, a new approach was applied to the problem of predicting time-dependent camber. The method uses a time-stepping approach. At each step, the curvature is established at a number of cross-sections along the girder, and is integrated to give the deflected shape. The curvature is computed for the relevant axial force and moment using time-dependent constitutive relationships. The calculations are iterative to account for the time-dependence. This algorithm has the following advantages over current methods

- The time-dependent concrete behavior, as well as its interdependence with strand relaxation and environmental loading in the form of shrinkage and thermal effects, is analyzed explicitly at every time step.
- The analysis starts when the strand is first stressed and includes all of the pre-release activities, so their effects on camber can be analyzed explicitly for a wide range of girder histories.
- The algorithm is modular which allows the exploration of alternative constitutive models for the material behavior.

CHAPTER 2 PREVIOUS WORK

The problem of predicting time-dependent camber is not new. The first prestressed pre-cast concrete girders were used in the early 1950's in the United States (Naaman, 2004). In the intervening time, the time-dependent issues described in Chapter 1 have been researched by many investigators. This chapter reviews the previous work that has been done in the various areas of importance.

2.1 Creep Modeling Methods

The most important factor in determining the time-dependent cambers is the creep of concrete. Many models have been proposed for predicting creep deformations in concrete. The most commonly used are:

- ACI 209R-08 (ACI Committee 209, 2008)
- Bazant-Baweja B3 (Bazant and Baweja, 1995)
- CEB MC90-99 (Muller and Hilsdorf, 1990)
- GL2000 (Gardner, 2004)
- AASHTO model (AASHTO 2013)

Creep is influenced by many attributes of the concrete, and each of the foregoing constitutive models considers a different subset of those attributes. This section outlines the key features of each model as described in the ACI Report 209.2R-08 (2008). Table 2.1 shows the different attributes and the models that consider them. This is not an exhaustive list of all the things that may affect concrete creep but these are the ones that have been studied.

Table 2.1 Effects considered by current creep models

Effect	Model				
	ACI 209R-08	Bazant-Baweja B3	CEB MC90-99	GL2000	AASHTO
Age of concrete when drying begins	X	X	X	X	X
Age of concrete at time of loading	X	X	X	X	X
Curing method	X	X			
Relative humidity	X	X	X	X	X
Volume-surface ratio	X	X	X	X	X
Cement type	X	X	X	X	X
Aggregate Content		X			
Cement content		X			
28-day compressive strength		X	X	X	
Specimen shape		X			
Water content		X			
Rate of strength gain					X

The model proposed by ACI Committee 209 was developed by Branson and Christiason. It is generally considered to under-predict the creep experienced in the measured results.

Bazant and Baweja's model, known as B3, is a much more mathematically intense model that explicitly models different attributes affecting creep. The compliance function developed in the model is based on three separate attributes; elastic deformation, drying creep, and basic creep. Although it is quite thorough in its accounting for the many different effects shown in Table 2.1, it is the most complicated to implement.

Muller and Hilsdorf developed the CEB MC90-99 creep model in 1990, and it was then modified in 1999 (ACI Committee 209, 2008) to include separate considerations for basic and drying creep. This model is highly sensitive to the relative humidity factor.

Gardner and Lockman developed the GL2000 model in 2001. Gardner then modified it slightly in 2004 (ACI Committee 209, 2008). This model is useful because it uses only the parameters available at the time of design. The ACI 209.2-08 report, from which this information was taken from, discusses how each of these models was calibrated and how they compare.

The AASHTO model (not included in the ACI 209 report) uses a series of factors to modify the creep coefficient as a function of time. This model is tailored for use in highway applications and is suited to modeling the creep in bridge girders (AASHTO, 2011). These models are discussed in more detail in Chapter 4.

2.2 Relaxation Loss Prediction Methods

The second, less important time-dependent factor to be accounted for is the relaxation of prestressing strands. This behavior is better understood than concrete creep because steel is a homogeneous material with consistent properties. The two commonly accepted models for predicting relaxation losses are the Magura (1964) model and the CEB (1990) model. Both describe the change in stress over time when the steel is subjected to constant strain.

The model proposed by Magura et al (1964) has been used for many years. It is based on a logarithmic degradation of stress due to a constant strain scenario. The original model was developed to replicate the relaxation of stress-relieved strands. Later, low-relaxation strand was developed and the model was modified by changing a numerical coefficient to account for the lower relaxation. Today low-relaxation strand is used almost exclusively. It loses about 1% of its initial stress over 1000 hours.

In the CEB (1990) model the stress decay is described by an exponential function. Again, the parameters in the CEB model have different values according to the type of strand being used.

Neither model is able to exactly match the stress decay measured in constant strain tests. Furthermore, and perhaps more important for use with girders, neither model is able to account for an applied strain that varies with time. Each these models and the selected model proposed by Bazant and Yue (2012) are discussed in detail in Chapter 5.

2.3 Camber Prediction Methods

In order to predict girder camber, the effects of creep and relaxation must be combined to develop a time-dependent camber response. This analysis is greatly complicated by the fact that both behaviors occur simultaneously and contribute to prestress loss. There are many different way in which this can be done and this section will discuss two of the main approaches used. They depend heavily on the way that prestress losses are computed.

2.3.1 Single Step Methods

In this approach, the total prestress loss at specific times is computed, and the corresponding camber is calculated. The total prestress loss is caused by the combination of creep, shrinkage and strand relaxation, but the way that these behaviors interact depends on properties such as the section shape. The interaction is accounted for by reduction factors on each effect, which leads to a solution that is simple but inevitably approximate. The PCI Method (2010) uses this approach. It applies empirically determined magnification factors to camber due to; prestressing force, self-weight deflections, and super-imposed dead load, to compute the predicted camber at the time of fabrication and the long-term camber. A separate set of factors is used for calculation at release and long-term. This method is useful due to its simplicity but has been shown to provide inaccurate results (Stallings and Eskildsen, 2001).

2.3.2 Time-Stepping Methods

In a time-stepping method, stresses and deformation in the girder and the deflected shape are computed at a number of explicit time intervals. The change in stress in each material is computed during each step, and the new stress is used to compute the changes in the next time step. The advantage over single step methods is that, for short enough time steps, the interaction of the stress changes in the different materials are properly accounted for.

In the conventional approach to implementing the time stepping method, the constitutive laws are the conventional ones (such as the Magura model for relaxation and the ACI 209 model for creep) that were derived from constant stress or strain tests. The consequence is that, at every step, a change in the stress on the concrete means that a new load-case must be added and tracked in addition to the previously existing time-varying stress. Thus, if N time steps are used and the stress changes during each one, it becomes necessary to superimpose N load-cases by the end of the analysis. If shrinkage and thermal effects are treated as uniform throughout the cross-section, the member can be analyzed using section properties and the computational effort is acceptable. Rosa (2007), for example, used this approach. If shrinkage and thermal effects are treated as varying over the girder height, the section must be broken into layers and each layer needs the superposition of N load-cases over N time steps, and the computational effort increases significantly.

To compute the camber at a given time, the following camber contributions are added together:

- Camber due to prestressing strands. This accounts for the prestress losses due to relaxation, elastic effects and in some cases the creep.

- The elastic camber due to self-weight and any superimposed loads applicable for the time step.
- The camber caused by creep under sustained loads from self-weight and superimposed dead loads.
- There are several models which employ this method. The difference in these models is the way they account for each of these effects.
- The AASHTO (2012) model uses the Magura (1964) model to predict relaxation losses and the AASHTO creep model to compute losses due to relaxation. These losses are combined with the elastic losses computed at release to generate a prestressing force. This force can then be used to compute the camber due to prestressing. The creep deflections employ the AASHTO creep model to magnify the cambers due to sustained loadings including self-weight. Note that a separate creep function must be used for loads applied at different times (i.e. slab weight at the time of construction). The total camber at any time is then computed as the summation of these various affects. The American Concrete Institute proposes a similar method for predicting cambers (ACI Committee 435, 1995).
- The second possible approach to implementing the time-stepping method is to use rate-type constitutive laws. These do not depend on constant stress or strain loading, so they are inevitably more complex than their constant load counterparts. However, for any given time, if the stress and strain are known, then the change in response during the ensuing time step can be computed with the need to know or record the previous history. This is essential if, for example, a full 3-D FEA is to be conducted. However, until recently it has seldom been undertaken because satisfactory material models have not

been available. (A conventional visco-elastic model is such a rate-type model and can be used. However, because the properties, such as the elastic modulus, remain constant over time, it fails to describe the true time-dependent behavior). Bazant, Yu, and Wendner were successful in applying this approach to the analysis of the Koror-Babeldaob Bridge in Palau (Yu et. al. 2012).

- There have also been several studies on prestress loss prediction. Prestress loss and cambers are closely linked and so these studies are also worth mentioning in the same context. Tadros et. al. (2003) and Zia et. al. (1979) each completed a comprehensive study on prestress losses in girders. These studies include the losses that result from elastic deflections, creep, and relaxation.

In his research, Mike Rosa (2007) generated a comprehensive program for analyzing several of these time-stepping methods for a given scenario. For this approach, Rosa used superposition to account for changing load conditions. This method is highly computationally expensive.

CHAPTER 3 ANALYSIS FORMULATION

3.1 Overview

This chapter discusses the analysis algorithm developed to predict camber in pretensioned concrete girders. The impetus for developing the algorithm is the need for an incremental time-stepping approach. This approach removes the need for superposition, creates a consistent method of tracking material behaviors, explicitly allows for the interaction between time dependent material behavior and all loadings, and allows the explicit analysis of pre-release effects. In Chapter 6, the predicted cambers are compared with cambers measured in the field. It should be noted that this comparison is a proof-of-concept calibration rather than a detailed, optimized calibration.

3.1.1 Analysis Setup and Geometry

Before discussing the details of the analysis procedure, it is important to understand the problem for which the algorithm has been formulated. Because the methods of fabricating prestressed girders vary among fabricators, the algorithm has been formulated to handle a wide range of scenarios. Figure 3.1 shows the typical setup for a fabrication system:

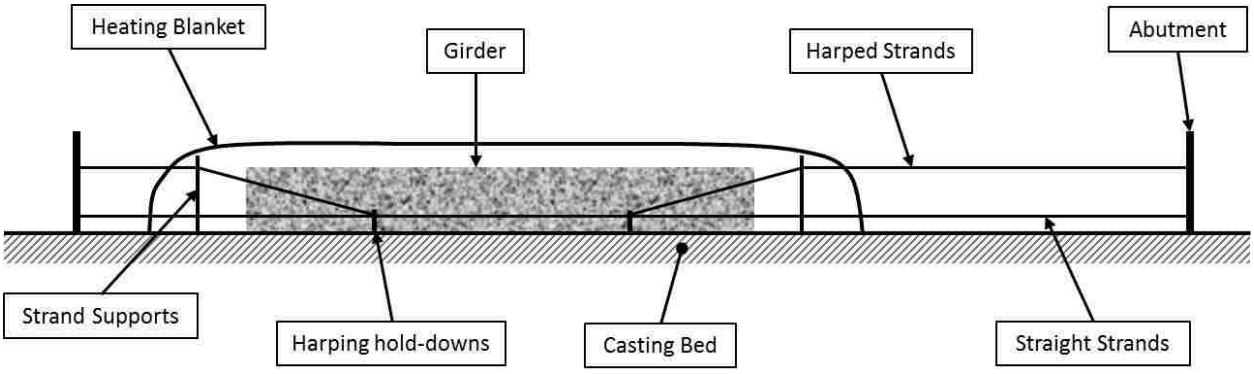

Figure 3.1 Typical casting bed configuration

This configuration includes the key features used in many precasting plants. As the girder is produced, different parts of this configuration are added, and the solution process for the analysis must change accordingly. Examples of differences in production methods include:

- Some fabricators use harped (or "depressed") strands, while others use only straight strands, partially de-bonded at the ends as necessary to avoid excessive top tension.
- Some plants use forms that are thermally insulated and electrically heated, while others use a heating blanket over the form under which steam heat is introduced. Differences in heating procedures lead to different thermal profiles in the girder.
- Some plants use a "Sure-cure" system that allows test cylinders to be cured in cylinders whose temperature is computer-controlled to be the same as the internal temperature in the girder. Others use cylinders that are cured under the heating blanket alongside the girder. These differences may affect the ratio of actual to design concrete strength at release.
- At release time, procedures for releasing the strand stress differ. Most fabricators lift at least one end of the girder to avoid its dragging in the form as the girder shortens elastically, but the ways in which this is done vary.

Several assumptions that are made in the entire analysis are summarized in Figure 3.1 and listed here.

- The casting bed length, defined as the distance between the two abutments, does not change during the fabrication process.
- The temperature under the heating blanket and in the exposed regions is assumed to be constant with respect to the height above the casting bed except within the girder concrete.

- The harping hold-downs and strand supports are frictionless and do not cause a change in stress along the strands.
- All material properties remain elastic with respect to instantaneous deformations.

Any necessary dimensions and properties of the system are defined in the subsequent discussion.

An important aspect of this analysis algorithm is that it accounts for variation in the girder temperature, both over time and over the height of the girder. Concrete in the girder is likely to experience a temperature profile over the height of the girder. This gradient is caused by the variation in the rate of heat loss due to differing volume-to-surface ratios along the height of the girder. The hydration of concrete also generates heat. This temperature profile changes with time as the girder. This algorithm accounts for the temperature profile and history by applying user-defined temperature histories at several locations along the height of the girder.

3.1.2 Analysis Sequence

The program uses a time-stepping method, in which conditions at time *t* are known, and those at time $t + \Delta t$ are computed based on instantaneous material properties and the applied loading.

The analysis is broken down into four phases:

- Strand Jacking (Section 3.2)
- Pre-Bonding (Section 3.3)
- Bonded, Pre-Release (Section 3.4)
- Post-Release (Section 3.4)

The separate treatment of the four phases is necessary because, although the same principles are used throughout, the topology and boundary conditions differ in each of the phases. For example, no concrete exists in the first phase, the concrete exists but has no stiffness or strength in the

second phase (but it can register temperature), whereas it is fully engaged in the third and fourth phases.

The flow chart in Figure 3.2 outlines the algorithm at its highest level and shows how these separate phases are integrated into the algorithm. The sections refer to the sections of this chapter in which that part of the algorithm is described in detail. In Figure 3.2, the third level of the flow-chart shows four options, one for each phase. The algorithm contains a conditional statement that selects only the analysis option appropriate for that phase

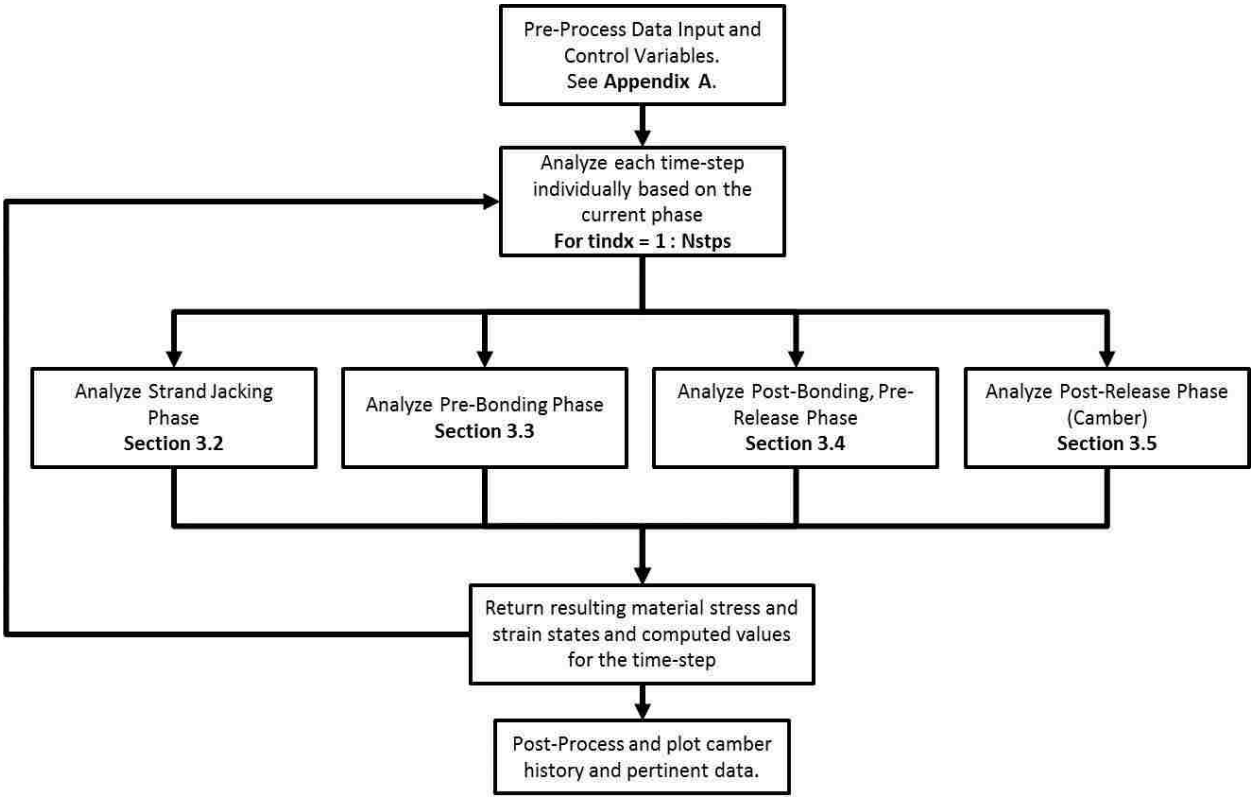

Figure 3.2 Top level algorithm flow chart

The *strand jacking* operation was treated as a separate phase in order to account for relaxation that occurs during the jacking of the strand. Relaxation occurs at its fastest rate during the time immediately after jacking, and because the jacking process is not instantaneous, it may be important to consider the relaxation that occurs during this time. Throughout this phase all

strands are assumed to be the same length (i.e. they are assumed to be stressed simultaneously) and are assumed to have a constant temperature.

The *pre-bonding phase* occurs after the strands have been jacked and anchored. During this phase the concrete is cast and may be externally heated with either a heating blanket or heated forms in addition to the inherent heat of hydration. These fabrication practices create significant variations in strand temperature along the length of the bed, and these variations affect the stress in the strands. During this phase the strands are not yet bonded to the concrete, and the total length of the strand is assumed to be constant. However, local longitudinal movement of the strand is possible in response to variations in temperatures along the length of the strand.

The post-bonding phase refers to the period of time when the concrete is assumed to have hardened and bonded to the strand and rebar, but the strand stress has not yet been released from the abutments. At this point the girder is modeled as a one-dimensional, axial element resting on the bed, which is treated as a foundation that is vertically rigid but has longitudinal flexibility. The system consists of five finite elements; one heated strand element and one exposed strand element on either side of the girder element. As the concrete hardens, it "locks" in a thermal profile to the concrete and strands within the girder. This temperature profile at bonding contributes to the post-release cambers and is investigated later in this document. Again, the casting bed length cannot change, and each of the three element types, exposed strands, heated strands, and hardened concrete elements, may be subjected to different temperature histories.

The post-release phase is the period likely to be most familiar to the reader. This phase begins once the prestressing strands have been cut and the girder is free to lift off the casting bed. Upon release, the girder is analyzed at several cross section locations to determine the curvature

and axial strain. The curvatures are then integrated to determine the deflected shape and camber of the beam. Allowance is made for a range of support conditions (e.g. lifting loops) at locations other than the end of the girder.

In this chapter, these four phases of the analysis are discussed in chronological order.

3.1.3 Analysis Approach

Some aspects of the analytical approach are the same for all four phases. For example, in all phases, the girder is modeled as a beam, in which plane sections are assumed to remain plane. This assumption was made in the interests of simplicity, because it allows the use of one-dimensional material models and the consideration of longitudinal strains alone.

The analysis is conducted using an incremental, time-stepping algorithm. Because the material properties and loads (including environmental loads) are time dependent, the calculations within each time step are iterative and are conducted using a Newton-Raphson procedure. Although the topology and boundary conditions are different for each phase, the final solution consists of a combination of force and displacement values that satisfy the applied equilibrium and kinematic constraints. The general formulation for this procedure is outlined in Figure 3.3 with a flowchart and in Figure 3.4 with a force-deformation plot.

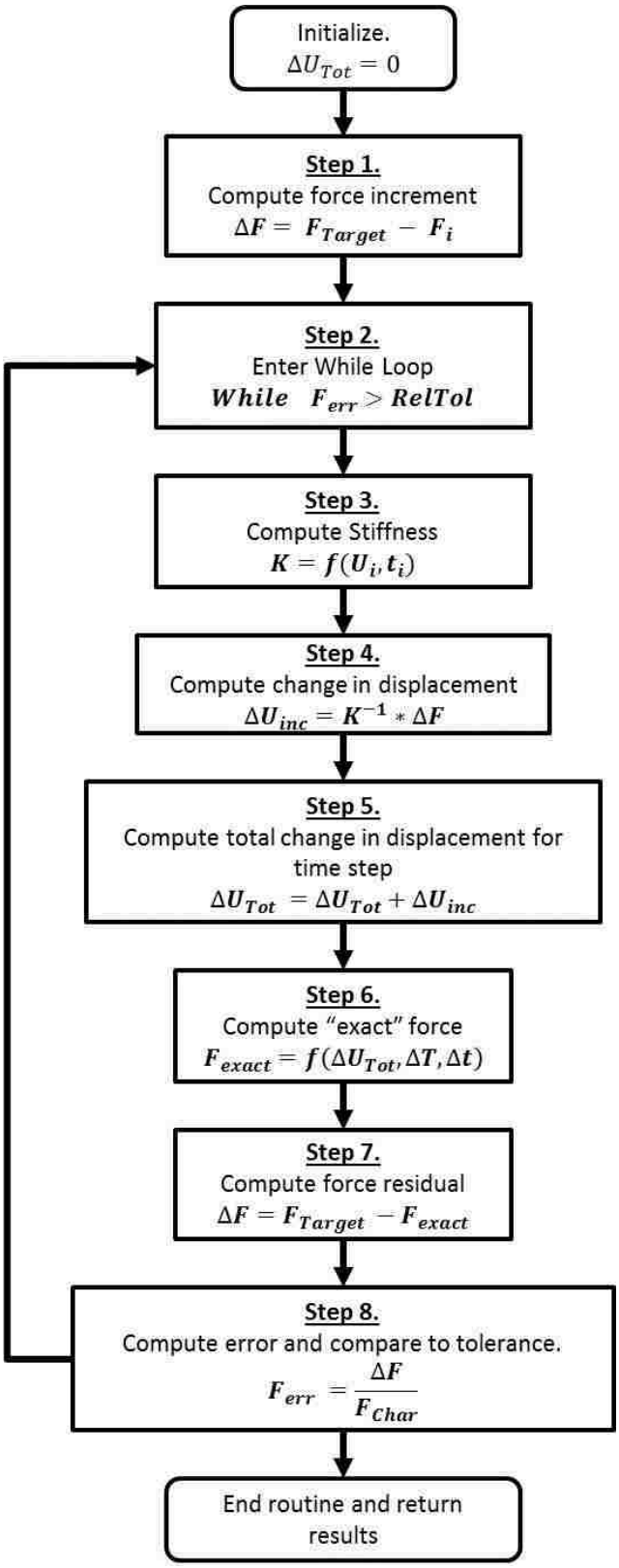

Figure 3.3 Flow chart for Newton-Raphson iteration scheme

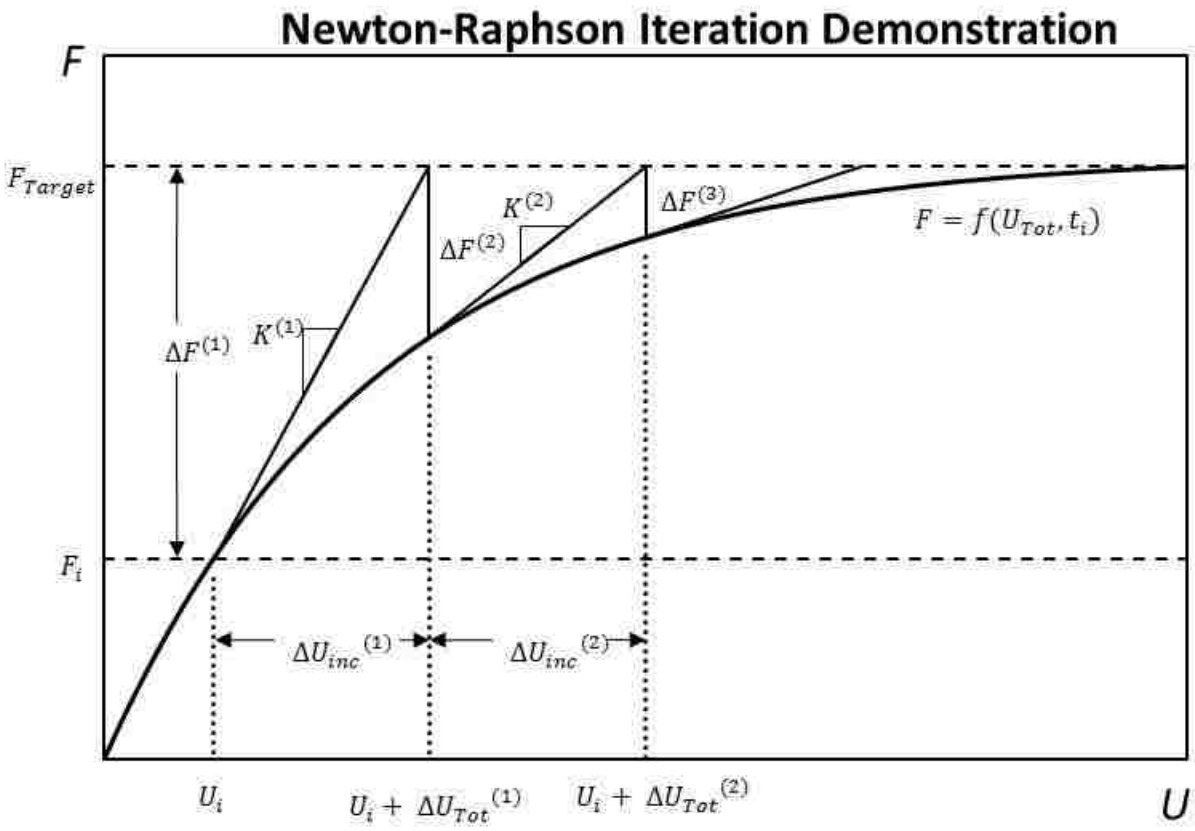

Figure 3.4 Graphical illustration of Newton-Raphson iteration scheme.

In Figure 3.4, the superscripts on *K* and *F* denote the iteration number for which these were input, and the superscripts on *U* denote the iteration number for which it was the result. For example, $\Delta U_{inc}{}^{(1)} = \left[K^{(1)}\right]^{-1}\Delta F^{(1)}$ and $\Delta U_{Tot}{}^{(2)} = \Delta U_{inc}{}^{(1)} + \Delta U_{inc}{}^{(2)}$.

This approach is used for the iterations in each of the four phases, but, in each case, the variables *F* and *U* represent different force and displacement quantities, and the governing equilibrium and kinematic constraints change.

During the strand jacking phase, the force term, *F,* represents the stress in each strand and F_{Target} is the target stress for the end of the time-step. *U* is the mechanical strain in the strand. The goal of the analysis is to compute the mechanical strain required to reach the target stress in the presence of relaxation during the non-instantaneous jacking.

Phase two is the pre-bonding phase during which the total strand length remains constant, albeit with possible temperature variations along its length. In this case, the displacement is known, and the stress in the strand is the dependent quantity. The variable representation from Figure 3.3 is less intuitive in this case, because *F* is used to denote the change in length of the strand and *U* represents the stress in the strand. In this case, the overall length of the strand must remain constant (target quantity) and the stress in each strand segment must remain equal for equilibrium. The strain in each segment is determined such that the change in length $\Delta L = F = 0$.

Phase three is the most complicated scenario in which a finite element formulation is used. Here the concrete has hardened and five distinct elements and four internal nodes exist between the two abutments. *F* in this case represents the applied nodal forces and, in a typical scenario where there are no external loads, *F* should converge to a target value of zero for each node. *U* is displacement of the internal nodes.

After release of the prestressing strands, the system becomes statically determinate and the iteration takes place at the cross-section level. Here, *F* is a vector containing the moment and axial force for the cross-section, and *U* is a vector containing the curvature and axial strain for the cross-section.

3.2 Strand Jacking Process Formulation

Strand jacking is the first event to occur in the time history of a prestressed girder. Before jacking, the strands are routed through the specified harping points and fixed to the abutment at one end of the casting bed. After the strands have been routed, a hydraulic jack is attached to the free end, and the strands are brought up to the specified jacking stress over a finite length of time. This setup is shown schematically in Figure 3.5.

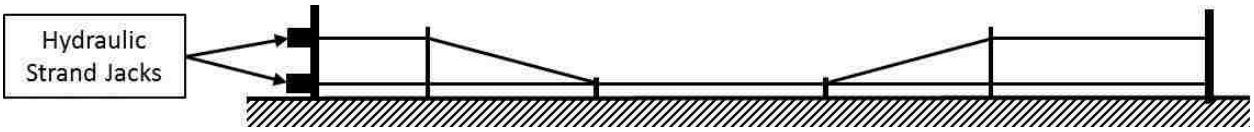

Figure 3.5 Strand jacking configuration

In the jacking portion of the analysis, the following assumptions are made within a single time step:

- All strands within each group (e.g. straight, harped) are stressed simultaneously with identical elongations, forces and temperatures.
- The strands are jacked to a specified target stress for the time interval
- Relaxation is allowed to occur during the process, so the final strain after jacking will be greater than $\frac{f_{pj}}{E_p}$.
- There are no temperature changes during the time step. This is a reasonable assumption, because jacking is a relatively fast process and significant changes in air temperature in the fabrication facility during jacking are unlikely. There are no other sources of heat as neither the concrete nor heating blanket is present during jacking. The effects of temperature on the rate of relaxation are considered. Thus the relaxation that occurs in girders cast during the summer may be expected to be slightly more than those cast in winter.
- The length of the casting bed between abutments does not change during jacking.

With these assumptions, the strand constitutive model (discussed in Chapter 5) is used to compute the mechanical strain required to reach the target stress for the end of the time step. For the analysis within this phase, each strand group (straight, harped, temporary) is considered separately so that differing jacking stresses can be applied.

Analysis of the jacking requires a target stress or strain path over time. Here, the stress was assumed to vary linearly with time. Using this relationship, the total time for jacking can be split into separate time steps for an incremental analysis. Note that, as will be discussed in Chapter 5, there is a threshold below which relaxation does not occur (this is noted in Figure 3.6 as γf_y). For this reason, the first time step length was selected so that the target stress at the end of the interval would be at this threshold, and the remaining stress increase should be split into a number of steps, *N*. This concept is shown in Figure 3.6.

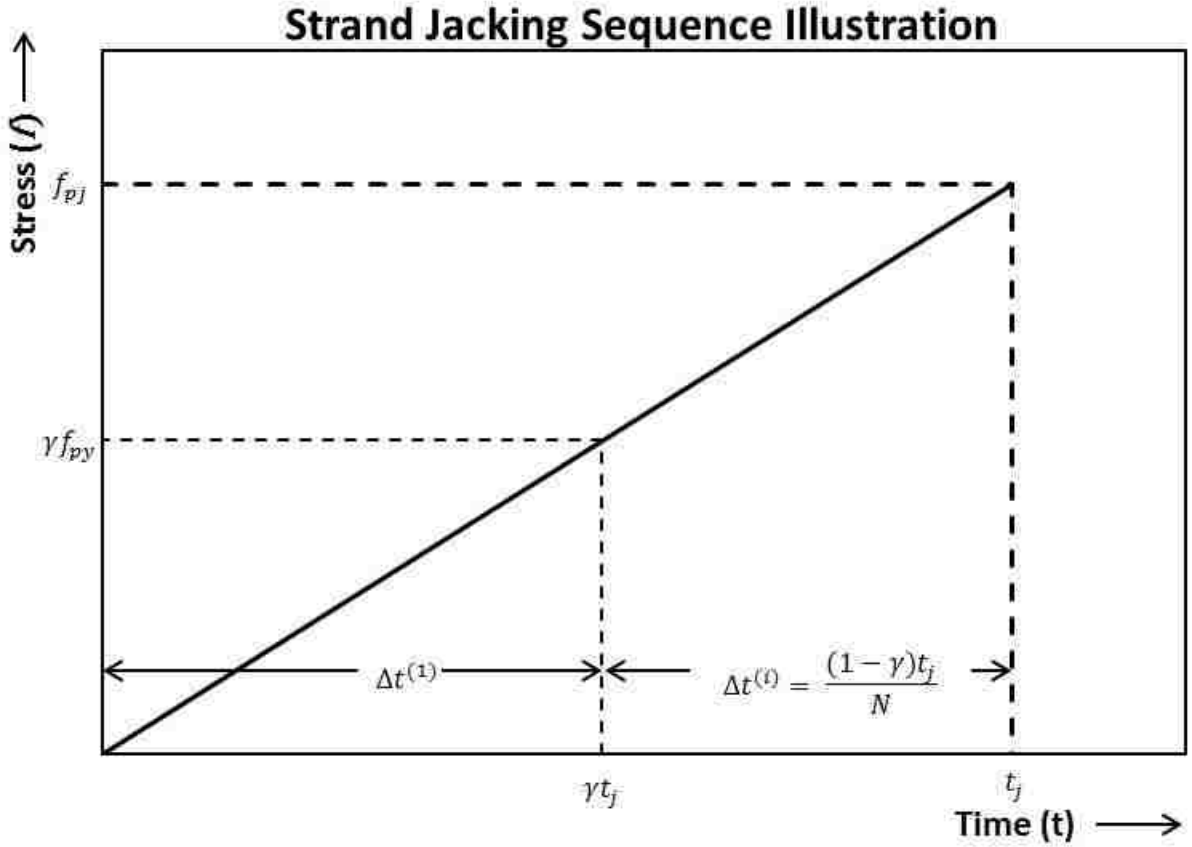

Figure 3.6 Jacking sequence time-step distribution

With the time steps and corresponding target stress values set, it is possible to complete the iteration for each step using the Newton-Raphson scheme and the strand constitutive model. For this analysis, stress is the dependent variable *F,* and mechanical strain is the independent

variable *U*. The constitutive model, which will be discussed in Chapter 5, can be expressed for now as:

$$\Delta\sigma(\Delta\varepsilon_{mech}, \Delta t) \tag{3.1}$$

where: $\Delta\sigma$ = the stress increment during the time step as a function of mechanical strain and time increments. This is the constitutive function that will be discussed in Chapter 5.

During the jacking phase, the assumption of zero temperature change means that there are no environmental strains and therefore $\Delta\varepsilon_{Tot} = \Delta\varepsilon_{mech}$. Using this equation within the Newton-Raphson procedure, the mechanical strain value required to reach the target stress can be determined.

The flow chart in Figure 3.7 outlines the process by which a time step occurring within the jacking phase of the girder time history is solved for the mechanical strain.

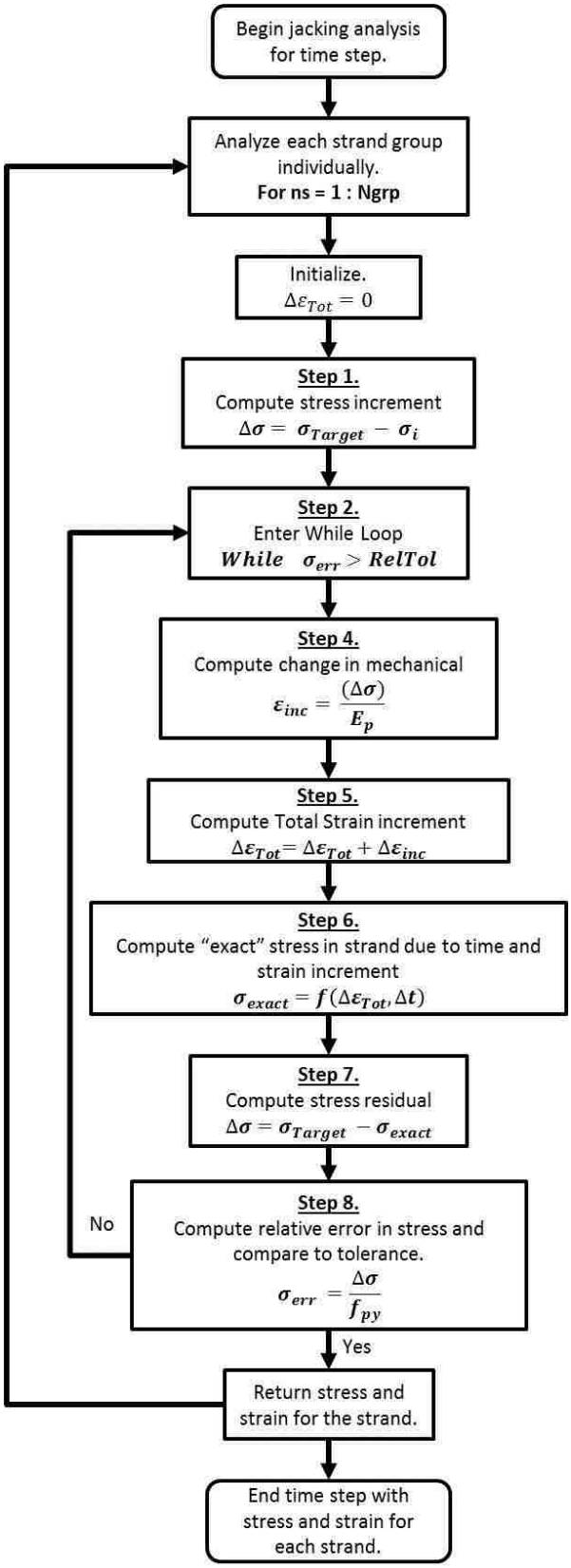

Figure 3.7 Jacking process flow chart

Notice that the flow chart has a Newton-Raphson procedure nested within the for-loop to deal with each of the input strand groups. This Newton-Raphson iteration has the same general approach outlined in Section 3.1.3.

Step 3 from the general Newton-Raphson procedure (finding the instantaneous stiffness) is omitted from Figure 3.7, because it is given by E_p and no further calculation is needed. For this iteration the true stiffness should be a tangent stiffness that is a function of the stress, strain, and time as described by the constitutive model. The simpler approach of using E_p is used. Note that after the calculation in each time step has converged, the final residual stress $\Delta\sigma$, is saved as an unbalanced load and is used to modify the target stress in the next time step. This step is followed for each of the strand groups at each time interval.

$$\sigma_{Target} = \sigma_{Target} + \sigma_{unbalanced} \tag{3.2}$$

After the stresses have converged, the stress and strain for each of the strand groups are stored.

3.3 Pre-Bonding

Once all strands are jacked to the target stress, the girder fabrication can begin. In the pre-bonding phase, the strands remain free to move independently from the surrounding concrete while the girder forms are placed and the concrete is poured. In most production plants, the fabrication schedule is critical to maintaining profits. For this reason, heat is applied to the concrete during curing so that higher concrete strengths are reached much faster. This is usually done in the form of either heated steel forms or by placing a large heating blanket over the length of the girder. This latter method creates three distinct regions of strand; the exposed region where strand is exposed to the ambient air temperature, the heated region where strand is within the heated blanket but outside the girder, and the girder region where the strand is affected by both

the hydration of the concrete and the supplementary heating mechanism. Figure 3.8 below shows the three types of regions of the strand that make up the entire system for which a solution is required.

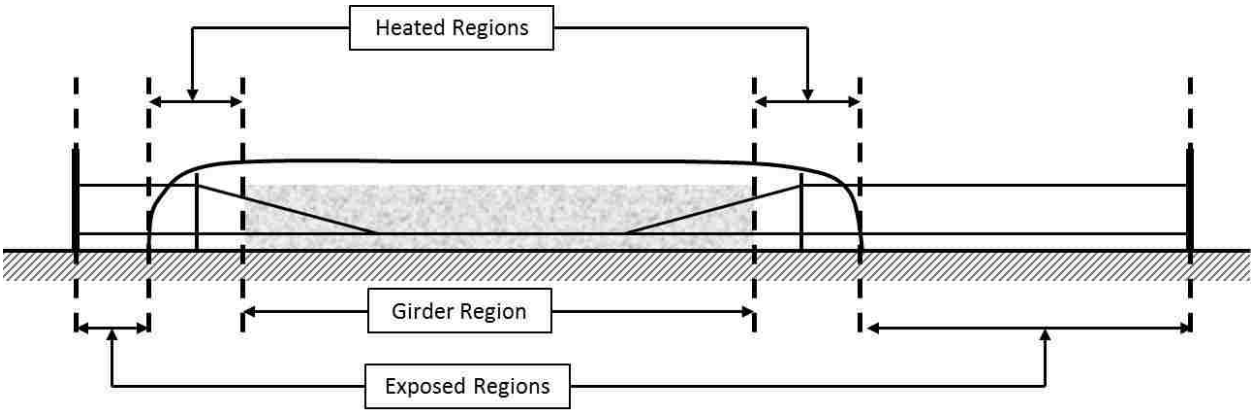

Figure 3.8 Pre-Bonding strand segment diagram

The heated region of the strand shown in Figure 3.8 may or may not exist depending on the type of heating system used by the fabricator. If a heated form system is used then this "heated" region shown above becomes part of the exposed region. For the purpose of this portion of the analysis both heated regions are lumped together into one length and the same is done for the exposed region. The result is three different segments of strand considered in the analysis.

The goal for each of the time steps in the pre-bonding phase is to converge on a single stress value for each strand group that accounts for the variations in temperature along the length as well as the relaxation that occurs during the time step. This process is governed by the fact that the length of the casting bed does not change. Each of the three segments of strand are subjected to its own temperature histories that have a significant impact on the stress in the strand due to the thermal expansion coefficient and the effect of temperature on the rate of relaxation.

While completing this analysis the following key assumptions are made:

- The total length of the strand groups does not change.

- The temperatures in the heated and exposed regions of the strand are constant with respect to the height, while the girder region may register a vertical temperature profile from the heat flow properties of the girder that arise due to applied heat and the heat of hydration.
- Each strand group has a constant stress over its entire length, (i.e., the harping points are frictionless).

For the strands to maintain equilibrium under these conditions, the mechanical strains must change so that the stress in each segment of strand is the same as in adjacent segments. It is important to note that if the thermal changes are ignored there would be no change in mechanical strain, and the problem becomes one of constant strain relaxation.

3.3.1 Solution Procedure

The governing parameter for this phase of the time history is the kinematic equation that defines the change in length of the casting bed.

$$\Delta L_{Bed} = \int_0^{L_{Bed}} \Delta\varepsilon_{Tot} dl \tag{3.3}$$

By breaking the total strain into a mechanical and an environmental component, and assuming that the strain in each strand region is constant, Equation 3.3 can be written in the form of a sum:

$$0 = \Delta L_{Bed} = \sum_{i=1}^{Nreg} (\Delta\varepsilon_{mech} + \Delta\varepsilon_{env})_i L_i \tag{3.4}$$

where: *Nreg* = the number of strand regions being considered (three in this case – heated, exposed, and girder).

L_i = length of the region

Notice that stress does not appear in this equation. The stress enters via the constitutive relation between the mechanical stress and strain. The same constitutive model used in the strand jacking

formulation above is used here, but it is re-formulated to give the change in strain due to an increment in stress.

$$\Delta\varepsilon_{mech}(\Delta\sigma, \Delta t) \tag{3.5}$$

where: $\Delta\varepsilon_{mech}$= is the increment in mechanical strain during the time step as a function of stress and time increments. This is the constitutive function that will be discussed in Chapter 5.

Using this in Equation 3.4:

$$\Delta L_{Bed} = \sum_{i=1}^{Nreg}(\Delta\varepsilon_{mech}(\Delta\sigma, \Delta t) + \Delta\varepsilon_{env})_i L_i \tag{3.6}$$

This governing equation is defined by a nonlinear relationship in time and must therefore be solved iteratively. In Equation 3.4, it is assumed that the change in bed length is zero and in order to ensure that this is true, the stress in the strand is iterated to change the mechanical strain to this end. The resulting equation is:

$$\Delta L = \Delta L_{Bed} - \sum_{i=1}^{Nreg}[\Delta\varepsilon_{mech}(\Delta\sigma, \Delta t) + \Delta\varepsilon_{env}]_i L_i \tag{3.7}$$

where: ΔL = the residual change in length that results from the increment in time, stress, and specified environmental strain.

ΔL_{Bed} = is the specified change in bed length. This is typically set to zero but is included in the formulation for completeness.

Equation 3.7 is now formulated in a manner that can be used in a Newton-Raphson scheme. Notice that the change in the independent variable. ΔL, is specified in terms of an increment in the dependent variable σ. Notice that this is the opposite variable dependence from the general formulation described above. This is because the governing Equation, 3.3, in this case is not equilibrium but is instead a kinematic relation. The Newton-Raphson iteration is continued until this resulting ΔL is within the specified tolerance of zero.

In order to complete the Newton-Raphson formulation, the additional change in stress must be expressed in terms of the residual change in length. This is done by applying the elastic stiffness for strand and results in the following stiffness equation.

$$\Delta\sigma_{inc} = \frac{E_p}{L_{Bed}}\Delta L \tag{3.8}$$

where: ΔL = the change in bed length resulting from Equation 3.7

$\frac{E_p}{L_{Bed}}$ = the inverse stiffness term K^{-1}, from the general Newton-Raphson formulation above.

The implementation of this Newton-Raphson formulation is outlined in the flow chart in Figure 3.9.

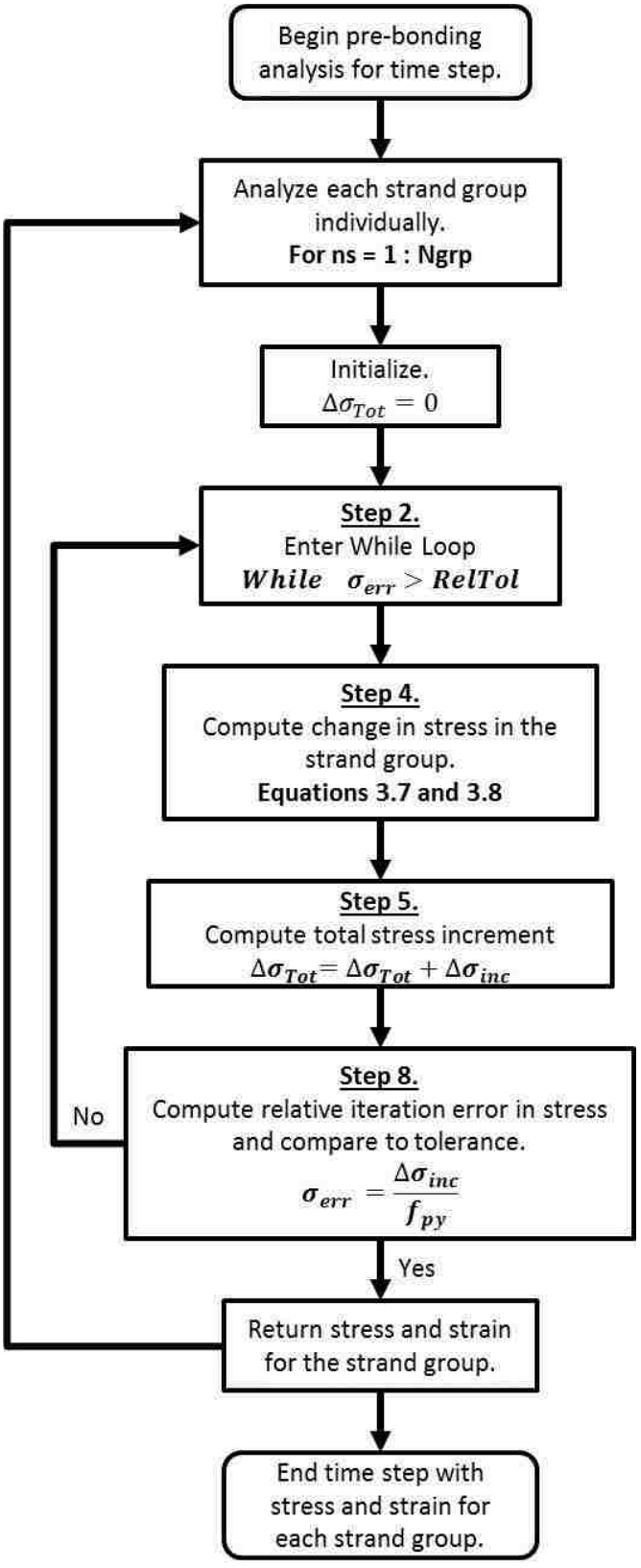

Figure 3.9 Pre-bonding analysis flow chart

As before, each strand group is analyzed individually. For the first iteration it is assumed that the total change in stress ($\Delta\sigma_{Tot}$) is zero. The time and environmental changes in the system are included in the residual stress that results after the first iteration when the assumed stress change is zero.

Due to the kinematic formulation of this problem, there are several differences from the general Newton-Raphson algorithm. In Step 4, the change in stress (dependent variable) is calculated based on the exact solution for ΔL rather than using an approximate stiffness approach. Because the exact solution at any point in the iteration is known, ΔL should always be zero. This increment in stress (from Equation 3.8) is then added to the total stress change for the time step (Step 5). The final difference is the computation of error. For this system, the error is calculated from the dependent variable, stress, rather than the independent variable, change in length. Although either could be used to generate an iteration error, a ratio between the stress change increment and the yield stress is used for a relative error. For an exact solution, the term $\Delta\sigma_{inc}$ would be zero and is therefore a good representation of the accuracy of the iteration. The yield stress is chosen as a convenient normalizing parameter.

After completing this phase of the analysis, the stress and mechanical strain for each of the strand groups in each region is stored.

3.4 Post-Bonding, Pre-Release Analysis

The next portion of the girder's time history occurs after the concrete in the girder has bonded to the strands and the girder becomes a composite steel-concrete element. For the sake of this analysis it is assumed that the concrete bonds suddenly at a specified time rather than gradually. The concrete is assumed to harden gradually with the elastic modulus increasing from zero to a release value in a linear fashion (see Chapter 4 for more details).

When bonding occurs two important things happen:

1) The girder is heated by both the intrinsic heat of hydration and external heating mechanism, if present. This may cause a vertical thermal profile.
2) The girder becomes a composite element containing prestressing strands, reinforcing bars, and concrete.

The girder typically rests on a casting bed raised above the ground, both to facilitate leveling and to allow access to the hold-down anchor points. The bed is supported on posts. Bending of the bed support posts leads to some shear flexibility between the bed and the ground. It is modeled here as an elastic foundation that deforms in shear. The stiffness of the bed is included because it affects any changes in length of the girder.

The problem is simplified into a one-dimensional system of axial elements. This idealized system is shown in Figure 3.10 below:

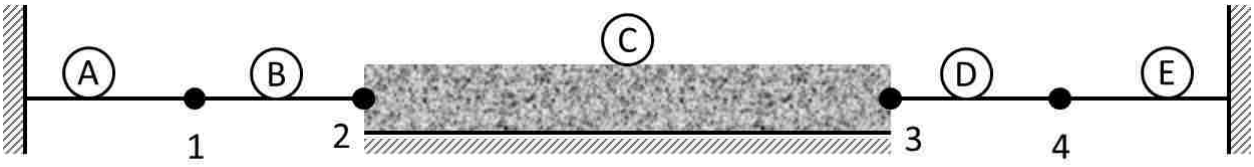

Figure 3.10 Post-Bonding idealized element configuration

In this figure the elements A and E are strand-only elements exposed to the external temperature of the casting facility, and elements B and D are strand-only elements that are under the heating blanket, if it exists. Element C is the girder resting on an elastic foundation. When completing this analysis the following assumptions are made:

- In the strand only elements (i.e., elements A, B, D, and E), the strand groups go through the same nodal displacements. This is different than the assumption made in previous phases, for which each strand group was analyzed separately and allowed to deform independently. This assumption is made because, in the girder element, the strands are

bonded to the concrete and forced to undergo the same nodal displacements. In the strand-only elements there are no driving factors that would lead do differential motion between strands. This assumption has the added advantage that all of the strands can be analyzed together as a single element, and the stiffness is related to the total area of strands.

- The girder does not undergo any curvature until release. It is assumed that the combination of self-weight and hold-down anchors counteracts any moment that could be induced on the girder due to thermal/shrinkage profiles.

3.4.1 Numerical Formulation

In the post-bond/pre-release phase of the girder history, the goal is to determine the stress and strain in each of the active materials. This means analyzing the strand-only elements as well as the composite girder element. This is accomplished using finite elements to determine the free node displacements that result in an equilibrium state. Because this is a non-linear solution in time, the Newton-Raphson approach is again used to iterate on the nodal displacements based on the nodal forces.

It is important to note that, although the final solution is in terms of nodal displacements, the actual data of importance is the final stress and strain results from each material element. The final nodal displacements are unimportant and for this reason it is only the change in nodal displacements during each time-step that are actually important to determining the material state at the end of the interval.

There are two constraints on this problem. The first is the kinematic requirement of zero change in length of the casting bed. This constraint is satisfied by using free nodes only, labeled as 1, 2, 3, and 4 in Figure 3.10; the two abutments are specified to have zero displacement. The

second requirement is for nodal equilibrium to be achieved at each of the four free nodes. Because there are no applied nodal forces, equilibrium requires that the force on either side of the node be equal, as shown in Figure 3.11.

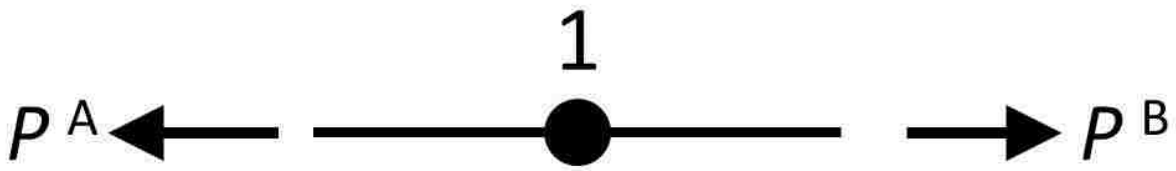

Figure 3.11 Nodal equilibrium requirement

With no applied loads, nodal equilibrium is achieved when $P^B = P^A$. For the Newton-Raphson iteration, a residual nodal load is needed to determine the next increment in displacement.

$$F^{res} = P^B - P^A \tag{3.9}$$

where the residual nodal force is zero once equilibrium is achieved. In terms of the Newton-Raphson scheme for this phase, nodal forces, *F,* are the dependent variables while the nodal displacements, *U*, are the independent variables to be iterated on.

The residual nodal forces and nodal displacements are related using the classical finite element approach where:

$$\Delta U = [K]^{-1} F^{res} \tag{3.10}$$

where: F^{res} = a 4x1 vector of residual nodal forces.

ΔU = a 4x1 vector of free nodal displacement increments

K = the stiffness matrix relating nodal forces and displacements.

For the stiffness matrix, *K*, the instantaneous linear-elastic stiffness provides an acceptable approximation for iteration purposes.

For the strand only elements where a simple 1-D element is used, the resulting stiffness for a single strand only element,

$$[K]^e = \frac{A_p E_p}{L^{(e)}} \begin{bmatrix} 1 & -1 \\ -1 & 1 \end{bmatrix} \tag{3.11}$$

where: A_p = the total area of strands from all groups in the element. This is the same for all of the strand-only elements.

E_p = the elastic modulus of the strand (typically 28500 ksi)

$L^{(e)}$ = the length of the element

The girder element is more complicated due to the effects of the elastic foundation it is resting on. The derivation of the stiffness matrix for this 1-D element is shown in Appendix B and results in the element stiffness equation:

$$\begin{Bmatrix} P_i \\ P_j \end{Bmatrix} = \frac{K_{Bed}}{\lambda L} \begin{bmatrix} \frac{1}{\tanh \lambda L} & \frac{-1}{\sinh \lambda L} \\ \frac{-1}{\sinh \lambda L} & \frac{1}{\tanh \lambda L} \end{bmatrix} * \begin{Bmatrix} u_i \\ u_j \end{Bmatrix} \tag{3.12}$$

where: L = the length of the girder

K_{Bed} = the total shear stiffness of the elastic bed along the entire length of the girder

$\lambda = \sqrt{\frac{\beta}{EA}}$, in which β is the bed stiffness per unit length given by $\frac{K_{Bed}}{L}$, and EA_{Tot} is the cross sectional axial stiffness of the composite girder.

It should be noted that the total bed stiffness, K_{Bed}, is specified as a user input. This stiffness matrix gives the standard axial element stiffness shown in Equation 3.11 if the term K_{Bed} approaches zero.

Using these element stiffness matrix types, the global stiffness matrix for the free nodes can be assembled as follows:

$$[K] = \begin{bmatrix} A_pE * \left(\frac{1}{L_1} + \frac{1}{L_2}\right) & \frac{-A_pE}{L_2} & 0 & 0 \\ \frac{-A_pE}{L_2} & \frac{A_pE}{L_2} + \frac{K_{Bed}}{\lambda L_3 \tanh \lambda L_3} & \frac{-K_{Bed}}{\lambda L_3 \sinh \lambda L_3} & 0 \\ 0 & \frac{-K_{Bed}}{\lambda L_3 \sinh \lambda L_3} & \frac{A_pE}{L_4} + \frac{K_{Bed}}{\lambda L_3 \tanh \lambda L_3} & \frac{-A_pE}{L_4} \\ 0 & 0 & \frac{-A_pE}{L_4} & A_pE * \left(\frac{1}{L_4} + \frac{1}{L_5}\right) \end{bmatrix} \quad (3.13)$$

Using this stiffness and Equation 3.10, the change in displacement due to residual nodal loads can be determined.

Equation 3.10 provides an estimate for the nodal displacements due to residual nodal loads, but in order to complete the iteration circle, a method of calculating the "exact" residual nodal loads due to prescribed nodal displacements. This is done through kinematics and the constitutive relation.

Equation 3.9 provides the residual nodal force provided the element forces are known. The forces in the strand-only elements are computed from the nodal displacements as follows:

$$\Delta\varepsilon_{Tot} = \frac{\Delta u_j - \Delta u_i}{L_e} \quad (3.14)$$

where: Δu_j and Δu_i are the increments in nodal displacements at the right and left ends of the element respectively.

L_e = the element length

The mechanical strain increment in the element can then be determined using the relationship:

$$\Delta\varepsilon_{mech} = \Delta\varepsilon_{Tot} - \Delta\varepsilon_{env} \quad (3.15)$$

where: $\Delta\varepsilon_{env}$ are the free thermal strains given by $\alpha\Delta T$.

Using this mechanical strain, the force in the element can be calculated using the constitutive relation that will be discussed in Chapter 5.

$$P^e = \int \sigma(\Delta\varepsilon_{mech}, \Delta t) dA \tag{3.16}$$

For the strand-only elements this equation becomes a summation of the force in each strand group. Each strand group must be considered individually because, although the change in strain is the same for each group, the beginning state differs from the result of the previous phase. So the total force in a strand-only element is:

$$P^e = \sum_{i=1}^{Ngrp} A_i * \sigma(\Delta\varepsilon_{mech}, \Delta t)_i \tag{3.17}$$

The girder element is more difficult because of the elastic foundation on which it rests. In order to compute the actual force on the element, the total strain must be related to the nodal displacements. This is complicated by the fact that the total strain is not constant along the length due to the bed stiffness contribution. The derivation of the governing equations for an axial element resting on an elastic bed with shear stiffness is shown in Appendix B. The resulting strain at any location along the girder is given by.

$$\Delta\varepsilon_{Tot}(x) = \frac{\lambda}{\sinh \lambda L}[-\sinh[\lambda(L-x)] \quad \sinh \lambda x] * \begin{bmatrix} \frac{1}{\tanh \lambda L} & \frac{-1}{\sinh \lambda L} \\ \frac{-1}{\sinh \lambda L} & \frac{1}{\tanh \lambda L} \end{bmatrix} * \begin{Bmatrix} \Delta u_i \\ \Delta u_j \end{Bmatrix} \tag{3.18}$$

where: x = the location along the girder measured from the left side of the girder and is positive to the right.

Note that because of the assumption of zero curvature in the girder element, the total strain does not vary over the height of the girder. This is not true for the thermal (and possibly shrinkage) strains which are likely to vary over the height of the girder. With this the mechanical strain increment may be computed at any height as follows:

$$\Delta\varepsilon_{mech}(y) = \Delta\varepsilon_{Tot}(x) - \Delta\varepsilon_{env}(y) \tag{3.19}$$

where: $\Delta\varepsilon_{env}(y)$ = the environmental strain increment at height y due to thermal and shrinkage effects depending on material type.

$\Delta\varepsilon_{mech}(y)$ = the mechanical strain increment at a location *y* in the girder at a given location *x,* along the girder.

Applying the same principle as before, the force at the location, *x*, can be calculated as:

$$P^e(x) = \int \sigma(\Delta\varepsilon_{mech}(y), \Delta t) dA \tag{3.20}$$

Notice that this integral is more complicated, because the stress changes along the height of the girder and there are also different types of material active in this cross-section. Equation 3.20 includes the integration of the stress in the prestressing strands, rebar and girder concrete. The method for dealing with this integration will be discussed in greater detail in Section 3.5.4.

The force in each of the five elements can now be calculated using Equations 3.17 and 3.20. These now are combined to generate the residual forces on each of the free nodes. This can be done as follows using Equation 3.9 to define the residual forces

$$\{F^{res}\} = \begin{Bmatrix} F_1 \\ F_2 \\ F_3 \\ F_4 \end{Bmatrix} = \begin{Bmatrix} P^B - P^A \\ P^C(0) - P^B \\ P^D - P^C(L^C) \\ P^E - P^D \end{Bmatrix} \tag{3.21}$$

where: (*x*) indicates the location in the girder element where the force was computed.

3.4.2 Numerical Implementation

The derivation above was completed with a Newton-Raphson iteration scheme. Figure 3.12 displays the flow chart for the implementation of this scheme.

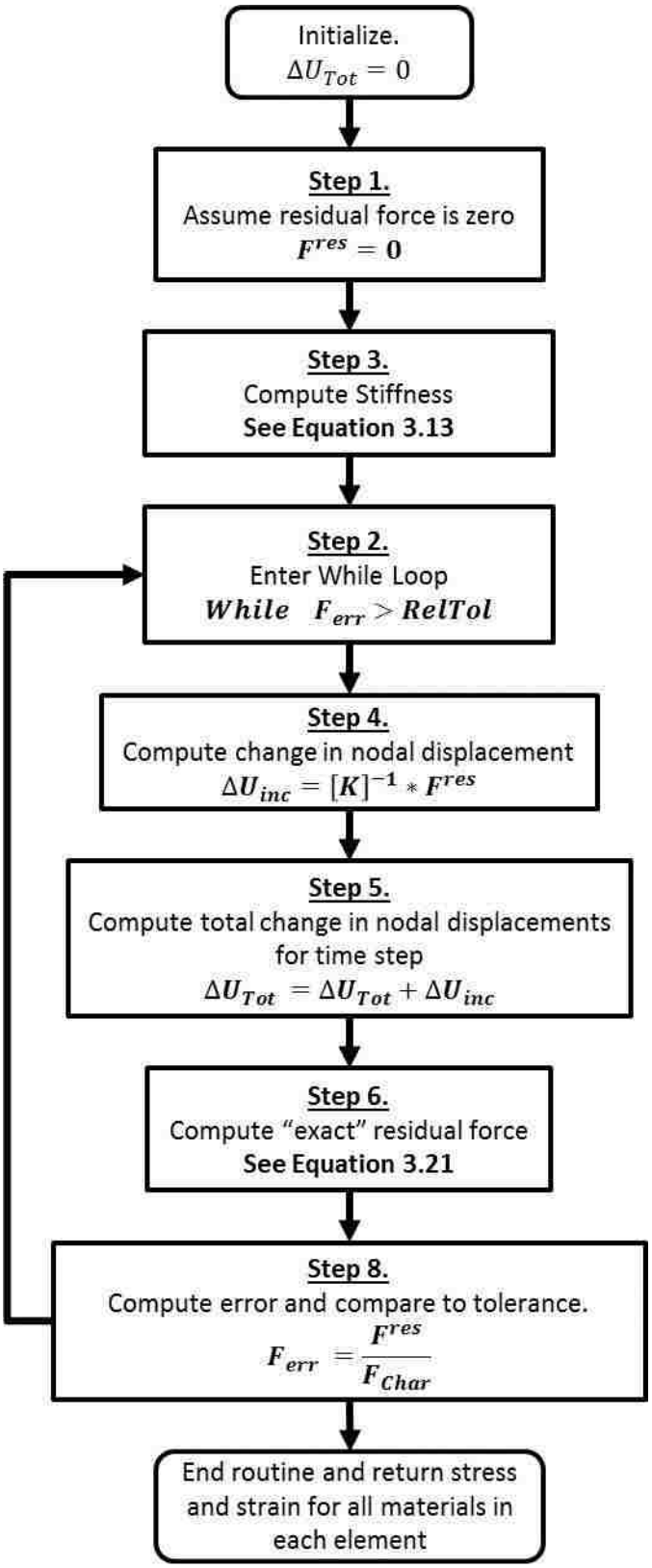

Figure 3.12 Post-bond, pre-release analysis flow chart.

The step numbering above matches that from the general Newton-Raphson scheme outlined in Section 3.1.3. Step 3 (computing the stiffness matrix) has been moved outside of the while-loop because it is not updated at each iteration. This is because the stiffness is computed based on the linear-elastic properties only. Step 7 is removed from this iteration scheme because the target value for F^{res} is always zero and therefore F^{res} is also the error.

The end result of this analysis phase is to obtain the stress and strain state for all of the material properties prior to release. These results are saved for use in the next time-step. In the post-release phase, which is discussed next, the girder element is analyzed at multiple cross-sections to determine the curvature. In order to include the pre-release phases, each of these cross-sections needs to be analyzed during this post-bond phase. In the formulation above only the end sections need to be analyzed to complete the analysis.

Because the results of this phase of the analysis are used in the next section, it is necessary to complete the material analysis for all locations needed in the future. This means that each of the cross-sections used in the post-release analysis (see Section 3.5) must be computed for each of the time-steps in the post-bond analysis. This is done so that the material state at the time of release is known for each of the material elements at each location. Note that these analysis locations are not used for the solution procedure described above.

3.5 Post-Release Analysis

The post-release phase is the one most commonly analyzed. In most analysis procedures (PCI, 2010; Tadros and Al-Omaishi, 2003; Stallings, 2001; AASHTO, 2012; ACI Committee 435, 1995) the stresses in the concrete and steel at the start of the phase are obtained from one-time calculations, such as the elastic shortening of the strand. Here, the starting conditions are

obtained from the output from the post-bonding phase, during which relaxation, temperature effects, etc., were tracked over time.

The goal is to compute the girder camber based on the constitutive models, applied loads, and environmental effects. The girder's camber history will be affected by the various events that occur during the fabrication process and service life.

At release, the girder formwork is removed; the strands are released at both ends of the girder, which becomes simply supported, as shown in Figure 3.13. Immediately after release, the girder is typically supported by a crane. The lifting loops are likely to be set in a short distance from the girder ends, rather than being at the ends, as shown in Figure 3.13, and this placement is taken into account when determining the moments at each cross-section location.

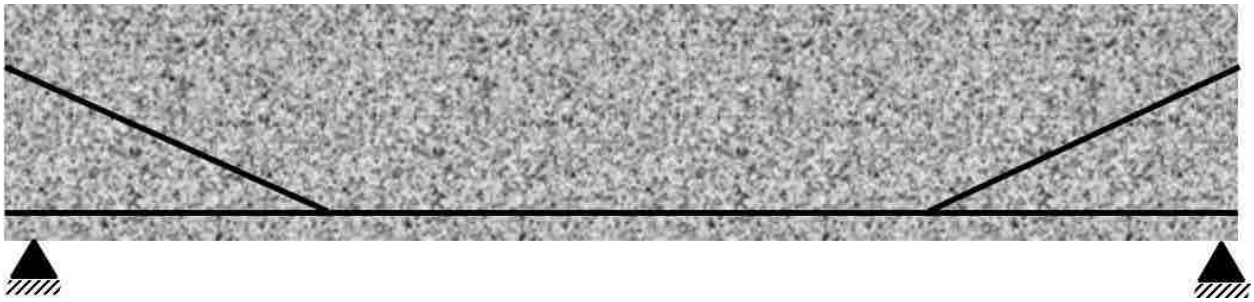

Figure 3.13 Released girder configuration

Camber is calculated at each time step by determining the curvature at several user-specified places along the girder and then integrating twice to determine the deflected shape and camber. The method consists of several different analysis levels which will be discussed in the following sections. The following assumptions are made when completing this analysis:

- Plane sections remain plane.
- Materials exhibit visco-elastic properties but remain in the elastic strain region. The girder remains uncracked.

- The supports have no friction and cannot induce longitudinal forces or moments in the beam.

3.5.1 Camber Calculation

Figure 3.14 shows the procedure for computing camber at any time step.

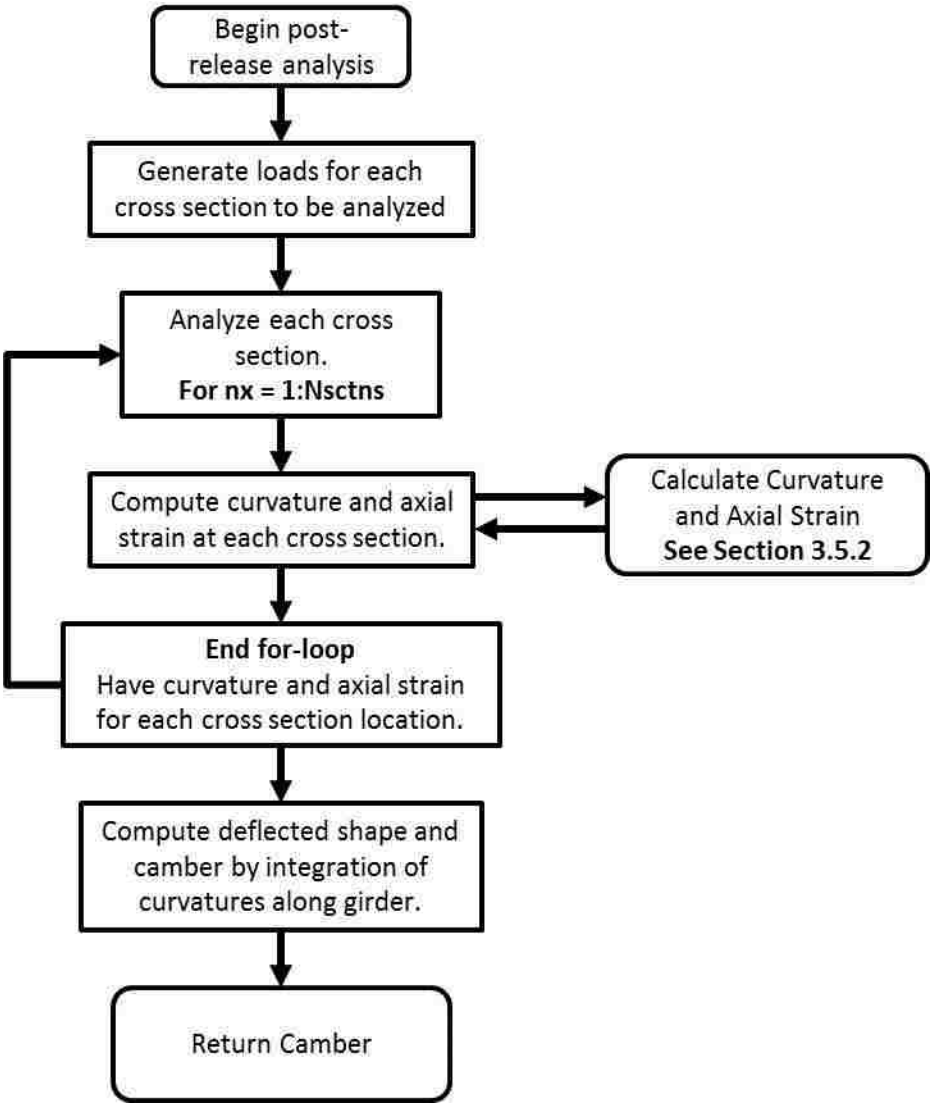

Figure 3.14 Post-release analysis flow chart

External load increments are generated for each cross section. They consist of axial forces and moments. In most cases the axial load at any location will be zero, but the moment will vary with the applied loads and support conditions.

For each cross-section, at the time step in question, the curvature and axial strain at the top of the girder are evaluated as described in Section 3.5.2. Those curvatures are integrated twice numerically (using the Simpson's rule) to give the deflected shape along the girder, and the camber is taken to be the deflection at mid-span relative to the ends. Loads and deflections are taken to be positive downwards, so an upwards camber is computed as a negative number. In reporting the camber for the camber history, this result is modified to match the common practice of stating camber as positive in the upward direction. The axial shortening of the girder is obtained by numerically integrating the strains at the centroid.

3.5.2 Curvature Calculation

Computing the curvature is done by completing a cross-sectional analysis. In order to illustrate the theory behind this analysis, the governing equations for a linear-elastic, time-dependent material will be developed. This will be useful in demonstrating the use of the Newton-Raphson approach that is used when the time-dependence is linked to the elastic changes as is the case for the constitutive models used in this algorithm.

For the cross-section analysis, the curvature and axial strain at the origin are determined by iteration until the moment and axial force on the cross-section are equal to the applied external loads.

The axial load will be derived first. In order for equilibrium to be satisfied,

$$\Delta P_{ext} = \int \Delta\sigma(\Delta\varepsilon_{mech}, \Delta t) dA \tag{3.22}$$

where: $\Delta\sigma(\Delta\varepsilon_{mech}, \Delta t)$ is the constitutive relation that gives the stress increment due to an increment in time and mechanical strain.

So:

$$\Delta\sigma = \frac{\partial\sigma}{\partial t}\Delta t + \frac{\partial\sigma}{\partial\varepsilon}\Delta\varepsilon_{mech} \tag{3.23}$$

So for a cross-section analysis where stress varies over the height of the girder

$$\Delta P_{ext} = \int \Delta\sigma(y)dA = \int \frac{\partial\sigma}{\partial\varepsilon}\Delta\varepsilon_{mech}(y)dA + \int \frac{\partial\sigma}{\partial t}\Delta t dA \tag{3.24}$$

But $$\Delta\varepsilon_{Tot} = \Delta\varepsilon_{mech} + \Delta\varepsilon_{env} \tag{3.25}$$

where: $\Delta\varepsilon_{env} = \Delta\varepsilon_{thermal} + \Delta\varepsilon_{shrinkage}$ and may vary over the height

$\Delta\varepsilon_{mech}$ = the strain increment associated with a stress change.

So

$$\Delta P_{ext} = \int \frac{\partial\sigma}{\partial\varepsilon}\big(\Delta\varepsilon_{Tot}(y) - \Delta\varepsilon_{env}(y)\big)dA + \int \frac{\partial\sigma}{\partial t}\Delta t dA \tag{3.26}$$

For this case where materials are assumed to remain linear

$$\frac{\partial\sigma}{\partial\varepsilon} = E(t) \tag{3.27}$$

And for a given cross-section subjected to both moment and axial loads, the total strain can be expressed as

$$\varepsilon_{Tot}(y) = \varepsilon_{Tot,O} + \phi_{Tot}y \tag{3.28}$$

Combining these equations and rearranging, the common stiffness formulation can be derived as

$$\int E(t)\Delta\varepsilon_{Tot,O}dA + \int E(t)\Delta\phi_{Tot}ydA = \Delta P_{ext} + \int E(t)\Delta\varepsilon_{env}(y)dA - \int \frac{\partial\sigma}{\partial t}\Delta t dA \tag{3.29}$$

A similar approach can be used to develop the following equation for the moment.

$$\int E(t)y\Delta\varepsilon_{Tot,O}dA + \int E(t)y^2\Delta\phi_{Tot}dA = \Delta M_{ext} + \int E(t)y\Delta\varepsilon_{env}(y)dA - \int \frac{\partial\sigma}{\partial t}\Delta t y dA \tag{3.30}$$

Equations 3.29 and 3.30 describe equilibrium on the cross-section in the classical stiffness form,

$$\{F\} = [K]\{U\} \tag{3.31}$$

Equations 3.29 and 3.30 can be combined to create a 2x2 system of linear equations

$$\begin{Bmatrix}\Delta M_{Tot}\\ \Delta P_{Tot}\end{Bmatrix} = [K(t)]\begin{Bmatrix}\Delta\phi_{Tot}\\ \Delta\varepsilon_{Tot,O}\end{Bmatrix} \tag{3.32}$$

where: $$[K(t)] = E(t)\begin{bmatrix}\int y^2 dA & \int y dA\\ \int y dA & \int dA\end{bmatrix} \tag{3.33}$$

$$\begin{Bmatrix}\Delta M_{Tot}\\ \Delta P_{Tot}\end{Bmatrix} = \begin{Bmatrix}\Delta M_{ext} + \int E(t) y \Delta\varepsilon_{env}(y) dA - \int \frac{\partial\sigma}{\partial t}\Delta t y dA\\ \Delta P_{ext} + \int E(t)\Delta\varepsilon_{env}(y) dA - \int \frac{\partial\sigma}{\partial t}\Delta t dA\end{Bmatrix} \tag{3.34}$$

$\Delta\phi_{Tot}$ = the increment in curvature

$\Delta\varepsilon_{Tot,O}$ = the increment in total axial strain at the user defined origin of the cross-section.

Equation 3.29 shows that the total change in load, ΔP_{tot}, consists of three components. The first is the external load component, the second is the environmental load component, and the third is the load change caused by the fact that the constitutive laws are time-dependent. The latter therefore constitutes the difference between the real load change (including creep effects) during the time step and that obtained assuming elastic behavior.

The variable *E(t)* represents the instantaneous elastic modulus, so the terms in the stiffness matrix, *K*, represent the instantaneous elastic stiffnesses, that is, the tangent stiffness at time *t*.

Because the stress is, in general, a function of both time and strain, the last term in the loading cannot be evaluated until the strain increment during the time step is known. This causes the need for iterative calculations. Thus the procedure is to:

- Formulate the incremental load vector (Equation 3.29 and 3.30)
- Estimate the increments in total curvature $\Delta\phi_{Tot}$ and strain $\Delta\varepsilon_{Tot,O}$ at the origin of the cross-section using Equation 3.31.
- Evaluate the total incremental strains throughout the section from $\Delta\phi_{Tot}$ and $\Delta\varepsilon_{Tot,O}$.

- Evaluate the stresses at the end of the time step throughout the cross-section using the time-dependent constitutive laws.
- Integrate the incremental stresses to obtain the calculated axial force and moment, ΔP_{exact} and ΔM_{exact}.

This formulation is easily written into the Newton-Raphson using the relationships described above. This scheme is outlined in Figure 3.15.

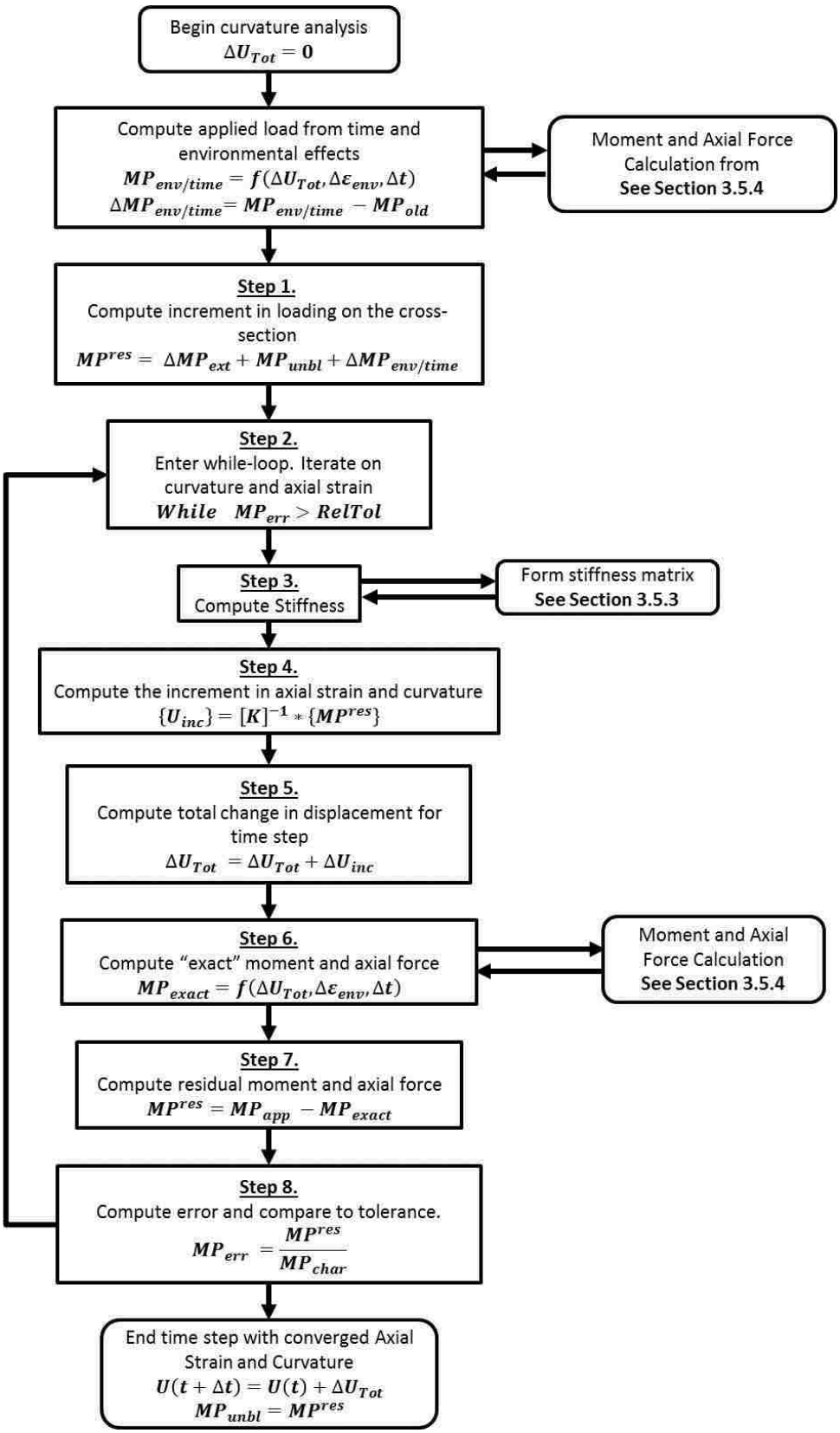

Figure 3.15 Curvature calculation routine flow chart

Notice that at two locations, a separate function is called to compute the moment and axial force at the end of the time-step (note that this is not the increment in load and therefore an increment is computed by subtracting the previously converged load). This calculation will be discussed in more detail in the Section 3.5.4. This is calculated based on an increment in time, environmental strains, and total strain and curvature expressed as ΔU_{Tot} .

In Step 1, the computed change in moment and axial force due to the time and environmental effects are added to the change in applied load. This load is computed assuming that there is a zero increment in total strain or curvature and is done for numerical efficiency. If the time and environmental loads are neglected in the first step, they will be accounted for in the residual force in the first iteration when time and environmental strains are incorporated in the moment and axial force calculation.

In Step 3, the stiffness is computed. In the original Newton-Raphson formulation, this stiffness is computed in each iteration with the updated state variables, while in the modified Newton-Raphson procedure the stiffness is computed only in the first iteration. The algorithm is formulated such that either method can be used depending on the user input. The method of computation is discussed in Section 3.5.3.

3.5.3 Stiffness Matrix Calculation

The stiffness matrix is determined using Equation 3.33 where the location *y* depends on the definition of the origin. If the origin is selected at the centroid of the section, the resulting stiffness matrix is given by.

$$[K] = \begin{bmatrix} EI & 0 \\ 0 & EA \end{bmatrix} \tag{3.35}$$

where: A and I are the transformed gross-section properties

E is the instantaneous elastic modulus during the time step.

Because the curvature calculation formulation must hold throughout the entire analysis, the origin of the section was selected as the top of the girder for this analysis. This is done because when a slab is added, the centroid changes and then the stiffness computation would need to change. The stiffness is then computed numerically following the procedure outlined in Figure 3.16.

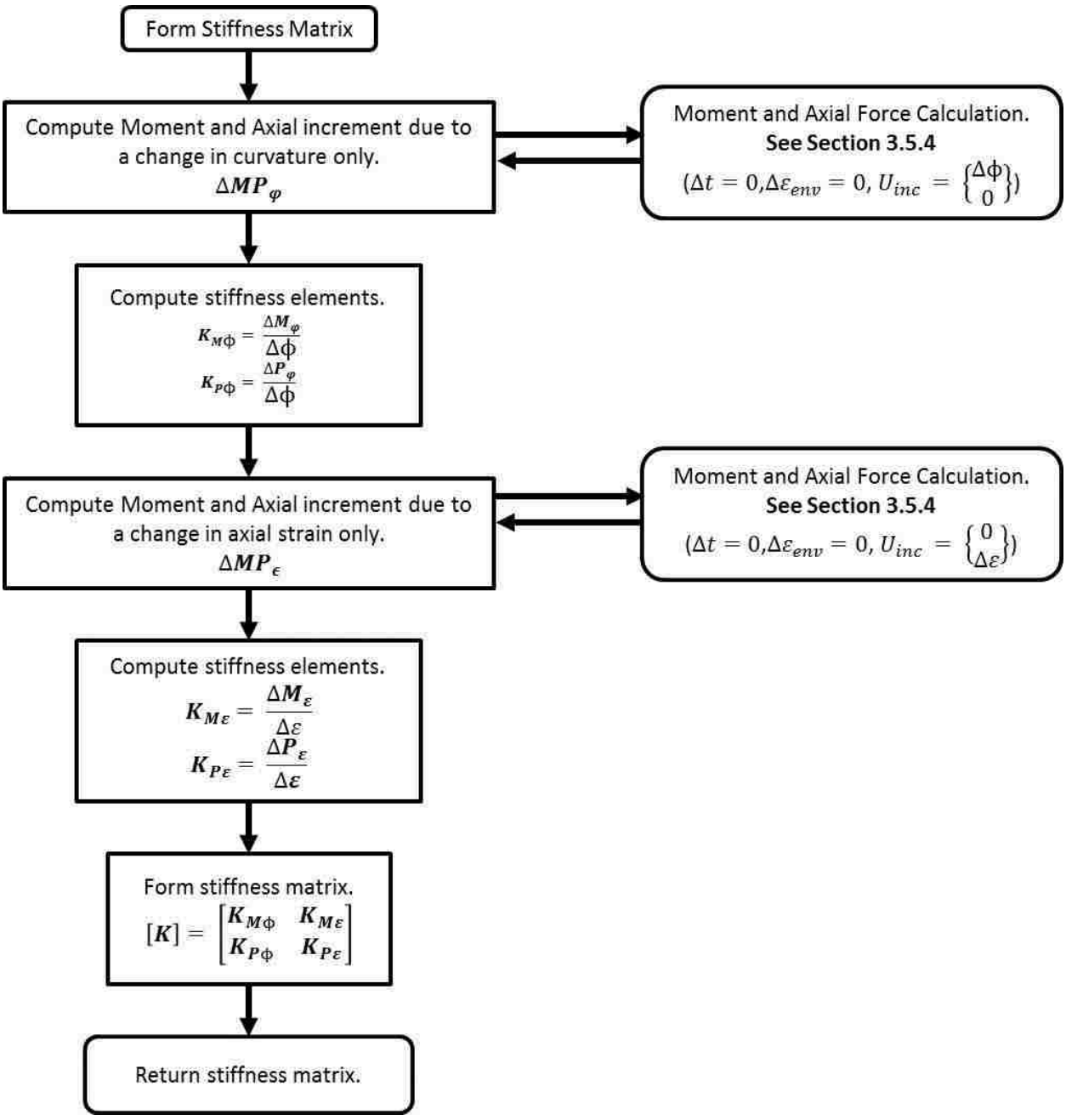

Figure 3.16 Flow chart for generating cross sectional stiffness matrix.

This formulation also has the added advantage of being universal and could be used in the case where nonlinear strains are reached.

By setting the time and environmental increments to zero when calling the moment and axial force calculation function, only the elastic stiffness is returned. In that case the elements of the stiffness matrix can be obtained with less computational effort as:

$$K_{P\varepsilon} = E(t) \int dA = A \tag{3.36}$$

$$K_{P\varphi} = K_{M\varepsilon} = E(t) \int y dA = A\bar{y} \tag{3.37}$$

$$K_{M\varphi} = E(t) \int y^2 dA = I + A\bar{y}^2 \tag{3.38}$$

where y is measured from the origin, in this case the top of the precast section, and $\bar{y}$ is the distance between the origin and the centroid.

3.5.4 Moment and Axial Force Calculation

The very lowest level of this iteration scheme is the routine supplied for computing the moment and axial force on a cross section due to an increment in curvature, axial strain, time and environmental effects. The routine is a relatively simple integration process, but it is worth describing to complete the discussion of the analysis algorithm. Several important points should be made about how this integration system is formulated:

- The origin for the y-axis is at the top of the girder and is oriented as positive downwards.
- The axial strain value $\varepsilon_{Tot,0}$ is specified at the origin.
- The concrete cross section is split into horizontal layers, following the concepts of a fiber element. The stress and strain are evaluated at each of these layer interfaces and then Simpson's integration scheme is used to compute the axial force and moment cause by the concrete on the section.
- Both the thermal and shrinkage strains may vary in the y-direction and must be evaluated at each calculation point.

- The strands and rebar in the section are treated as points and the strain and stress are assumed to be constant over the bar or strand area.

The routine used to compute the moment and axial force is shown in Figure 3.17.

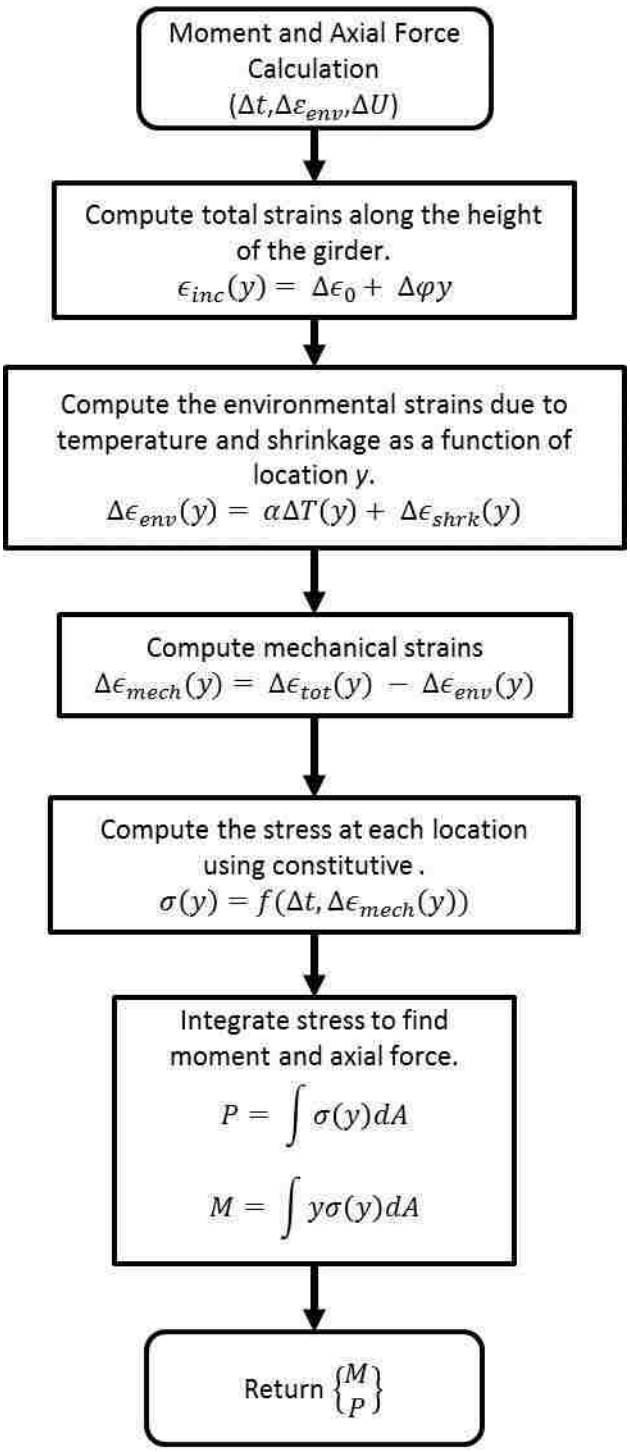

Figure 3.17 Moment and axial force calculation routine

The time-dependent constitutive models compute the stress at the end of the time-step based on an increment in mechanical strain and time. Note that the constitutive model does not compute the increment in stress but the final stress.

Each of the three material types was considered separately when calculating the axial force and moment. The strands and rebar elements are easily considered by using the point assumption made above but the integration over the concrete section is a little more complicated.

The user defines the geometry of the cross-section by inputting a series of trapezoids (see Appendix A). These major trapezoids can be subdivided further for better accuracy, and this is done by defining the target sub-layer thickness. These sub-layers are used to integrate using Simpson's rule.

Simpson's rule is an approximate method for integrating a function. It uses coefficients applied at sets of three locations where the function is known to integrate the parabolic equation described by these three points. These coefficients are come from Simpson's derivation where the integration is exact for functions of order two or less.

In this algorithm, Simpson's rule is applied in a numerical fashion where, rather than a function, the concrete stress is known at pre-determined locations along the height of the cross-section. This done using Equations 3.25, 3.28 and the constitutive model described in Chapter 4. These locations are the interfaces of the sub-layers described above. Each major trapezoid is divided into an even number layers and the strain and stress is analyzed at the interface of these layers (an odd number). The force at each interface is computed from the stress acting over the area tributary to it. These forces are integrated multiplying by the specified Simpson's coefficients and summing.

For a simple I-beam section, the Simpson's coefficient distribution would look like the

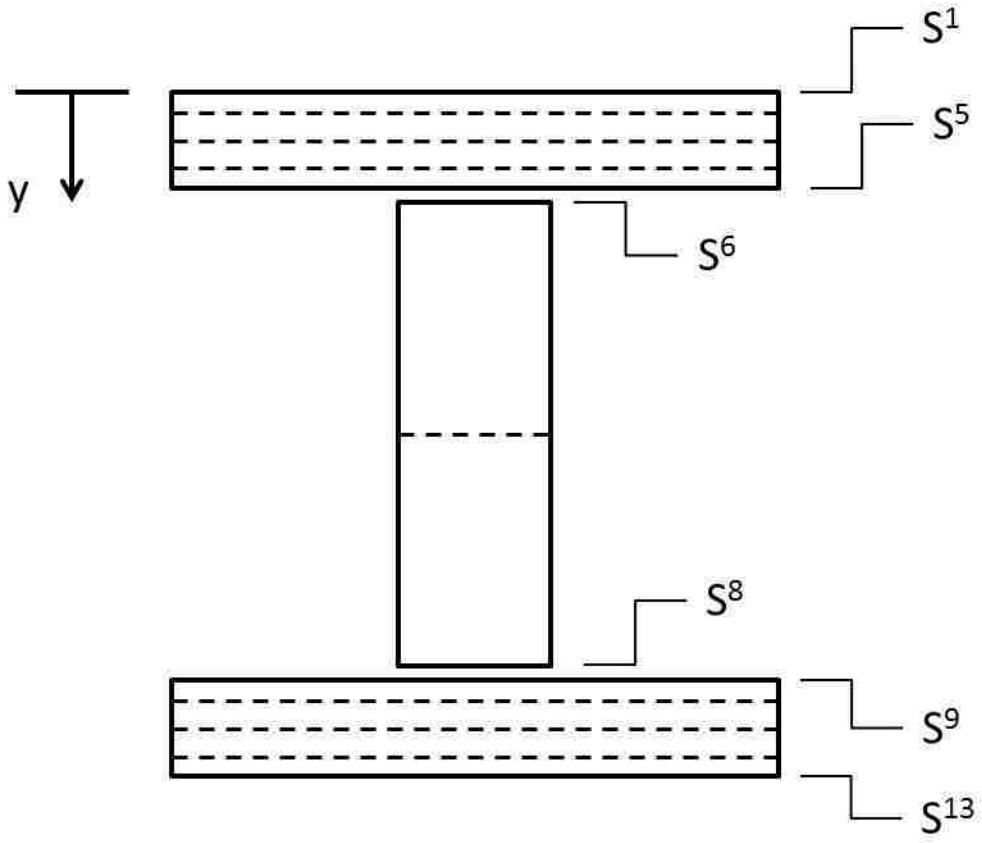

following.

Figure 3.18 Simpson's Rule demonstration

In this diagram, the solid lines represent the trapezoids input by the user and used to define the section geometry. The dashed lines are the sub-layers used to increase the accuracy during the integration. Each pair of the sub-layers is integrated separately using Simpson's Method.

Using Simpson's integration rule for the girder, the closed form integration for *P* noted in Figure 3.17 is computed as follows.

$$P_{Rebar} = \sum_{n=1}^{nbar} A_n \sigma_n \tag{3.39}$$

$$P_{Strand} = \sum_{n=1}^{nstnd} A_n \sigma_n \tag{3.40}$$

$$P_{Concrete} = \sum_{n=1}^{nInt} S_n A_n \sigma_n \tag{3.41}$$

where: $P = P_{Rebar} + P_{Strand} + P_{Concrete}$

S_n is the Simpson's coefficient for the concrete interface.

n_{Int} = the number of sublayer interfaces in the section (used for the concrete integration only).

Similarly the moment M is computed as follows.

$$M_{Rebar} = \sum_{n=1}^{nbar} y_n A_n \sigma_n \quad (3.42)$$

$$M_{Strand} = \sum_{n=1}^{nstnd} y_n A_n \sigma_n \quad (3.43)$$

$$M_{Concrete} = \sum_{n=1}^{nInt} y_n S_n A_n \sigma_n \quad (3.44)$$

where: $M = M_{Rebar} + M_{Strand} + M_{Concrete}$

S_n is the Simpson's coefficient for the concrete layer.

n_{Int} = the number of sublayer interfaces in the section (used for the concrete integration only).

CHAPTER 4 CONCRETE CONSTITUTIVE MODEL

The creep of the concrete is the most important fact in analyzing the long-term deflection behavior of precast, prestressed, concrete girders. The effects of creep are magnified in prestressed members because long-term deflections are increased not only by creep, but also by prestress losses resulting from creep deformations. In order to link the effect of creep to the prestress loss, it is preferable to use a model formulated in a time-incremental manner. This chapter describes the formulation of a new rheological model for simulating creep that has significant advantages over current methods. Most existing models exhibit the following drawbacks, while the new model avoids them:

- They are formulated to predict the outcome of creep tests, in which the stress is known and the strain is sought. This is the opposite of the need in most displacement-based numerical simulations of structures.
- They are formulated for constant stress loading, such as is found in creep tests, and are not amenable to use with time-varying stress, which is the usual condition in a pre-tensioned girder.
- Their inability to address time-varying stress leads to an inability to predict the special but important case of creep recovery when the stress changes.
- The models are mostly phenomenological and consist of empirical equations that fit test data. Guaranteeing thermodynamic validity is essential but may be difficult.
- They do not include the observed time variations in elastic modulus and other properties.

This proposed model is based on visco-elasticity and is intended to provide a framework sufficiently versatile to replicate a variety measured results, including creep recovery.

Following its formulation, the model will be calibrated against the currently available creep prediction models. Because this thesis is focused on the development of a camber prediction algorithm and not the intricacies of creep modeling, the versatility of this model will be demonstrated but a more thorough calibration to actual creep data will not be conducted. This calibration will be demonstrated using a typical girder concrete mix and the resulting material parameters will be applied for the rest of the comparisons.

4.1 Model Formulation

The model is shown schematically in Figure 4.1. It consists of a chain of Kelvin elements, to the end of which is attached a pure elastic spring element. A Kelvin element consists of a linear spring in parallel with a linear dashpot, in which the resistance is proportional to the strain rate, $d\varepsilon/dt$. The figure shows a model with three Kelvin elements, but as many as desired can be used. All of the material parameters, such as springs and dashpots in the Kelvin units, have properties that can vary with time. It is questionable whether the experimental data presently available are sufficiently reliable to calibrate all of the time-varying features, but the time-variation feature is included in preparation for such time that the data are available. Some time-variation is needed to model creep recovery, and that characteristic is shown here. However, suitable calibration data are available for the variations of elastic modulus over time, so at least that element of the model can vary with time using realistic values. The model can, of course, be used with constant values for the parameters in the absence of data for calibrating the time-varying.

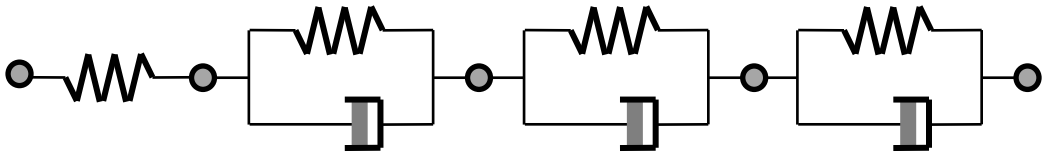

Figure 4.1 Rheological diagram of the model

4.1.1 Governing Equations

The governing equations for a single Kelvin element are derived first, and they are then incorporated into the chain. In each case the parameters are assigned time-varying properties.

To maintain thermodynamic consistency, the parameters may not vary arbitrarily. The primary requirement is that the unit should not be able to generate energy under any loading scenario. That goal is achieved here by basing the equations on a particular physical form; at each time step, each element is thought of as being supplemented with an additional, unstressed, element in parallel with the original one. Because the model describes the behavior of a real physical system, it must be thermodynamically consistent. The predicted response will depend slightly on the length of the time step, but it is expected to converge to a unique value as the time step is reduced towards zero. The use of finite time steps is a consequence of having to solve the equations numerically.

The way in which the properties change with time can be chosen to fit any particular set of measured data. Here, the variation with time of the elastic modulus is taken to be of the form

$$E(t) = E_0 + (E_{\inf} - E_0)(1 - e^{-t/T}) \tag{4.1}$$

where: T = a user-specified intrinsic time constant that controls how rapidly the properties change.

This form fits the available elastic modulus data well and is quite simple. It is illustrated in Figure 4.2. The same general form of time dependence is used for the Kelvin element spring stiffnesses and dampers, E_K and η.

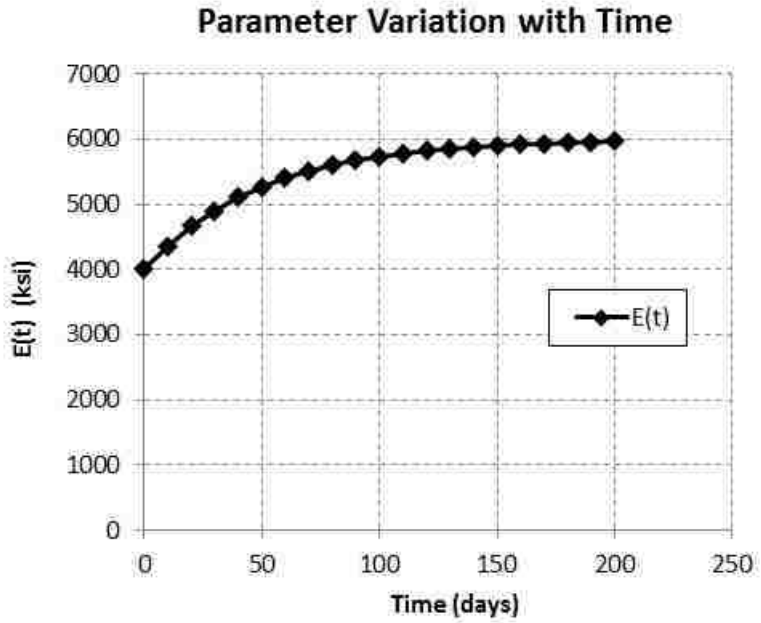

Figure 4.2 Assumed variation of *E* with time.

The general constitutive equation for a Kelvin unit with fixed properties is:

$$\sigma = E_K \varepsilon + \eta \dot{\varepsilon} \tag{4.2}$$

where a dot indicates differentiation with respect to time. To address the time variations this must be differentiated to give the incremental form

$$\frac{d\sigma}{dt} = \frac{dE_K \varepsilon}{dt} + \frac{d\eta\dot{\varepsilon}}{dt} \tag{4.3}$$

or:

$$\frac{d\sigma}{dt} = E_K \frac{d\varepsilon}{dt} + \varepsilon \frac{dE_K}{dt} + \eta \frac{d\dot{\varepsilon}}{dt} + \dot{\varepsilon} \frac{d\eta}{dt} \tag{4.4}$$

However, Equation 4.4 contains the term, $\varepsilon \frac{dE_K}{dt}$, which should not be present if the incremental stiffness element is unstressed when it is added. The term must therefore be dropped, to give:

$$\frac{d\sigma}{dt} = E_K \frac{d\varepsilon}{dt} + +\eta \frac{d\dot{\varepsilon}}{dt} + \dot{\varepsilon} \frac{d\eta}{dt} = \dot{\varepsilon}\left(E_K + \frac{d\eta}{dt} \right) + \eta\ddot{\varepsilon} \tag{4.5}$$

or:

$$\dot{\sigma} = \dot{\varepsilon} E_f + \eta\ddot{\varepsilon} \tag{4.6}$$

where: E_f = the effective stiffness, given by $E_K + \dot{\eta}$,

Equation 4.6 can also be obtained from first principles, by considering the force in each element. Note that this formulation causes creep to be treated in the same fashion for both tension and compression.

To find the relationship between the stress and strain rates in the Kelvin element at the end of a time step, either the stress rate or the strain rate is needed; in the absence of both, the problem specification is incomplete. Here it is assumed that the stress varies linearly with time, so $\dot{\sigma}$ is constant. The solution to Equation 4.6 is then

$$\dot{\varepsilon}_K(t) = \dot{\varepsilon}_{K0} e^{-t/\tau} + \frac{\dot{\sigma}}{E_f}\left(1 - e^{-t/\tau}\right) \tag{4.7}$$

where: $\tau = \eta/Ef$ = the intrinsic decay time of the unit

$\dot{\sigma}$ = the rate of change of stress with time

$\dot{\varepsilon}_{K0}$ = strain rate in the Kelvin element at the start of the time interval

4.1.2 Numerical solution procedure

Equation 4.7 provides the strain rate throughout the time step, and it must be integrated with respect to time to obtain the strain at the end of the time step. However, the property E_f is

time-dependent, and so the form of its dependency must be known in order to complete the integration. Two approaches were considered. In the first, E_f was treated as constant during the time step with a value equal to the average of the starting and ending values. This approach is referred to as the "Constant Average" approach. In the second approach, the compliance, $1/E_f$, was assumed to vary linearly during the interval. That approach is referred to as the "Linear" approach, (the compliance, rather than the stiffness, was taken as linear because doing so simplifies the integration). For the Constant Average approach, the strain at any time t during the time step is given by:

$$\varepsilon_K(t) = \varepsilon_{K0} + \tau\dot{\varepsilon}_{K0}\left(1 - e^{-t/\tau}\right) + \frac{\dot{\sigma}}{E_{f,ave}}\left[t - \tau\left(1 - e^{-t/\tau}\right)\right] \tag{4.8}$$

and for the Linear approach:

$$\varepsilon_K(t) = \varepsilon_{K0} + \tau\left(\dot{\varepsilon}_{K0} - \dot{\sigma}\left(J_0 + \tau J_1\right)\right)\left(1 - e^{-t/\tau}\right) + \dot{\sigma}t\left\{J_0 + J_1\tau\left(\frac{1}{2}\frac{t}{\tau} + e^{-t/\tau}\right)\right\} \tag{4.9}$$

where: J_0 and J_1 are the (known) compliances, or $1/E_f$ values, at the start and end of the time step.

In order to select from these two integration schemes, trials were conducted using both approaches to investigate convergence. A single Kelvin unit was loaded with a user-selected, time-varying stress, consisting of an initial value plus a constant stress rate thereafter.

For arbitrary time variation in E_f, no closed form solution exists against which to evaluate the numerical results, so the strain was calculated at a specific time (100 days in this case), using time steps of decreasing size. At the shortest step size used (0.5 days), the strain at 100 days had converged to within 0.05% of the same value using both techniques. That converged value was then taken as the true solution for the strain at 100 days, and the errors between it and the computed values using larger time steps were plotted against time step size on a log-log plot.

The result is shown in Figure 4.3. The time step size was normalized with respect to τ, the inherent time constant of the system. Because the material properties varied over the 100 day calculation period, τ also varied, so its starting value was used in all the normalizations. The parameters used for the plot are: $E_K = 4000$, $\eta = 300{,}000$ at $t = 0.0$, $E_K = 8000$, $\eta = 600{,}000$ at $t = \infty$, $\sigma_0 = 0.7, \dot{\sigma} = 0.001$. Units are inch, kip, days. The strain was evaluated at 100 days.

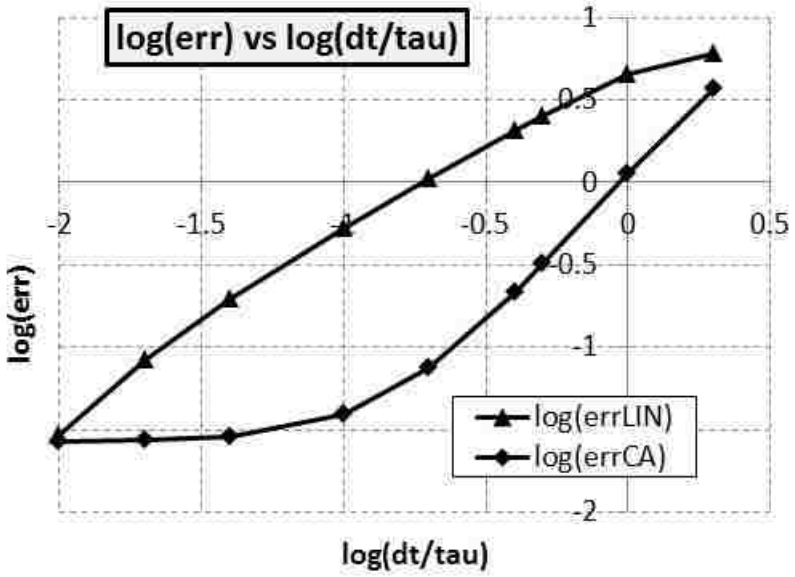

Figure 4.3 Error in predicted strain at 100 days vs. time step.

Both curves contain an approximately linear region, in which the error is dominated by truncation. The slopes (of 1.0 and 2.0) imply that the Linear and Constant Average techniques converge with $(\Delta t/\tau)$ to the first and second power respectively, suggesting that the Constant Average method is the better choice. The Constant Average curve also departs from linearity at low $\Delta t/\tau$ values. This occurs because round-off starts to control the error, and further reduction in $\Delta t/\tau$ provides no corresponding reduction in error, and might, if taken too far, even cause the error to increase. The Constant Average approach was selected, because of its superior convergence properties at all but very small time steps, and because the formulation is slightly simpler.

The Kelvin units can now be assembled to form the chain. For each unit, equilibrium requires that the stress variation with time within the interval be the same. Thus, the strain change in each unit at the end of the time step can be established as a linear function of the unknown stress rate, $\dot{\sigma}$. The strain change in the elastic unit is:

$$\Delta\varepsilon_e = \frac{\dot{\sigma}}{E_e}\Delta t \tag{4.10}$$

where: for consistency with choice made in the Kelvin units, E_e is taken to be the average value over the time step.

The total strain change is then:

$$\Delta\varepsilon_{tot} = \Delta\varepsilon_e + \sum_{j=1}^{Nlink}\Delta\varepsilon_{K,j} \tag{4.11}$$

Or,

$$\Delta\varepsilon_{tot} = \frac{\dot{\sigma}\Delta t}{E_e} + \dot{\sigma}\sum_{j=1}^{Nlink}C_j + \sum_{j=1}^{Nlink}D_j\,\dot{\varepsilon}_{K0,j} \tag{4.12}$$

where:

$$C_j = \frac{\Delta t - \tau_j\left(1 - e^{-\Delta t/\tau,j}\right)}{E_{f,j}} \tag{4.13}$$

$$D_j = \tau_j\left(1 - e^{-\Delta t/\tau,j}\right) \tag{4.14}$$

Equation 4.12 can now be solved for $\dot{\sigma}$ if the total strain change, $\Delta\varepsilon_{Tot}$, is known. The result is:

$$\dot{\sigma} = \frac{\Delta\varepsilon_{tot} - \sum_{j=1}^{Nlink}D_j\,\dot{\varepsilon}_{K0,j}}{\frac{\Delta t}{E_e} + \sum_{j=1}^{Nlink}C_j} \tag{4.15}$$

This value for $\dot{\sigma}$ can now be used to find the stress change, given by:

$$\Delta\sigma = \dot{\sigma}\Delta t \tag{4.16}$$

and can also be substituted into Equations 4.7 and 4.8, with Δt in place of t, to find the strain and strain rate in each individual Kelvin unit at the end of the time step. The calculations can then proceed to the next step.

Equations 4.13 and 4.14 may lead to significant loss of accuracy through cancelation at low $\Delta t/\tau$ values. If desired, they may be replaced by their Taylor Series expansions for use in such circumstances,

$$C_j \approx \tau_j \left[\frac{\phi^2}{2!} - \frac{\phi^3}{3!} + \frac{\phi^4}{4!} \ldots \right] \tag{4.17}$$

$$D_j \approx \tau_j \left[\frac{\phi}{1!} - \frac{\phi^2}{2!} + \frac{\phi 3}{3!} \ldots \right] \tag{4.18}$$

where: $\emptyset = \Delta t/\tau$

4.1.3 Comparison of Model Parameter to Conventional Material Constants

In the derivation above, a series of material parameters were developed in the form of rheological model constants. It is convenient to correlate these parameters to the conventional constants used to describe concrete creep. Although many models exist using a variety of approaches and constants, the most commonly used constants to describe concrete deformations are the elastic modulus at 28 days and the ultimate creep coefficient. The ACI 209R-92 creep model (ACI Committee 209, 2008) also gives an equation that defines the rate of progress with time of the creep effects. These general parameters are compared to the rheological constants below.

Elastic modulus, E_c. This maps directly to E_e, the stiffness of the elastic spring element. This can be assigned the (measured) E_c value at 28 days if no better information is available, and

E_e may be taken as constant. It is very likely that E_c will vary with time, and the variations should be included if possible.

Ultimate creep coefficient, C_{cu}. This is normally taken to be the ratio of the creep strain to the initial elastic strain (for a constant load). However, in practice, the initial elastic strain is often computed using $E_{c,28}$, rather than the instantaneous value at the time of loading, because data on the early modulus is often unavailable, and because many models do not account for the time variation in E_c. If both E_c and the model parameters are treated as constant with time, C_{cu} is related to the model parameters by:

$$C_{cu} = \frac{E_e}{E_k}$$

Note that, in this case $\dot{\eta} = 0$, so $E_f = E_K$. If more than one Kelvin element is used, E_k in Equation 4.14 should be replaced by $E_{k,eq}$, defined by:

$$E_{k,eq} = \left[\sum_{j=1}^{N} \frac{1}{E_k} \right]^{-1}$$

Dashpot stiffness, η. This is related to the intrinsic time constant, τ, for the system by

$$\tau = \eta / E_f$$

and, for a system with parameters that do not vary with time, in which case E_f is simply E_k, τ represents the time needed to complete 63.2%, i.e. (1-1/*e*), of the creep deformation.

If the model parameters are chosen to be functions of time, the relationships between the conventional constants and the model parameters depend on the functional form of the time variation of those parameters. It is then necessary to conduct trials, guided by the foregoing results for fixed parameters, to achieve a model that replicates the desired combination of

conventional parameters. This process was used in the following section to calibrate the model to several data sets.

4.2 Model Calibration

Ideally the Kelvin model would be calibrated thoroughly enough that each of the rheological parameters and accompanying time dependent factors could be related to the key factors that affect creep such as mix properties, relative humidity, temperature, and member geometry. Due to limits on time, resources, and adequate experimental data, this was not feasible. In order to demonstrate the versatility of the model and its ability to at least model the correct behavior, it be calibrated to each of the following five accepted creep models using constant stress loading; AASHTO, ACI 209R-92, B3, CEB MC90-99, and GL2000 (ACI Committee 209, 2008). In each of these models, some or all of the important factors, such as relative humidity and member geometry, are accounted for in determining the strain history due to a constant applied stress. By generating a good fit of the Kelvin model to each of these models, it is demonstrated that with proper calibration the model has the ability to account for these effects.

In order to conduct this calibration effectively, each of these models was analyzed under the same test scenario. The important properties of the concrete specimen to be used in the calibration of the model are shown in Table 4.1. The constants used in each of the five models can be determined from the data in Table 4.1.

Table 4.1 Concrete creep specimen properties

Mix Properties		
Coarse Aggregate	2010	pcy
Fine Aggregate	1235	pcy
Cement Content	705	pcy
Water Content	219	pcy
Air Content	1.5	%
Slump	3	in
Specific Weight	150	pcf
Specimen Properties		
Volume-to-Surface Area Ratio	2.95	in
Relative Humidity	0.7	
f_{cm28}	9.35	ksi
Loading Conditions		
Time of Loading (Moist Curing)	7	days
Load magnitude	1	ksi

This mix design was taken from the NCHRP Report 496 (Tadros and Al-Omaishi, 2003) and corresponds to a typical mix used by Concrete Technology Corporation in the manufacture of a W74G bridge girder. This girder is the one for which measured camber data is available for comparison with the complete camber prediction algorithm. That comparison is done in Chapter 6.

Important things to notice are; the temperature is assumed to be constant at room temperature for the duration of the analysis and the volume-to-surface ratio is assumed to be constant for all the concrete in the sample. The CEB model has the capability of considering temperature in creep prediction but when trying to apply that feature to the present loading regime, highly unrealistic answers resulted. For this reason, the effect of temperature was ignored for this calibration. The volume-to-surface ratio was taken to be constant over the cross-section, and given by the area of the cross-section divided by its perimeter. This approximation is

highly questionable; the thin web and large volumes of concrete at its junction with the bottom and top flanges suggest that these different regions have very different "effective" volume-to-surface ratios based on the distance from the center of mass of the region to the nearest free surface. Using these parameters, the Kelvin model was calibrated to fit each of the five creep models.

4.2.1 Elastic Element Calibration

For the elastic spring in the model, the time dependent function used was that specified by the model under consideration. As previously mentioned, the time dependent properties can be selected to follow any function as long as it increases monotonically with time. Each of the five existing models defines a method for determining the elastic modulus as a function of time based on specific constants and the 28 day parameters (E_{cm28} or f_{cm28}). Rather than calibrating a new function (i.e. the exponential function in Equation 4.1), the currently accepted functions were used directly.

Figure 4.4 shows a comparison of the development of the elastic modulus as predicted by the models above. Note that there is no model for the AASHTO code because the AASHTO code references the ACI 209R model (AASHTO, 2012).

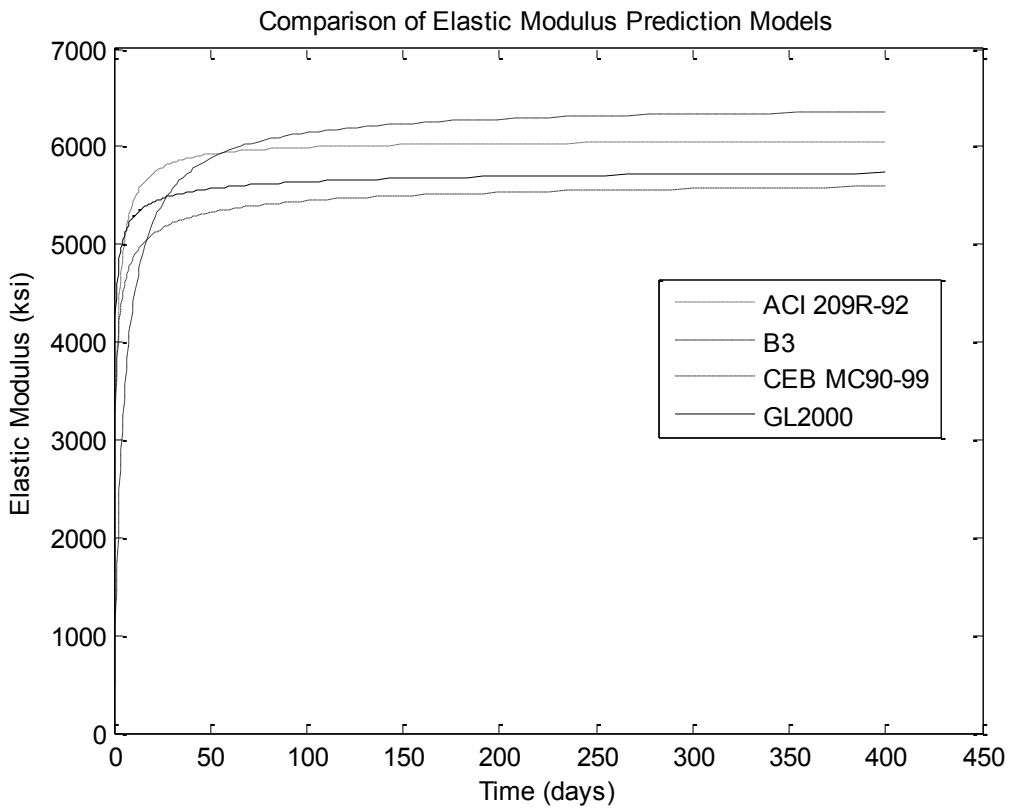

Figure 4.4 Elastic Modulus development models

Figure 4.4 shows that all of the models are reasonably close to each other. In the calibration of the Kelvin model to each of the different models, the corresponding elastic modulus parameter will be used to represent the spring only element. It should be noted to that in the NCHRP Report 496 (2003), the elastic modulus at release and at time of casting (190 days) were specified for the mix defined in Table 4.1. These values match the closest with the ACI 209 model for the elastic modulus.

In the elastic modulus predictions above, all the models use t_0 to be at the time of concrete casting and assume that the concrete is moist cured. In most girders, the concrete is heated and is then release after as little as 16 hours. Then, this time scale does not work as cleanly. The AASHTO LRFD Specifications (2012) state that the accelerated curing process can be approximated by assuming that at release, the girder has a maturity equivalent to seven days

of moist curing. Using this assumption the elastic modulus function above can be applied by using an offset in the time used for the girders concrete age.

In this thesis, pre-release conditions are included in the calculations. During that time, the concrete is hardening and the material parameters are changing, in ways that are unknown at this point. As an approximation of the concrete properties, a linear variation will be used, where all properties are zero at the time of bonding and increase linearly up to the time of release where properties have values equivalent to concrete with 7 days of moist curing. This approximation will be used for all the Kelvin unit properties derived.

4.2.2 Kelvin Element Calibration

Now that the elastic element has been calibrated/determined, the Kelvin unit properties must be calibrated. After some initial experimentation, it was determined that the use of two Kelvin elements in the rheological model provided sufficient flexibility to allow good fits to presently available data without creating excessive variables. It is possible that as more detailed data becomes available, additional Kelvin elements will be needed to ensure good accuracy.

The Kelvin element parameters were calibrated to the predicted creep histories provided by each of the five existing models. The history was generated by applying a 1-ksi stress at time of 7 days and holding this constant stress until 10^4 days (27.5 years). For each model the mix properties and test scenario were the same. The Kelvin unit spring and dashpot each need three variables to fully describe the time dependence. This means that for each Kelvin unit there are a total of six variables that can be modified, and for the two Kelvin elements used in this calibration, a total of 12 variables can be modified to achieve the best possible fit.

Figure 4.5 demonstrates the need to calibrate the Kelvin element over the entire time range considered. In this plot, the Kelvin model is calibrated against the AASHTO creep

prediction model using data for 500, 1000, and 10000 days. When projected out to 10000 days, each of these calibrations gives significantly different results.

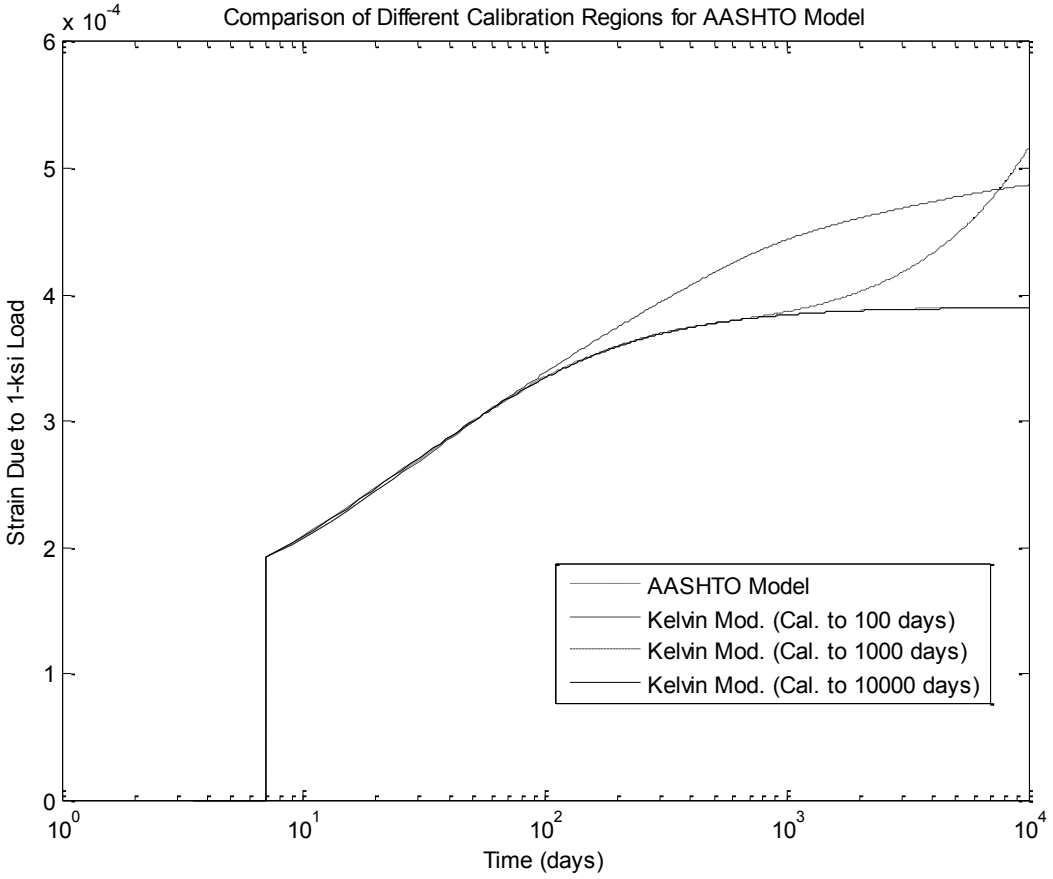

Figure 4.5 Demonstration of calibration range effects

From Figure 4.5 it can be seen that when using the Kelvin model, it is necessary to calibrate the Kelvin element parameters to the complete time period for which the model will be used.

The remaining four models were also calibrated separately and the results are shown in Figure 4.6. Again, for these calibrations the elastic modulus was calculated using the prescribed model associated with the creep prediction method.

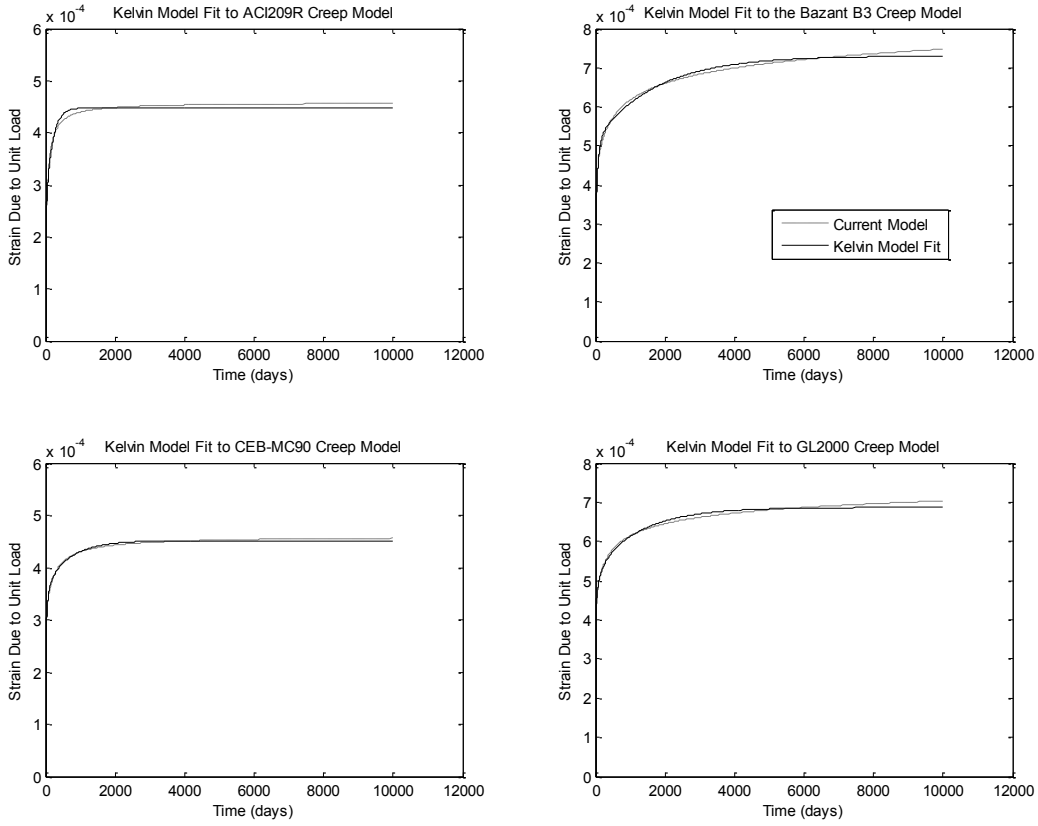

Figure 4.6 Kelvin model calibration to ACI209R, B3, CEB-MC90-99, and GL2000

This figure demonstrates the ability of the Kelvin model to replicate a variety of creep behaviors and indicates that with a complete calibration, the model parameters could be related to the important factors affecting creep discussed above.

The Kelvin parameters used in each of the model fits in Figure 4.5 and Figure 4.6 are shown below in Table 4.2. Note that for the AASHTO model the parameters are based on the calibration out to 10000 days.

Table 4.2 Calibrated Kelvin model parameters for various creep models

Fit Model	Element Type	Initial Value	Ratio of Infinite to Initial Value	Intrinsic Time Constant
AASHTO Model	*Spring Stiffness*	326.59	35.35	106.14
		9491.54	611.18	235.73
	Dash-Pot Viscosity	77709.83	220.63	1386.00
		2162413.37	49.70	211.20
ACI Model	*Spring Stiffness*	874.49	5.65	0.01
		3218.99	15.46	44.59
	Dash-Pot Viscosity	52019.56	16.81	3.47
		252391.62	1.21	10.32
B3 Model	*Spring Stiffness*	770.26	5.38	7.18
		691.87	7.21	157.88
	Dash-Pot Viscosity	32613.93	9.23	23.16
		3441172.19	2.52	0.00
CEB Model	*Spring Stiffness*	708.14	9.45	1.06
		3828.21	2.93	0.00
	Dash-Pot Viscosity	26085.05	19.04	37.44
		474764.36	16.58	0.75
GL2000 Model	*Spring Stiffness*	1070.92	5.03	7.81
		462.91	9.52	52.87
	Dash-Pot Viscosity	14220.62	3.04	24.72
		467885.06	12.39	305.40

From this table it is seen that the values describing the Kelvin element vary greatly. This is because there are an excess number of variables available to generate a fit. This results in a non-unique solution. A more thorough calibration program is needed to relate the Kelvin element parameters to the important factors and create a unique solution for determining the creep model parameters.

One of the key reasons for creating this rheological model is to create an incremental model in which the problem is not constrained to a constant stress test, but has the ability to predict creep recovery. For this reason the model needs to be calibrated against variable stress

data. Little such data is available, but one source is provided by creep recovery data. The end goal for the calibration of the model is to obtain a set of material parameters that can be used in the girder analysis where the concrete is the mix described in Table 4.1. Because this is a very specific girder mix, there is no available creep data and especially no creep recovery data. For this reason a different method is needed for calibrating creep recovery.

Yue and Taerwe conducted significant research in the area of creep recovery (1993). The method they developed for predicting the behavior of creep recovery provides a very useful model for verifying the ability of the Kelvin model to predict creep recovery. The formulation if this model uses a two-function approach, where one function is used to predict the increasing creep strain under constant strain loading and a second function is used to predict the creep recovery after some or all of the load was removed. Strain at a time *t* is computed as follows:

For $t_0 \leq t \leq t_1$, $$\varepsilon(t, t_0) = \sigma_0 \varphi(t, t_0) \tag{4.19}$$

The φ term in this function is the basic creep compliance function. In their research, Yue and Taerwe used the CEB MC90 model equations to generate this compliance function.

For $t \geq t_1$,

$$\varepsilon(t, t_0) = \sigma_0 \varphi(t_1, t_0) - \Delta\sigma_r[\varphi(t, t_0) - \varphi(t_1, t_0)] - \Delta\sigma_r \varphi_r(t, t_0, t_1) \tag{4.20}$$

where: σ_0 = initial applied stress

t_0 = time of initial loading

$\Delta\sigma_r$ = the reduction in stress that occurs

t_1 = the time at which the stress is released.

$\varphi(t, t_0)$ = the standard creep compliance function for a constant stress creep test

$\varphi_r(t, t_0, t_1)$ = the creep recovery compliance function developed and shown below.

The generic loading scenario for which this model was developed is shown in the Figure 4.7.

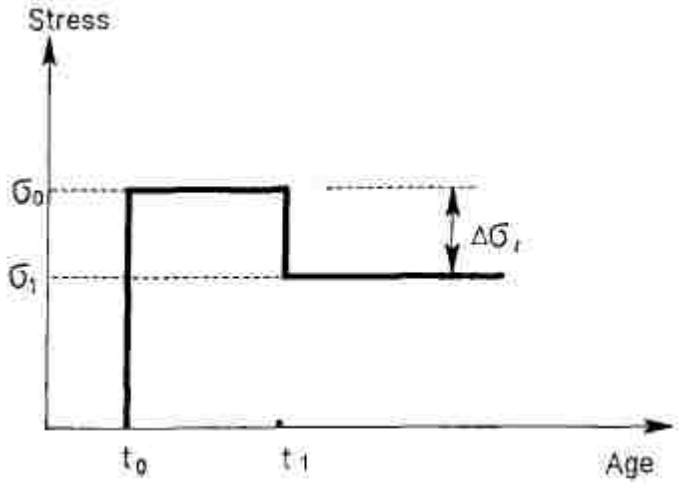

Figure 4.7 Creep recovery loading history. (Yue and Taerwe 1993)

The creep recovery compliance function, φ_r, was determined by Yue and Taerwe to be:

$$\varphi_r(t, t_0, t_1) = \frac{1}{E(t_1)} + \frac{1}{E_{28}}\left(\frac{0.35}{\alpha^{.5}}\right)\left(\frac{t - t_1}{t - t_1 + 300\alpha}\right)^{.24} \quad (4.21)$$

where: $\alpha = 1 - e^{-0.1[t_0 + 0.05(t_1 - t_0)]}$

Yue and Taerwe have shown that their creep two function creep recovery model does a remarkable job of matching several specific creep recovery tests (Yue and Taerwe 1993).

This general formulation shown in Equations 4.19 and 4.21, provides a very convenient method for predicting creep recovery behavior. The standard compliance function $\varphi(t, t_0)$ can be selected as any of the five models from above which all formulate creep in terms of a compliance function. By using the AASHTO model for standard creep (φ), and the creep recovery compliance function, (φ_r) from above, in Equation 4.20, a recovery model can be generated with which to calibrate the Kelvin model using two Kelvin units.

For calibration of the model, four separate tests were calibrated simultaneously. In each test an initial stress of 1ksi was applied after seven days of moist curing. The following four variations on this loading scenario were included:

- The first test was completed as a constant creep test with no load release. This is the same case as analyzed above.
- In the second test, 75% of the load was removed 1 day after loading had occurred (8 days after casting).
- In the third test 50% of the load was removed 7 days after loading (14 days after casting).
- In the fourth test 25% of the load was removed 93 days after loading (100 days after casting).

Each of these tests was carried out to 10000 days. The parameters were optimized to create the best fit to all four test cases simultaneously. When computing the error in the creep recovery curves, only the portion of the test after partial stress release was considered. This is because the curve up to the release is the same as the first load case.

Figure 4.8 below shows each of the four load cases with the Kelvin model calibrated to the predicted result using Equation 4.20 with a combination of the AASHTO model of basic creep and the Yue/Taerwe model for creep recovery.

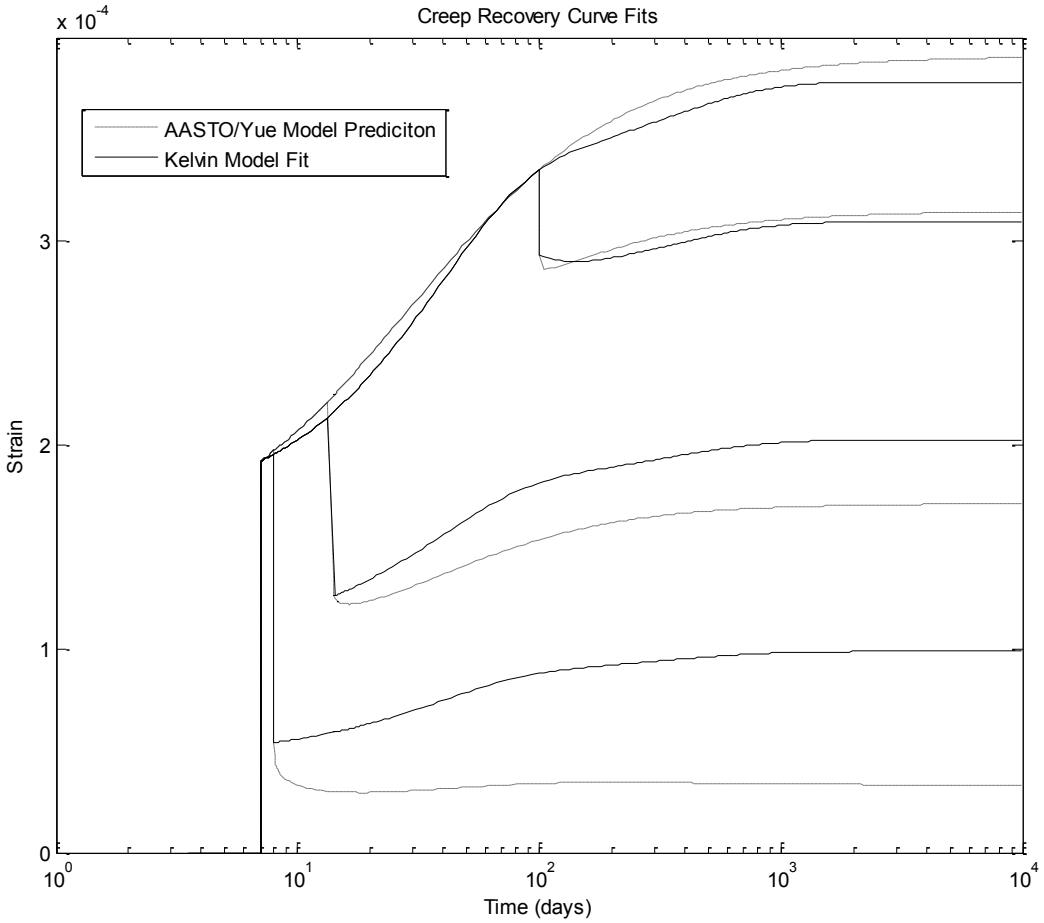

Figure 4.8 Calibration of creep recovery

The Kelvin model provides responses that follow the general trends of the Yu and Taerwe predicted behavior, with the best correlation occurring when the sudden stress drop and consequent creep recovery are the smallest. The resulting error is an average of 5% with respect to the final predicted strain in the constant stress test. This error is the average error from all of the data points in the calibration. It is worth noting that the data being used for comparison in Figure 4.8 is response predicted by Yu and Taerwe's model rather than actual test data. However, their model showed a good fit with measured data in most of their tests.

The resulting Kelvin unit parameters are shown in Table 4.3 below.

Table 4.3 Calibrated creep recovery Kelvin unit parameters

Element Type	Initial Value	Ratio of Infinite to Initial Value	Intrinsic Time Constant
Spring Stiffness	1007.54	26.64	136.02
	6492.24	3.23	1.66
Dash-Pot Viscosity	272345.14	9.33	1058.12
	1029774.47	6.73	4.43E-09

This table shows the Kelvin element parameters that will be used in the following girder camber analysis. These parameters were selected because they not only match the constant stress creep results predicted by the AASHTO, but also provide a reasonable approximation for the effects of creep recovery.

CHAPTER 5 PRESTRESSING STRAND CONSTITUTIVE MODEL

Behavior of the prestressing strand is the second important component of the long-term behavior of prestressed concrete girders. Under high stress, prestressing strand relaxes and the stress decreases over time without a reduction in strain. The lower strand stress leads to lower concrete stress and a corresponding change in camber. The relaxation of the strands and the creep and shrinkage of the concrete are the causes of time-dependent changes in camber. In modern girders, the effect of prestress relaxation is mitigated partially by the improved low-relaxation strand currently available.

For the purpose of this analysis a comprehensive constitutive model is necessary to accommodate several important properties of the relaxation behavior. The following criteria were used in selecting a steel relaxation model:

- The model must be incremental. In an incremental model the stress can be computed uniquely from the state variables at the current time. No time-dependent history needs to be stored.
- The model must be able to accommodate arbitrary changes in stress or strain during the load history, (i.e. load histories more complex than just a constant strain relaxation test or a constant stress creep test). This feature is critical for incorporating the interaction between the creep of the concrete and the relaxation of the strand.
- The model must reflect the experimentally-determined behaviors of strand relaxation such as the effect of temperature on relaxation rates and the short-term and long-term relaxation behaviors seen in typical strand relaxation tests. The temperature effects on the

strand are especially important to the current analysis algorithm in which pre-release behavior is analyzed. During the fabrication process the strands are exposed to significant temperature ranges which could have a significant impact on their relaxation.

The CEB (1990) and Magura (1964) models are the ones most commonly used for predicting relaxation in prestressing strands. Although these models give plausible results for constant strain tests performed on various strand types, they do not satisfy the criteria specified above. The CEB model is formulated as follows:

$$\frac{\sigma_0 - \sigma(t)}{\sigma_0} = \rho_1 \left(\frac{t}{\lambda_1}\right)^k \tag{5.1}$$

where: t = time since the strand was stressed

$\sigma(t)$ = axial stress in the strand at any time t

σ_0 = initial stress in the strand

λ_1 = time constant of 1000 hours

ρ_1 = constant specified in CEB related to the amount of initial stress in the strand

k = constant specified in CEB related to material type considered (ie. strands, wires, improved strands, or bars).

The model proposed by Magura *et al.* is:

$$\sigma(t) = \sigma_0 \left[1 - \frac{\log(t)}{K}\left(\frac{\sigma_0}{\sigma_y} - .55\right)\right] \tag{5.2}$$

where: K = 45 for low relaxation strands,

t = time in hours since strand was stressed,

σ_0 = the initial stress in the strand, and

σ_y = the yield stress of the strand.

Equation 5.2 is valid only for $t \geq 1$ hour.

Figure 5.1 shows the stress responses predicted by these two models to constant imposed strain. In the simulation, low-relaxation strand is stressed to an initial stress of 202.5 ksi at *t=0.*

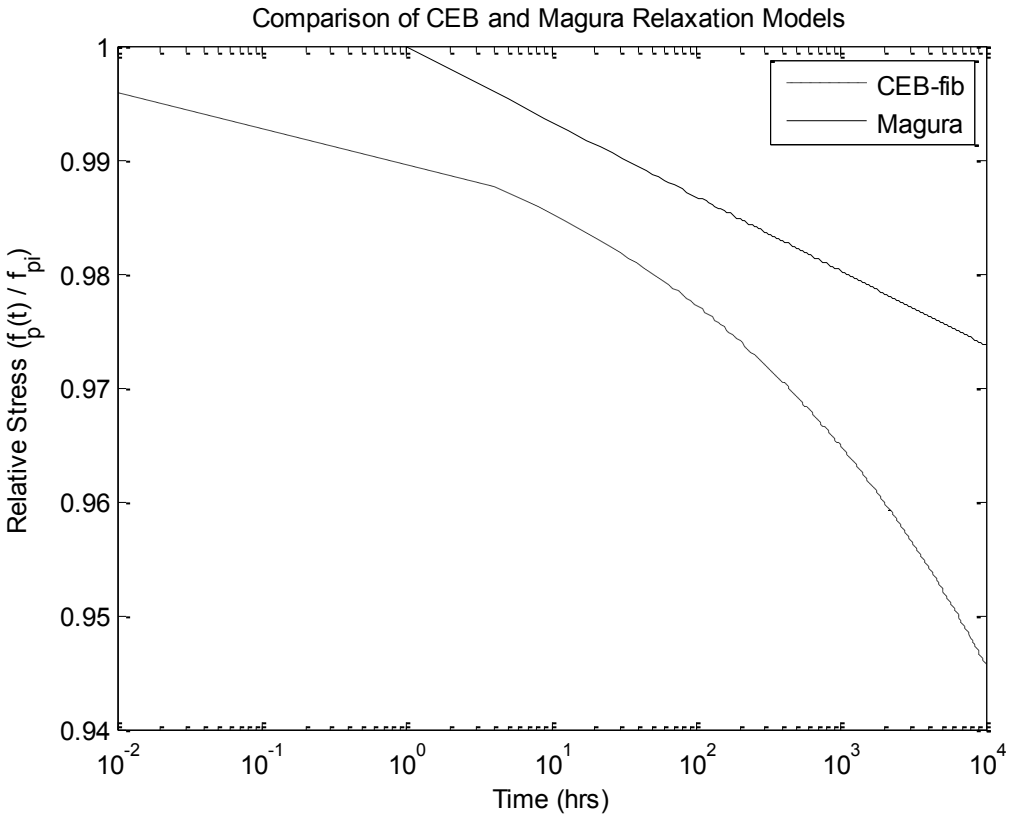

Figure 5.1 Comparison of CEB and Magura relaxation models

In this test a ρ_1 value of 3.5% was used for the "improved" strand type (Class 2, taken here to be equivalent to US "low-relaxation: strand)) and a jacking stress of 75% of ultimate strength. The value of *k* was 0.19 for class 2 strands specified by CEB. The material parameter *K* in the Magura model was set to 45 for low-relaxation strand.

The stress histories predicted by the models differ significantly. For low-relaxation strands it can be seen that the overall effect of relaxation is not great, with typical losses of 2-3% at 1000 hours, but the stress histories predicted by the models nonetheless differ significantly. The stress loss due to relaxation is much less significant than that due concrete creep, which helps to

mitigate effect of the differences between the models. Each model has advantages and drawbacks.

- The Magura model is not valid for times less than *t=1* hour. This results in poor estimation of the relaxation behavior during short times.
- The Magura model exhibits good long-term behavior and asymptotically approaches a stress limit of $0.55f_{py}$ rather than relaxing to infinite stress loss.
    - The CEB model continues to relax without bound so that at very long times (i.e. $t > \lambda\rho^{1/k}$) the stress in the strand becomes compressive. Although the time frame in which this occurs is outside the reasonable lifetime of the strand, it is an unrealistic result.
- The strength of the CEB model lies in its ability to predict the relaxation in the very short-term. This benefit comes with the slight drawback that the slope of the relaxation curve is infinite at time *t=0*. This has negative implications in the incremental formulation as will be discussed later in this chapter.

The early stages of the relaxation curve are quite important for this algorithm because of the inclusion of pre-release effects. Before the concrete hardens, the strands are allowed to relax and this loss is an important contributor to the proper prediction of the camber history.

The model that was selected was proposed by Bazant and Yu (2012), and incorporates the best features of both models in an incremental formulation. The sections below will outline the formulation of this visco-plastic formulation which leads to a versatile model that exhibits good relaxation behavior in both the short and long-term time regions.

5.1 Model Formulation

The model used here is an incremental version developed by Bazant and Yu (2013) of the CEB fixed-stress model described above. The modifications introduced by Bazant and Yu include:

- The model was formulated in incremental terms.
- This formulation allows it to accept variable strain loading.
- A threshold was added that eliminates relaxation when the stress falls below a user-defined value (similar to the $0.55f_{py}$ in the Magura model).
- The model was made temperature sensitive, to reflect that fact that relaxation typically occurs faster at high temperatures.

Each of these features is described in the following sections.

5.1.1 Incremental formulation and variable stress capability

An incremental relaxation function describes the stress at the end of each time step based on the length of the time step and the time derivative during the step. Equation 5.1 is reformulated as:

$$\sigma(t) = \sigma_0 \left(1 - \rho_1 \left(\frac{t}{\lambda_1}\right)^k\right) \tag{5.3}$$

Taking the derivative of this function with respect to time gives

$$\dot{\sigma} = -\frac{\sigma_0 \rho_1 k}{\lambda_1} \left(\frac{t}{\lambda_1}\right)^{k-1} \tag{5.4}$$

This function is in incremental form but is not a valid constitutive law because it explicitly contains time, *t.* This is remedied by solving Equation 5.3 in for the term $\frac{t}{\lambda_1}$,

$$\frac{t}{\lambda_1} = \left(\frac{\sigma_0 - \sigma(t)}{\rho_1 \sigma_0}\right)^{1/k} \tag{5.5}$$

Replacing $\frac{t}{\lambda}$ in Equation 5.4 and doing some rearranging gives,

$$\dot{\sigma} = -\frac{\rho_1 k}{\lambda_1}\sigma_0 \left(\frac{\rho_1}{1-{}^{\sigma(t)}/_{\sigma_0}}\right)^{\frac{1}{k}-1} \tag{5.6}$$

Equation 5.6 is a nonlinear ordinary differential equation that describes the change in stress with time, assuming all other state variables, including strain, remain constant. In it, the initial stress, σ_0, is defined by

$$\sigma_0 = F(\varepsilon_0)$$

where ε_0 is the applied (constant) strain, and $F(\varepsilon)$ is the instantaneous constitutive law.

Equation 5.6 is still only valid for a constant applied strain. For variable strain loading, the change in stress can be broken into independent components due to change in time and strain.

$$d\sigma = \frac{\partial \sigma}{\partial \epsilon} d\epsilon + \frac{\partial \sigma}{\partial t} dt \tag{5.7}$$

The principle is illustrated in Figure 5.2.

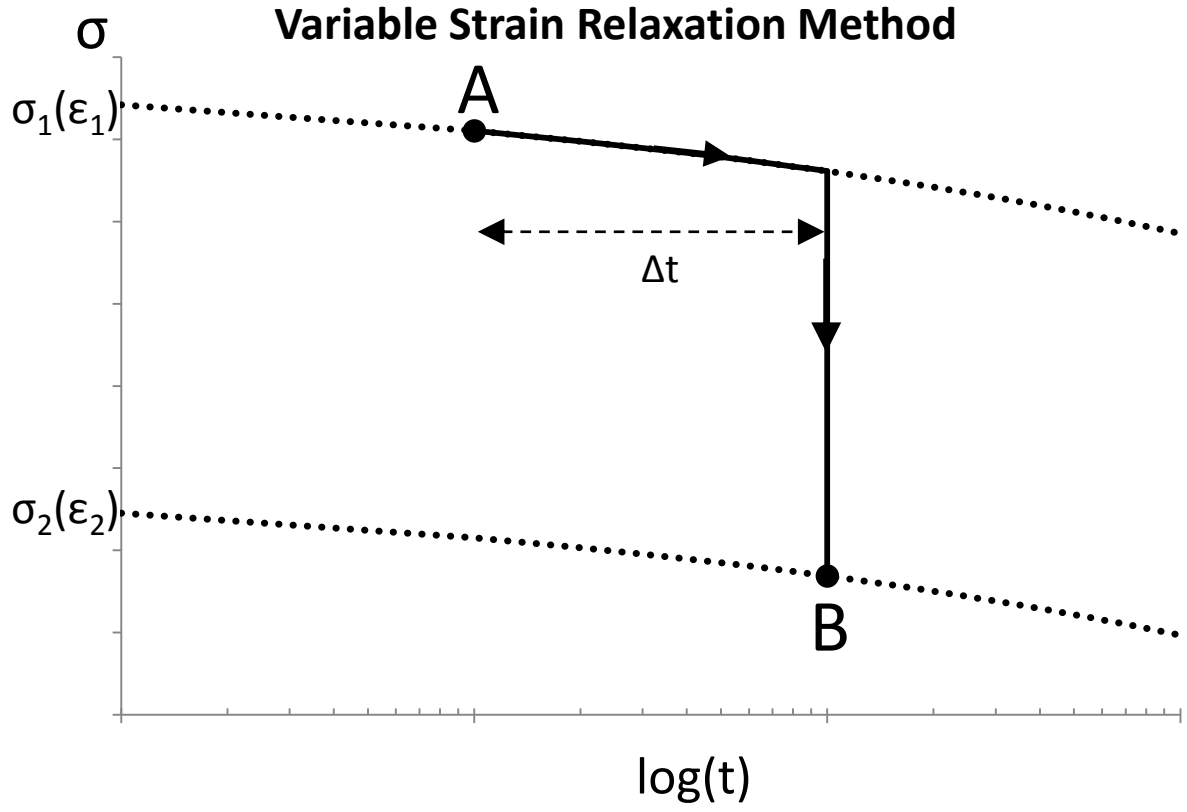

Figure 5.2 Variable strain time step relaxation method

The first term represents the instantaneous elastic change in stress due to a change in strain, and is shown in the figure as a jump (in zero time) from the ε_1 strain curve to the ε_2 strain curve. If the instantaneous stress-strain curve for the strand is given by

$$\sigma = F(\varepsilon_{mech}) \tag{5.8}$$

then the derivative is

$$\frac{\partial \sigma}{\partial \epsilon_{mech}} = \frac{\partial F(\epsilon_{mech})}{\partial \epsilon_{mech}} \tag{5.9}$$

In the special but common case of elastic behavior, $F(\varepsilon_{mech}) = E_p \varepsilon_{mech}$, and

$$\frac{\partial \sigma}{\partial \epsilon_{mech}} = E_p \tag{5.10}$$

This is invariably the case in pre-tensioned girders.

The second term in Equation 5.7 represents the visco-elastic change in stress that would occur during the time step if the strain were to remain constant. The question of what path it will follow is open. For a constant strain loading, the stress by definition decays along the path defied by Equation 5.3 for the constant strain that corresponds to the initial stress, σ_0, given by the $\varepsilon_{mech,0}$that satisfies

$$\sigma_0 = F\left(\varepsilon_{mech,0}\right) \tag{5.11}$$

and is characterized in the figure as movement along the constant ε_1 curve. It is assumed here that, during any time step, the visco-elastic stress change will follow the constant strain curve for the mechanical strain that exists at the start of the time step. As pointed out by Bazant and Yu (2012), this behavior is consistent with visco-plastic theory. The same principle was also used by Hernandez and Gamble (1975) to allow the use of the Magura (1964) model with strains that changed over time. The result is illustrated in Figure 5.2, in which the strain at the end of the previous time step ends at the point A, with the strain value ε_1, and the visco-elastic stress decay then follows the constant strain curve for $\varepsilon = \varepsilon_1$, for which the stress at time zero was $\sigma_0 = F(\varepsilon_1)$

The total rate of change of stress with time is then

$$\frac{d\sigma}{dt} = \frac{\partial F(\epsilon_{mech})}{\partial \epsilon_{mech}} \frac{d\epsilon_{mech}}{dt} - \frac{\rho_1 k}{\lambda} F(\epsilon_{mech}) \left(\frac{\rho_1}{1 - {\sigma(t)}/{F(\epsilon_{mech})}} \right)^{\frac{1}{k}-1} \tag{5.12}$$

Note that, in developing Equation 5.12 from Equation 5.6 σ_0 has been replaced with $F(\varepsilon_{mech})$

Equation 5.10 gives stress rate as a function of strain. If strain rate is needed as a function of strain and stress, Equation 5.12 can be inverted to give

$$\dot{\varepsilon_{mech}} = \frac{\dot{\sigma}}{E} + \frac{\rho_1 k}{E\lambda}(E\varepsilon_{mech})\left(\frac{\rho_1}{1-\sigma/E\varepsilon_{mech}}\right)^{\frac{1}{k}-1} \quad (5.13)$$

where: E = elastic modulus

ϵ_{mech} = current strain in the strand

σ = current stress in the strand

This formulation provides a constitutive model that links the stress, strain, stress rate and strain rate at any given time and does not require knowledge of the previous history. If any three of the quantities are known, the fourth can be computed. This model can be easily formulated numerically to give finite differences in strain. The simplest approach is to use the Forward Euler integration scheme, in which the tangent values at the beginning of the time step are used to predict the ending value.

$$\Delta\varepsilon_{mech} = \frac{\Delta\sigma}{E} + \left[\frac{\rho_1 k}{E\lambda}(E\varepsilon_{mech})\left(\frac{\rho_1}{1-\sigma/E\varepsilon_{mech}}\right)^{\frac{1}{k}-1}\right]\Delta t \quad (5.14)$$

If this method is used, a numerical problem results at the time *t=0*. When the strand has just been jacked, the term $\left(1-\sigma/E\varepsilon\right)$, is equal to zero and the solution to Equation 5.13 becomes undefined. The solution adopted for the purposes of this algorithm was to use a very short time step at *t=0,* ignore the change in strain during the interval, and use Equation 5.3 to determine the stress at the end of the time step.

5.1.2 Incorporation of a lower threshold stress

The formulation above allows for variable strain, but still contains the problem of infinite stress loss due to relaxation that was present in the initial CEB-*fib* formulation. It has been experimentally determined that relaxation stops if the stress drops below γf_{py}, where γ is

typically taken to be 0.55 but varies slightly with steel type. In order to combat this Bazant and Yu propose the following constant strain formulation:

$$\sigma(t) = \min\left(\gamma f_{py}, \sigma_0\right) + \langle \sigma_0 - \gamma f_{py} \rangle \left[1 + \frac{\rho}{c}\left(\frac{t}{\lambda}\right)^k\right]^{-c} \tag{5.15}$$

where: γ = the relaxation threshold usually taken as 0.55

k = material constant to be calibrated

c = material constant to be calibrated

ρ = material constant to be calibrated

$\langle\ \rangle$ = are Macauley brackets defined as $\langle x \rangle = \max(x, 0)$

This model is a constant strain formulation that approaches the relaxation threshold of γf_{py} for $t \rightarrow \infty$, and asymptotically approaches the CEB-*fib* formula for short times. This model is not a complete constitutive formulation for the same reasons that Equation 5.3 was not sufficient. Following the same procedure used to develop Equation 5.14, Bazant and Yu propose the following constitutive formulation:

$$\dot{\varepsilon} = \frac{\dot{\sigma}}{E} + \frac{\langle E\varepsilon_{mech} - \gamma f_{py} \rangle}{E} \frac{k\rho^{1/k} c^{(1-1/k)}}{\lambda \varsigma^{(1+\frac{1}{c})}} \left(\varsigma^{1/c} - 1\right)^{(1-1/k)} \tag{5.16}$$

where: $$\varsigma = \frac{E\varepsilon_{mech} - \gamma f_{py}}{\sigma - \gamma f_{py}} \tag{5.17}$$

$$\rho = \rho_0 e^{h\xi} \tag{5.18}$$

k,c,h,ρ_0 = material constants to be calibrated.

$\sigma, \varepsilon_{mech}$ = current stress and mechanical strain respectively

For current low-relaxation strands, Bazant and Yu recommend using $h=0$, which reduces Equation 5.17 to $\rho = \rho_0$, where ρ will be used for the rest of this thesis. This reduces the variables that need to be calibrated to k, c, and ρ.

Equation 5.16 can be written in the Forward Euler integration scheme as follows:

$$\Delta\varepsilon_{mech} = \frac{\Delta\sigma}{E} + \left[\frac{\langle E\varepsilon_{mech} - \gamma f_{py}\rangle}{E}\frac{k\rho^{1/kc\left(1-1/k\right)}}{\lambda\varsigma^{\left(1+1/c\right)}}\left(\varsigma^{1/c} - 1\right)^{\left(1-1/k\right)}\right]\Delta t \qquad (5.19)$$

This formulation is an incremental constitutive model that converges to Equation 5.15 for $\varepsilon_{mech} = constant$ and sufficiently short time steps Δt. Note that the term ς, represents the difference between the calculated stress due to the instantaneous stress-strain relationship and the actual stress existing in the strand including all previous relaxation. This term leads to the same numerical problems discussed previously at zero time when $E\varepsilon$ is equal to σ, and $\varsigma = 1$. In this case the time rate of relaxation becomes infinite and the forward finite difference is undefined. Again this was solved by choosing a very short time-step, ignoring the change in strain during the interval, and applying Equation 5.15 to determine the stress at the end of the interval.

5.1.3 Modification for Relaxation at Elevated Temperature

Steel relaxes faster at high temperature. That behavior is reflected in the model by modifying the time scale based on the temperature of the strand. Equation 5.16 represents the slope of the strain versus time relationship at a certain time in the history where stress and mechanical strain are known. To compute the strain at the end of the next time step, it is necessary to multiply by a step size. It is here that the temperature effect is applied:

$$\Delta t = A_T \Delta\xi \qquad (5.20)$$

where:
$$A_T = e^{\left[\frac{Q}{k_B}\left(\frac{1}{T_0} - \frac{1}{T(t)}\right)\right]} \qquad (5.21)$$

Here $\Delta\xi$ represents the real increment in time and the term Δt is a fictitious time step length used to compute the change in stress and strain. In Equation 5.21

Q = the activation energy,

k_B = Boltzmann constant, and

$\frac{Q}{k_B} \approx 14{,}600°K$.

T_0 = the reference temperature, 293°K, and

T(t) = the current temperature of the strand expressed in °K.

With the constitutive model developed, it is now possible to discuss the intricacies of implementing this into the algorithm. In the analysis formulation described previously it is necessary to be able to compute the change in stress, based on an increment in strain, or vice versa. Equation 5.16 can be derived in the incremental form to determine the stress at the end of the time step due to an increment in strain.

$$\Delta\sigma = E\Delta\varepsilon_{mech} - \left[\langle E\varepsilon_{mech} - \gamma f_{py}\rangle \frac{k\rho^{\frac{1}{k}} c^{\left(1-\frac{1}{k}\right)}}{\lambda\varsigma^{\left(1+\frac{1}{c}\right)}} \left(\varsigma^{\frac{1}{c}} - 1\right)^{\left(1-\frac{1}{k}\right)}\right]\Delta t \qquad (5.22)$$

Similarly the change in strain due to an increment in stress can be determined as:

$$\Delta\varepsilon_{mech} = \frac{\Delta\sigma}{E} + \left[\frac{\langle E\varepsilon_{mech} - \gamma f_{py}\rangle}{E} \frac{k\rho^{1/k} c^{\left(1-\frac{1}{k}\right)}}{\lambda\varsigma^{\left(1+\frac{1}{c}\right)}} \left(\varsigma^{1/c} - 1\right)^{\left(1-\frac{1}{k}\right)}\right]\Delta t \qquad (5.23)$$

These two versions of the constitutive model can be written into a numerical analysis routine. In each of these formulations the value at the end of the time-step can be computed by adding the increment to the value at the beginning of the time-step.

5.2 Numerical Implementation

The incremental version of the model was implemented in a numerical procedure to predict increments in stress caused by increments in strain and time. Several special features were added to improve the running of the model. They are:

- A special procedure was introduced for the first time step to overcome the fact that $d\sigma/dt$ is infinite there.
- Intermediate steps are added to prevent excessive time step size from stopping the entire analysis.
- An iterative central difference method is used to improve the time step accuracy.

In order to illustrate these details a sample constant strain relaxation test is shown in Figure 5.3.

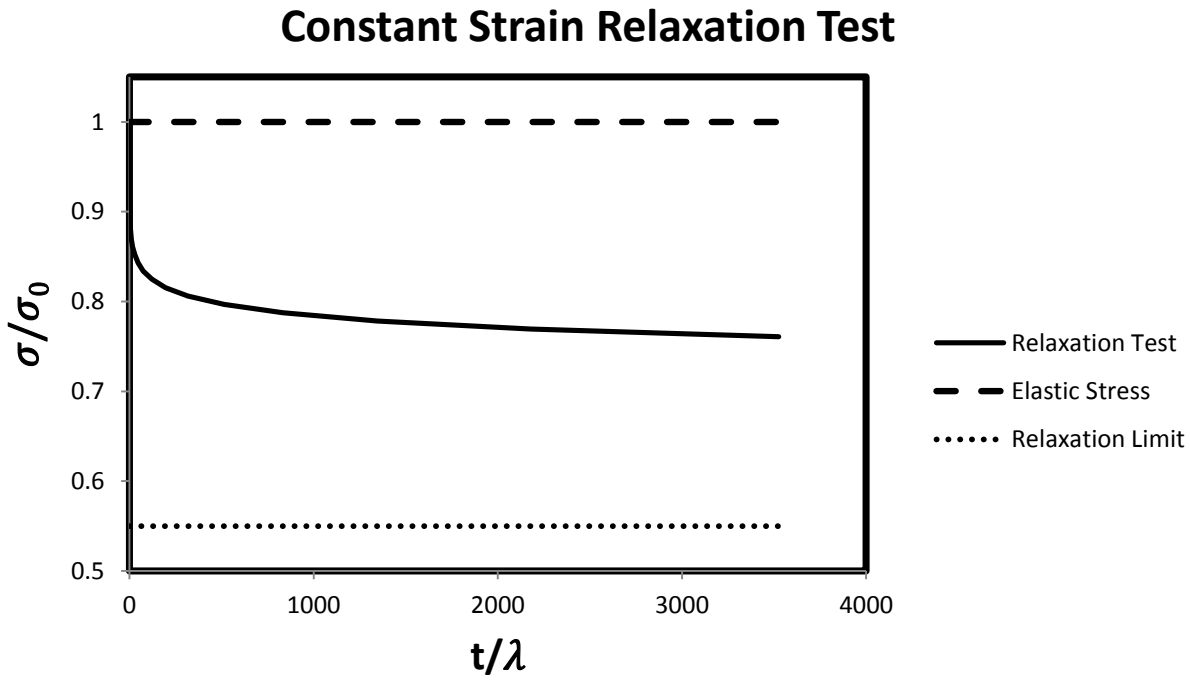

Figure 5.3 Constant strain relaxation test

Figure 5.3 shows the predicted stress history during a relaxation test at constant strain. The dashed line represents the stress due to the applied strain, $\sigma = E\varepsilon$, and the dotted line indicates the relaxation threshold The solid line is the time dependent stress for a constant strain relaxation test computed using the Equation 5.15.

5.2.1 Starting procedure

The first special feature arises from the numerical formulation in Equation 5.16 where the ς term is equal to 1 and results in an infinite slope for the relaxation rate. This infinite slope can be seen in Figure 5.3. When $\varsigma = 1$, the visco-plastic portion of Equation 5.16 is infinite and therefore cannot be used. To combat this problem, the strain in the first time step is assumed to be constant and Equation 5.15 is used to evaluate the stress at the end of the time step. The first time step should be small to minimize the error introduced by this approximation.

For the algorithm described in Section 1.2, this first time interval occurs during the jacking process during which the strain is changing as the strand is stressed to its specified initial stress. In the first time step, the strand is stressed up to the relaxation threshold, γf_{py}. This is an entirely linear step that requires no iteration as there is no relaxation occurring. In the second time step, relaxation begins and the stress at the end of the interval is specified by a jacking sequence. As described in the algorithm formulation, the strain required to reach the specified ending stress is determined through iteration. When using Equation 5.16 for the second time step, the initial stress value should be computed as:

$$\sigma = \sigma_i + \frac{1}{2}\mathrm{E}\Delta\varepsilon \tag{5.24}$$

where: σ_i = is the stress at the start of the time step from the previous step

$\Delta\varepsilon$ = the change in strain calculated from the previous iteration

This approach considers the relaxation that occurs due to the average stress during the time step. This is consistent with the forward finite difference approach used above in which the relaxation occurs at the beginning stress and strain and the change in mechanical strain is not considered. Keeping the time and target stress increments small minimizes the error from this approximation and gives a method for jump-starting the incremental approach in Equation 5.16.

5.2.2 Stress Overshoot

The second feature is also related to the infinite slope at the beginning of the relaxation curve. If the time step is too large, the resulting stress from Equation 5.22 may fall below γf_{py}. Note that this could happen at any time when the selected interval is too large but is more likely to occur in early time steps when the time rate of change is highest. This result is not acceptable for two reasons. First, tests show that strand does not relax below the threshold. Second, and more importantly, in a case where this occurs the next time step cannot be solved because $\varsigma < 1$, and the solution is undefined. To prevent this, the algorithm for applying Equation 5.22 includes the ability to break a time step into intermediate steps should the initial time step size result in a stress below γf_{py}. This is done by increasing the number intermediate steps used. Figure 5.4 illustrates how an excessively long time step is analyzed is broken into intermediate steps for a more stable performance.

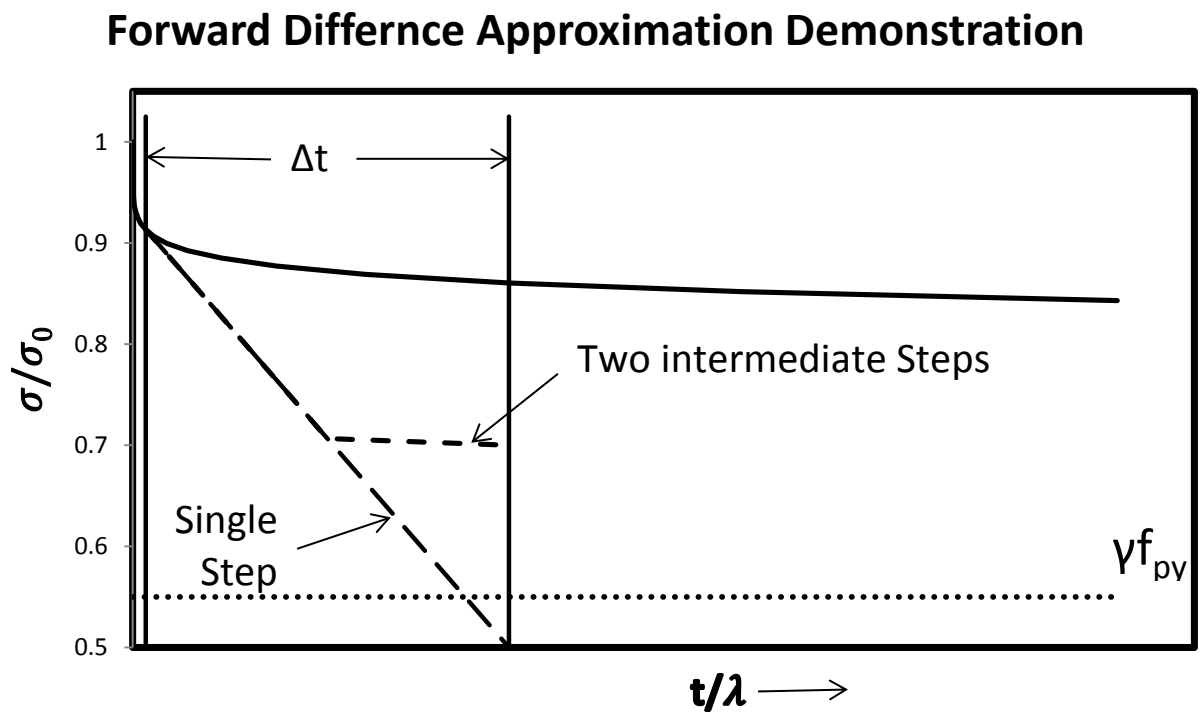

Figure 5.4 Forward difference approximation demonstration

As shown in Figure 5.4, a single long time step from t_i to $(ti + \Delta t)$ leads to a predicted stress below the relaxation threshold. Breaking the time step into two or more smaller ones improves the accuracy of the predicted stress and prevents it from incorrectly falling below the threshold. It is important to realize that this approach does not mean the accuracy for the time step is good, but it does ensure that the analysis will continue for the future time steps without becoming undefined. Three important notes should be made:

- First, the intermediate time steps are added to the numerical analysis of the strand constitutive model only. The overall time step for the algorithm remains the constant.
- This numerical fix is formulated such that it only takes effect if the strand relaxation causes a stress below the threshold at the end of the time step. Should an elastic stress reduction (or combination of elastic and relaxation losses) cause a stress below the

threshold, the time step is not divided up to try reduce this stress loss unless the relaxation alone causes an overshoot.

- The error between the final prediction and the true stress (shown in by a solid line in the figure) is still significant. The user should still select step size carefully to ensure good accuracy. It is recommended that time steps be kept below 0.1 hours for the first 24 hours of analysis and grow slowly beyond this time. Note that the user must consider the increase in fictitious time that may occur due to elevated temperatures (see Equation 5.21) when selecting these steps.

5.2.3 Accuracy Improvement

The final modification made is to improve the accuracy of the prediction. Equations 5.22 and 5.23 use a forward finite difference approach for predicting values at the end of the time step. In a classical forward finite difference approach, the values known at the beginning of the step are used to predict values at the end of the step. To improve the accuracy of this approximation, rather than using initial values, the average value is used for all of the specified increments except time (i.e. temperature and stress or strain). This takes on the following forms:

- For Equation 5.22, the value of σ, which represents the current stress in the strand, can be improved to be $\sigma = \sigma_i + \frac{1}{2} E \Delta\varepsilon_{mech}$.
- For Equation 5.23, the value of ε_{mech}, which represents the current strain in the strand, can be improved to $\varepsilon_{mech} = \varepsilon_{mech,i} + \frac{1}{2}\frac{\Delta\sigma}{E}$.
- And the average temperature is used to modify the time step size for temperature effects.

where $\Delta\varepsilon$, $\Delta\sigma$ and ΔT are all specified increments occurring over the time-step. Each of these modifications is used in the numerical procedure to improve the accuracy of the forward finite difference by including information about the changes that occur during the time step.

The essential feature of this formulation is its incremental nature. Equations 5.22 and 5.23 are used to compute the changes during the time increment, and the only variables needed to do so are the stress and strain from the previously converged time step and the increment in either stress or strain, depending on the formulation being used. No previous response history needs be stored. This form of the constitutive model is essential for the architecture of the overall analysis formulation described in Chapter 3.

5.3 Model Calibration

Values are needed for the material constants in the relaxation model. Two approaches are possible. In the first, the relaxation model could be calibrated against relaxation test data, while in the second; the constants could be determined by calibrating the entire girder model against measured girder cambers. The former is preferable, because it eliminates the possibility that an error in the relaxation model is (incorrectly) compensated for by changes in the concrete model. In this section, the material parameters will be optimized through the comparison to measured stress losses under constant strain relaxation tests.

Bazant and Yu (2013) used data collected from relaxation tests performed on older "stress-relieved" strands. This data is not consistent with the behavior of modern, low-relaxation (Low-Lax) strands. The production process for today's strands includes a stabilization process in which strands are held at high stress under elevated temperatures to reduce the amount of relaxation that occurs in the field. For this reason, the results of Bazant and Yu's (2013) calibration are not valid for use in the current model.

The model was therefore calibrated against the data available that is relevant to low-relaxation strands.

In calibrating the models, the material constants *k, c, h,* and ρ are available to be modified. For low-relaxation strand, Bazant and Yu (2013) recommend that *h* be set to zero. This leaves three parameters available for calibration. The following sets of data are used to determine the material constants:

- A set of three relaxation tests shown in Naaman (2004), taken from tests conducted on stabilized wire by Somerset Wire and Strands in England. Each test was carried out at a different level of initial stress. The data therefore provides an opportunity to determine the model's ability to model different levels of initial stress. The wire is believed to represent the material subsequently spun into 7-wire strand.
- A single test on low-relaxation 7-wire strand provided by Sumiden Wire Products Corporation. This data is valuable because it was conducted recently on the low-lax strands used by many west coast precasters. However the test duration was quite short.
- Tests carried out on stabilized wire by Somerset Wire and Strands in England at different temperatures.
- Finally, the model predictions were compared with those of the Magura et al. (1964) model. The comparison is not directly against measured data, but that model was derived from a range of tests and is widely used today. The strands tested were Stress-Relieved rather than Low-Relaxation, but the original constants in the model were subsequently adjusted to match the response of Low relaxation strands.

In each calibration, the predicted stress was computed using the present model, and the sum of the squared errors was taken as the cost function to be minimized. The optimization was

done allowing all three parameters to vary at once, using routines from the Matlab suite. The three separate calibrations described above lead to the material parameters shown in Table 5.1:

Table 5.1. Optimum material parameters for calibration scenarios

Calibrated To…	ρ	c	k
Naaman's f_{pu} Dependence Data	0.0344	0.1988	0.277
Sumiden Relaxation Test	0.0471	0.2341	0.0771
Magura Model	0.0563	2.5376	0.1743

As is shown in Table 5.1, the variation in these material parameters can be significant. For this reason, no attempt will be made in this thesis to fully calibrate the model to many data sets.

The first calibration was completed against the data shown in Figure 5.5, which shows the relaxation data for three separate tests carried out at 60%, 70%, and 80% of the ultimate strength of the strand. Each test was made at 20°C. (The data were digitized from the published figure using AutoCAD.)

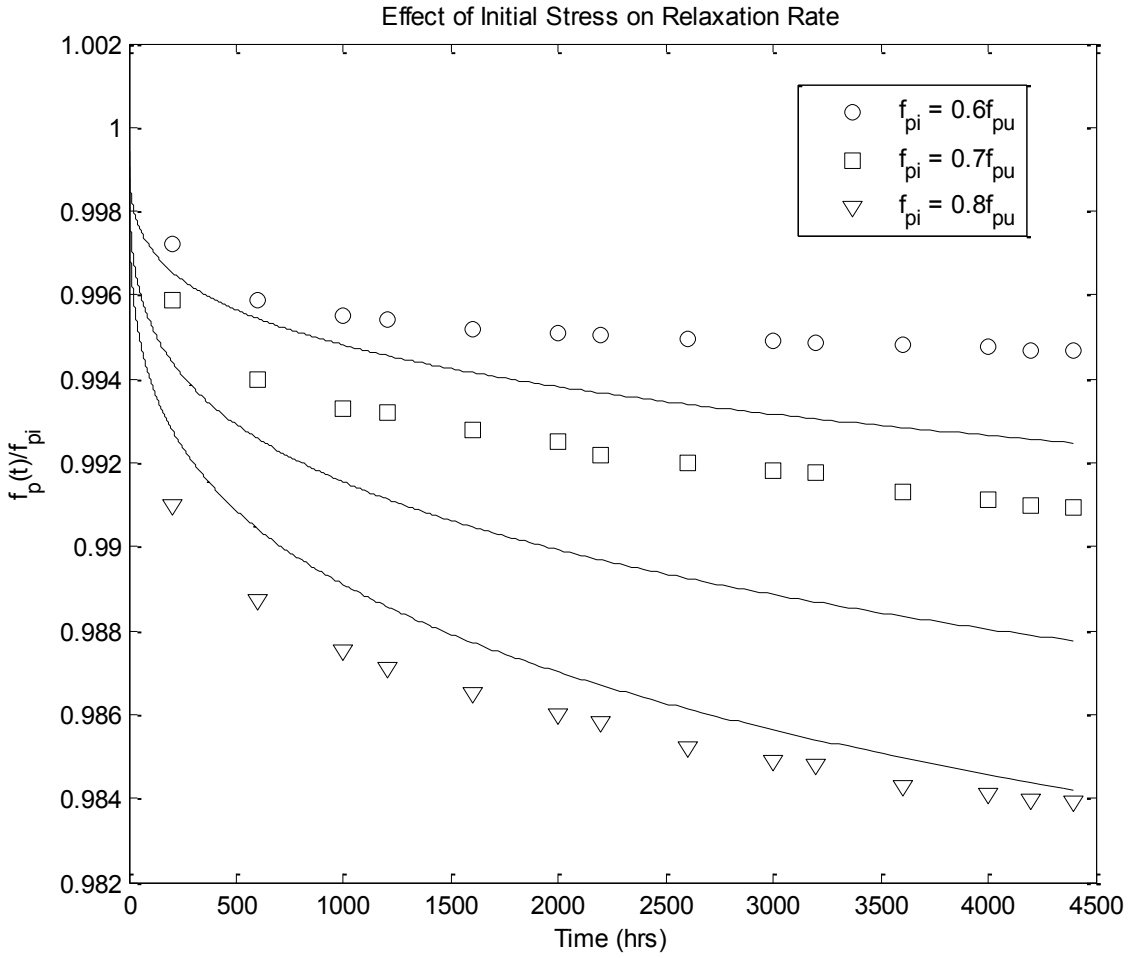

Figure 5.5 Calibration to Relaxation Tests under varying initial stress at room temperature. Measured data from Figure 2.7 in Naaman (2004)

Figure 5.5 shows the measured and predicted stresses for the three sets of data with different initial stresses. The constants for this plot were determined by fitting the data of all three tests simultaneously.

A number of points are worthy of note.

1. The stress loss is a small percentage of the initial stress in all cases. The largest loss is about 1.5% (wire stressed to $0.80f_{pu}$, loss at 4500 hours).
2. The predictions overestimate some measured stress curves and underestimate others. The relatively poor fit occurs because of the way the material parameters

affect the curve shape. For the fit of multiple curves, the parameter *c* is the most critical. In Figure 5.5, modifying *c* changes not only the rate of relaxation for each curve, but it also adjusts the spacing between the three curves. For this reason, the fit shown above cannot be improved by modifying *c.* The other constants do not help the fit of multiple curves.

The second data set was for 7-wire Low-Relaxation strand that was tested at 20°C. It was obtained from Sumiden Wire Products Corporation in 2014 and is shown in Figure 5.6.

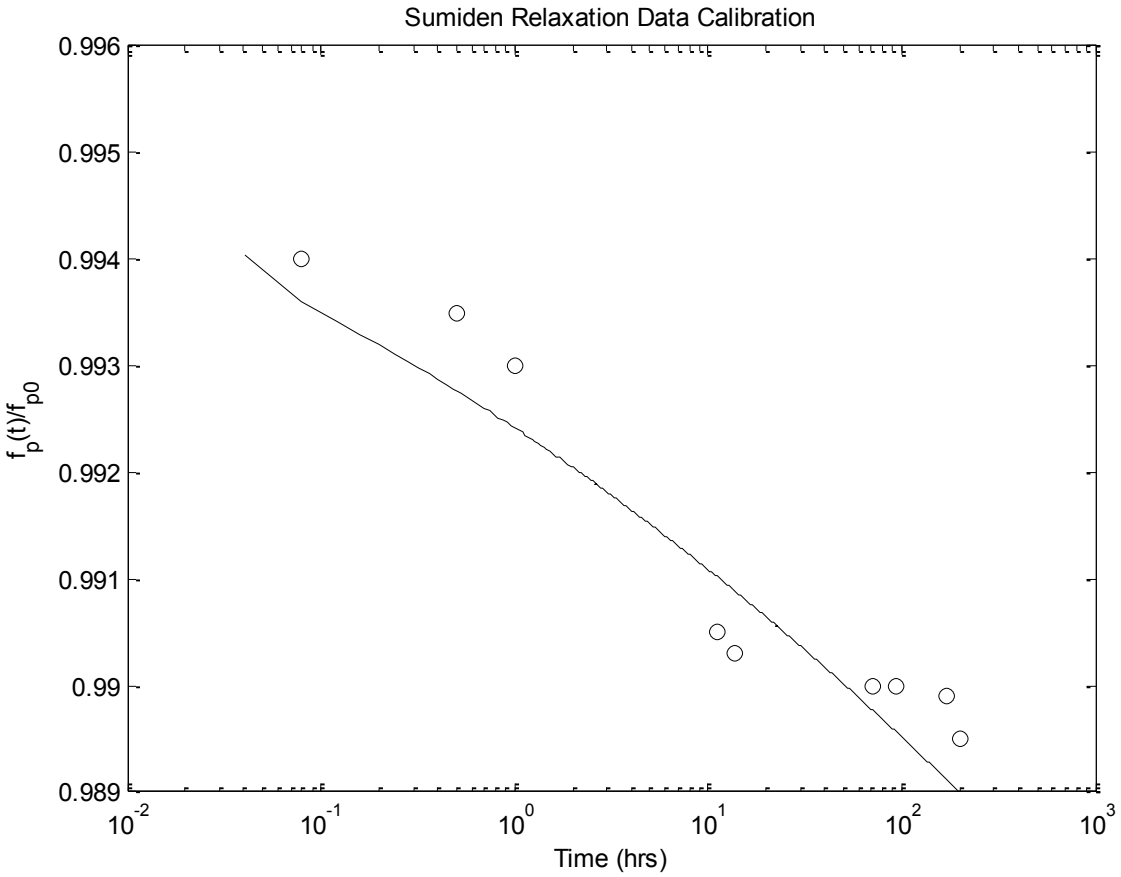

Figure 5.6 Calibration to constant strain relaxation test. Data provided by Sumiden Wire Products Corporation

This fit is reasonably good but, because the data extends only out to 200 hours, it is of limited value. However, its value lies in the fact that the material tested was the modern Low-Relaxation strand.

The final comparison was made against the Magura et al. (1964) model. It and the one used here are compared in Figure 5.7, where the initial stress at *t=0* was 202.5 ksi. The cost function was chosen to be the sum of the squared errors for 5000 points geometrically spaced between zero and 10000 hours (the smaller spacing was for shorter times). The constants *c*, *k* and ρ were adjusted to minimize the difference between the two sets of stresses.

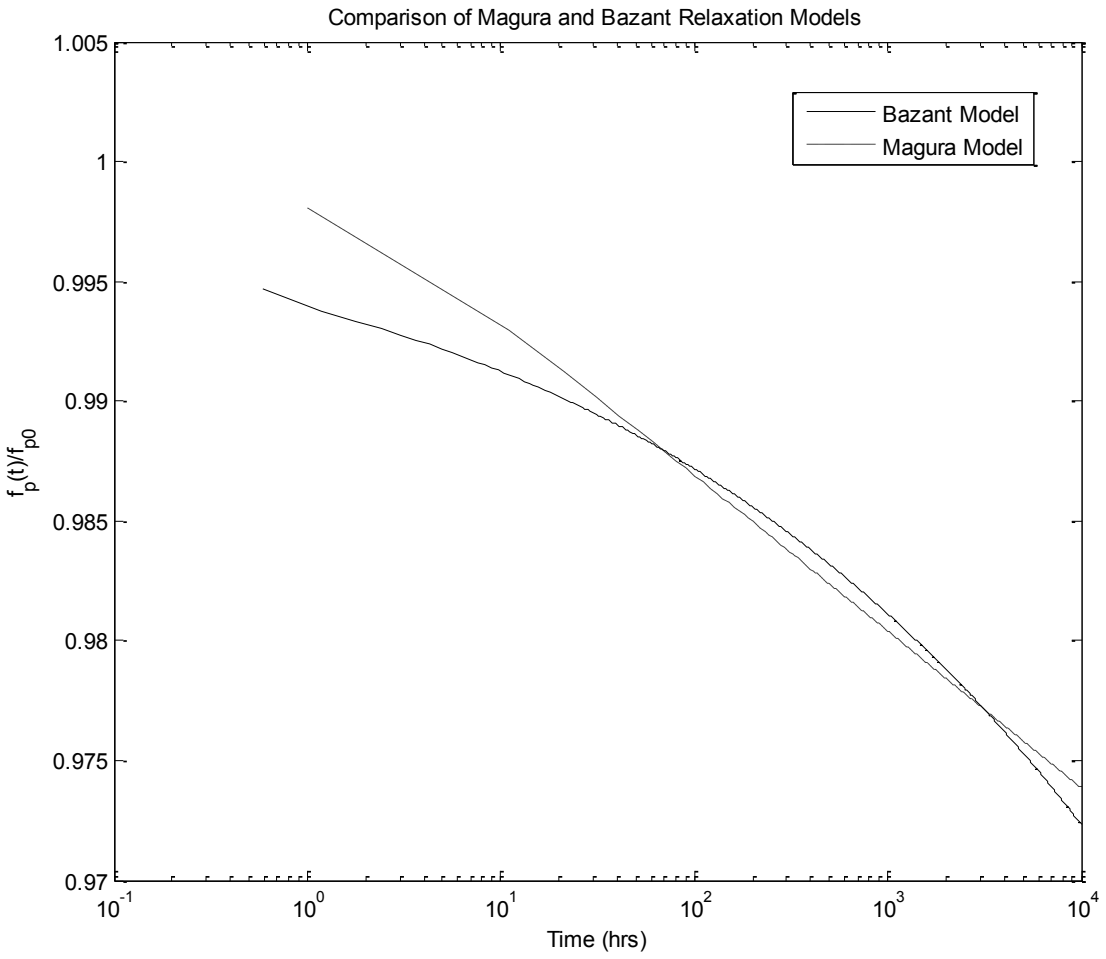

Figure 5.7 Calibration to the Magura et al. (1964) model

As is shown in Equation 5.2, the Magura model is not valid for times less than 1 hour and gives a zero stress loss at $t=1$. For this comparison, the Magura model was modified to use a $log(t+1)$ term rather than $log(t)$. Notice that in the short-time range the Magura model diverges from the model used here. This is due to logarithmic versus exponential formulations.

This calibration was included merely to show the significant difference in the two methods of prediction. Because the response curves for these two models have very different shapes, the time range used in calibration must be selected carefully. For Figure 5.7, Bazant's model was fit to the Magura model between 1 and 10000 hours (1.14 years). This is the time during which the most of the relaxation occurs and has the most significant impact on the deflection of the girder. From the previous calibrations it is evident that the Bazant model exhibits a very good match to the relaxation shape for these strands especially in the short term.

Using the material parameters from the foregoing f_{pu}-dependence calibration at room temperature, Bazant's model can be compared to the data provided by Naaman (2004) regarding the effect of temperature on the rate of relaxation. Figure 5.8 shows the data from Naaman's book as well as the fits from Bazant's model using the parameters, $k = 0.277$, $c = 0.1988$, and $\rho = 0.0344$.

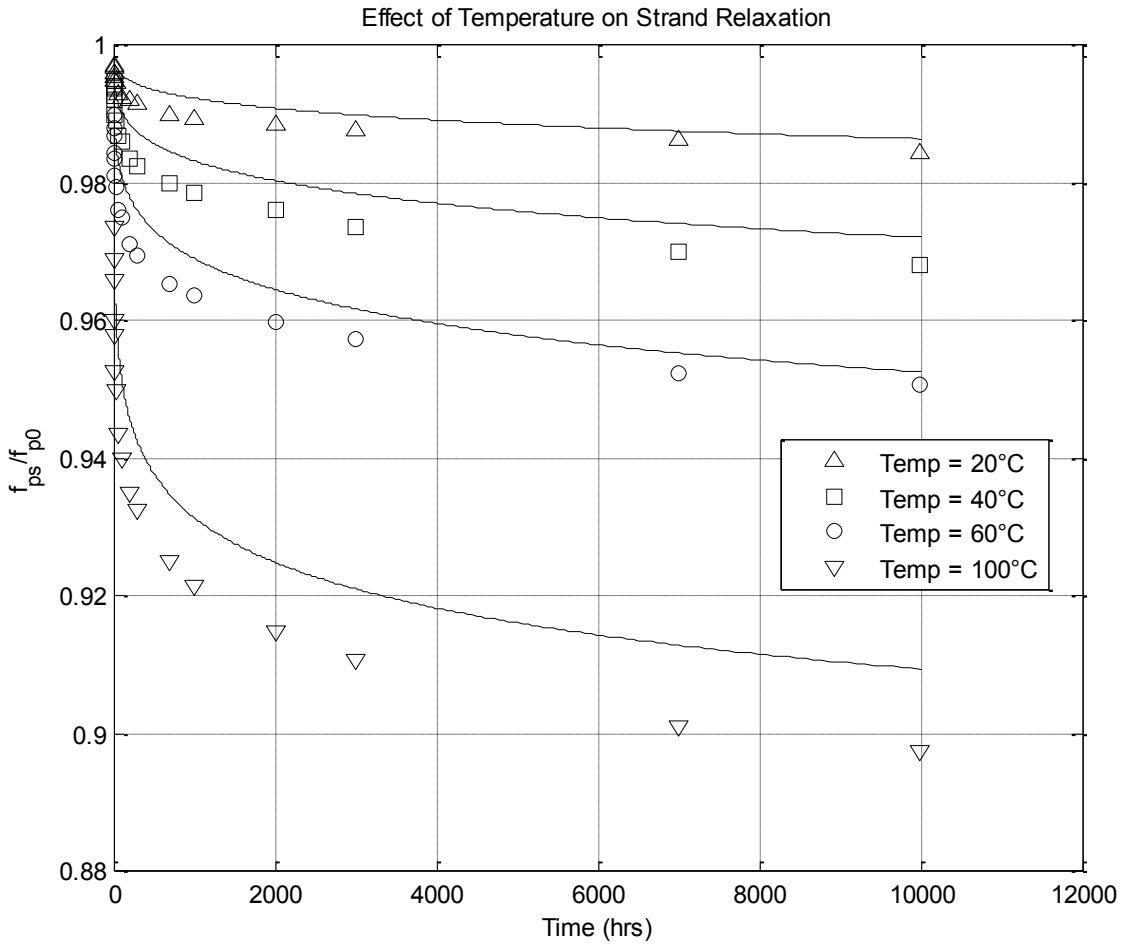

Figure 5.8 Data fits for different temperatures using previously calibrated material constants.

Figure 5.8 shows the temperature correction achieved using Bazant's model. This is an excellent demonstration of the not only the significant effect that temperature has on relaxation, but also the capabilities of Bazant's model to predict this effect with accuracy. This effect is potentially important because, during the casting and bonding period, it is common for pre-casters to heat the girder for faster curing. This heat could have a significant effect on relaxation, and thus on the stress in the strands and the camber of the girder after release.

After examining these calibrations, it is necessary to determine which material parameters are best for use in the remainder of this thesis. The parameters developed from the calibration to Naaman's data for different initial stress tests (i.e. k=0.1743, ρ = 0.563, etc) have been selected for the following reasons:

- The data set is the most complete available for calibration.
- When using the strand constitutive model within the analysis, it will be subjected to variable strain conditions due to the creep of concrete and elastic changed at release and slab casting. By calibrating to multiple initial stress relaxation curves simultaneously, the resulting parameters are more likely to be stable for a wide range of strains experienced.
- Figure 5.8 demonstrates that these parameters, when combined with Bazant's recommendations for adjusting the time scale to reflect the effects of temperature, also give good fits to high-temperature data.

The parameters, k = 0.277, c = 0.1988, and ρ = 0.0344 will be used for the remainder of this thesis.

In order to demonstrate the predicted relaxation response to a realistic temperature history, a strand history was generated using the following steps.

1) Jack the strands over 0.5 hours up to a jacking stress of 202.5 ksi. This portion is not shown in order to keep the scale of the y-axis small.
2) Allow the strands to rest for six hours to simulate the time taken to prepare forms and reinforcing in the casting bed.
3) Cast the concrete at six hours and begin a thermal history that is linearly interpolated between the following points:

Table 5.2 Sample Strand Thermal history.

Time (hrs)	6.5	12	16	22
Temperature (°F)	68	160	160	68

4) Release the girder after 22 hours and allow to it to cool at room temperature. Note that for an actual strand the strain would change in this time region depending on the creep properties. This has been ignored for this demonstration.

The resulting stress history for a strand is shown in Figure 5.9.

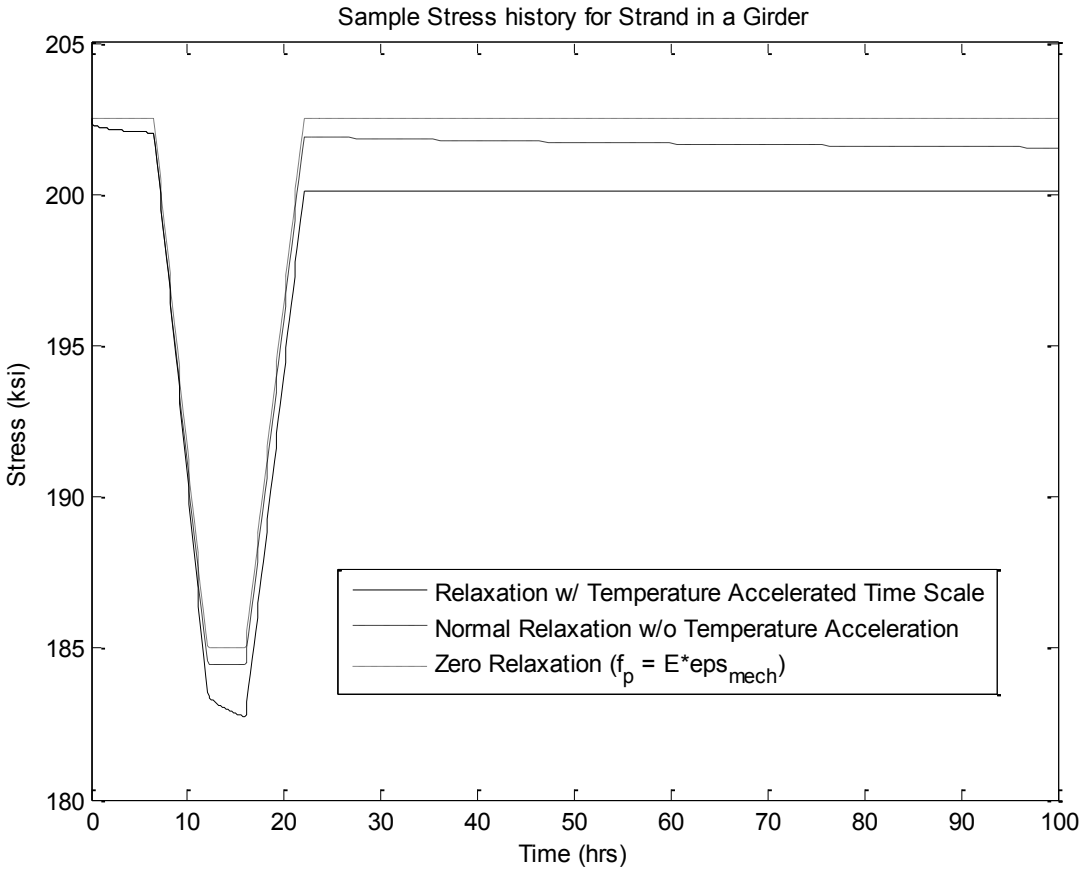

Figure 5.9 Sample strand stress history.

In Figure 5.9, the dotted line shows the stress history resulting from the mechanical strain in the strand without considering relaxation but including the effects of thermal expansion. That thermal expansion causes much larger stress changes than any due to relaxation, but most of it is recoverable when the stand cools. (The interactions with the concrete, discussed in Chapter 7 show that some strand stress is lost due to "locked in" stress effect, but they are ignored in this stress history.) The dashed line considers both the effects of thermal expansion and relaxation at room temperature and the solid line considers thermal expansion and the accelerated relaxation due to high temperatures as described in Equations 5.20 and 5.21. Notice that when accelerated relaxation is considered there is a 0.7% increase in relaxation after 100 hours. It is also interesting that when accelerated relaxation is considered, there is very little relaxation that occurs after cooling back down to room temperature (22 hours in Figure 5.9). This is because the strand is behaving like an older strand in which most of the relaxation has already occurred.

5.4 Concluding remarks

The following conclusions can be drawn from the development of the relaxation model:

- Current low-relaxation strands have little relaxation. The Sumiden data show a 1% loss at 200 hours and 1.2% when projected out to 1000 hours. This means that the effect of the relaxation on long-term deflections is much smaller than the effect of concrete creep.
- Although the model proposed by Bazant is versatile and is capable of modeling all of the key features of strand relaxation, further calibration against a wider array of measured data from low-relaxation strand tests is desirable.

CHAPTER 6 MODEL VERIFICATION

This chapter provides an example of the ability of the algorithm to predict the camber history of a girder for which measured camber data is available. Ideally, a complete calibration and statistical analysis of the model's capabilities would be conducted, but such an undertaking lay beyond the scope of the thesis. Furthermore, large variation in materials, as well as casting and curing procedures exist across the country, so the data required for a complete calibration would be extensive. This data was collected by Hang Nguyet Nguyen in her thesis research (Nguyen, 2013). Hang monitored the fabrication temperature profile and the post-release camber history for a WF74 girder from Concrete Technology Corporation (CTC) in Tacoma Washington. Using this data, a proof-of-concept calibration is conducted to demonstrate that the model provides reasonable predictions for camber.

The sources of uncertainty in the predictions lie in:

- The kinematic assumptions (plane sections remain plane)
- The numerical integration procedures
- The rebar steel constitutive model
- The prestressing strand constitutive model
- The concrete constitutive model
- The loading (including thermal and shrinkage loads)

Of these, the largest potential errors lie in the concrete constitutive modeling and in the loading. For example, the error in the kinematic assumption can be judged by the ratio of shear deflections (which are ignored) to bending deflections; in a typical prestressed girder with a span/depth ratio of 25, this ratio is about 0.005, or 0.5%. The numerical integration can be

conducted to any desired accuracy by using more layers in the cross-section and more integration points along the girder. The values used here led to an error no greater than 1%. The total relaxation loss in the strand was in all cases less than 3%, so the error caused by modeling it in accurately is much less than that. The rebar steel remains elastic and does not relax, and the combined uncertainty in its Young's modulus and bar area is on the order of 5%, but its effect on camber and deflection is no more than on tenth of that (i.e. 0.5%), partly because the rebar contributes so little to the moment of inertia anywhere, and partly because, at the critical mid-span location, almost no rebar exists.

The concrete constitutive model has already been shown to replicate a wide range of behaviors, although an accurate correlation between its numerical coefficients (e.g. E_K values) and the relevant physical parameters (e.g. volume/surface ratio) still needs to be conducted. The more difficult problem lies in the loading. In particular, detailed measured data on the thermal gradients in practice is sparse.

The girder used for this comparison was a 147.5 foot-long, WF74 girder cast in early December 2012 at CTC. The key gross cross-sectional properties for a WF74 girder are listed in Table 6.3

Table 7. Cross-Sectional Properties

Height (in)	74
I_{xx} (in^4)	733363
Area (in^2)	923
CGC Location From Top (in)	38.3

In the CTC casting plant, girders are fabricated in the following steps:

1) The prestressing strands are routed through the harping points (if necessary) and then stressed up to the specified jacking stress. This takes approximately a half an hour.
2) The formwork and reinforcing bars are assembled.
3) The forms are closed around the strands and rebar and concrete is cast. The total time between the start of jacking and the casting of concrete is approximately 6 hours.
4) After the concrete is cast, the forms are heated and the concrete cures for 16 hours before the strands are cut and the girder is released at 22 hours after jacking.
5) In her research, Hang investigated the effect of the assumed bonding/hardening time for the concrete. She found that, for this girder, the best agreement between predicted and measured release camber occurred when the concrete was assumed to bond and begin hardening 4 hours after casting (10 hours after jacking). In this analysis, her resulting hardening time is used (4 hours) for the beginning of concrete hardening.

This sequence of events is encompassed by the four phases used in the formulation of this algorithm.

Another important part of the analysis is the girder support conditions, which change throughout the life of the girder. For this girder, there are three separate support conditions: lifting, storage/transportation, and final site conditions. Just after release, the girder is picked by lifting loops located 3 feet from each end. Approximately 2 hours after release, the girder is then placed on storage bunks located 6 feet from each end. Once the construction site is ready, the girder is transported to it and placed in its final configuration. This girder was placed 74 days after release on supports located 1 foot from each end. These changing support conditions are accounted for in this analysis.

Throughout this cycle, there is a thermal history within the girder. Hang took detailed readings of the temperature profile within the girder during fabrication of the girder and up to nine hours after release. In Figure 6.1, the temperature history collected for the top, centroid, and bottom of the girder is shown for the fabrication period.

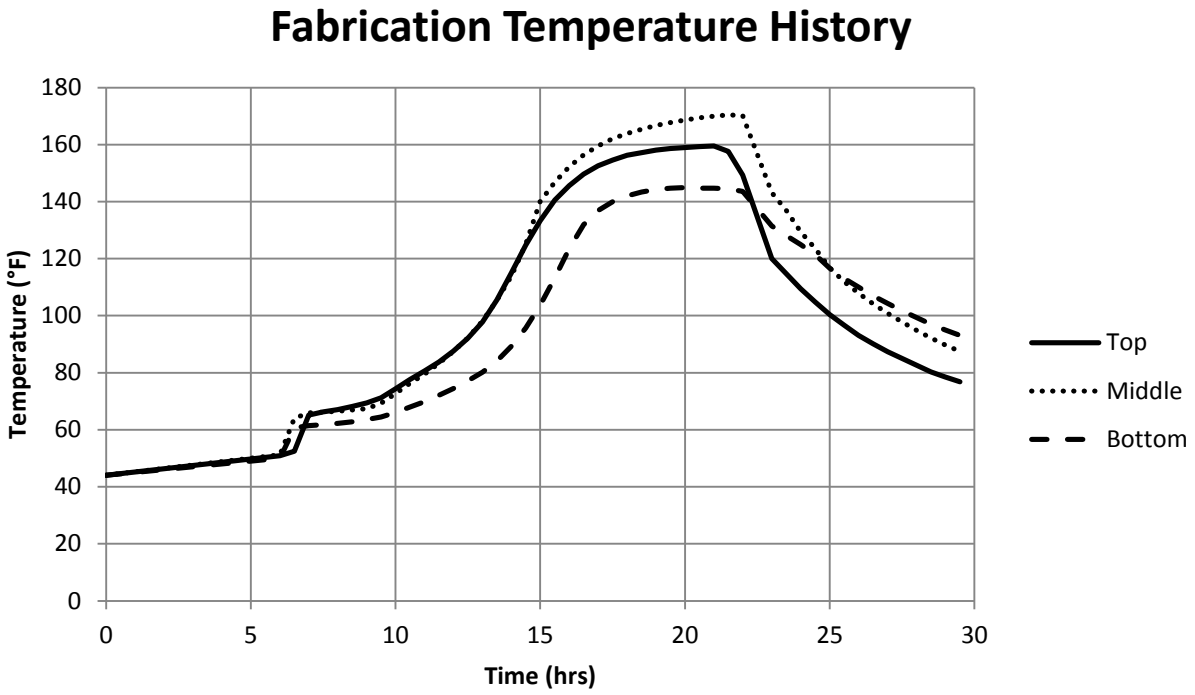

Figure 6.1 Fabrication thermal history for precast girder (Nguyen, 2013)

In Figure 6.1 it is important to note three key times; the time scale begins at the start of stressing, casting begins at 6 hours, and release occurs at 22 hours. Because the data shown above stops before the girder has completely cooled, the ending slope is used to project that the girder will reach a constant temperature over the height of 45°F (air temp) at a time of 43 hours. This temperature is maintained for the rest of the analysis for the lack of a better estimation. The external air temperature was 45°F during the casting and was assumed to remain at this temperature throughout the analysis. In collecting this data, Hang used 11 thermocouples distributed over the height of the girder. Data from all 11 sensors was used in the analysis;

Figure 6.1 shows data from only three sensors in the interests of clarity. The eleven sensors were distributed both vertically in the web and laterally in the flanges. They showed that the temperature varied in both directions. Because the analysis is based on the assumption that all conditions (including temperature, stress and strain) are constant across the width of layer, the measured temperatures were averaged across the width at any given level. This procedure inevitably introduced some error, because the number of sensors was insufficient to define accurately the complete 2-D thermal profile. Thus, some error exists in the "measured" data.

The strand layout in this girder is as follows:

- 17 harped strands. The strands are harped at points 14'-9" to the left and right of the girder centerline, i.e. at 0.40L and 0.60L. The vertical location of the centroid of these strands is 11.53" at the ends and 69.4" at mid-span, both measured from the top of the girder (62.47" and 4.6" respectively when measured from the bottom of the girder).
- 40 straight strands located at 70.4" down from the top of the girder (3.6 from bottom of the girder).
- 2 straight, temporary strands located 2" down from the top of the girder. These strands are cut after the girder reaches the site.

Each of these strands was 0.6 inches in diameter and was jacked to a stress of 203ksi.

Other key inputs are:

- The girder was analyzed at a total of 25 cross-sections
- The total bed stiffness was assumed to be 0.001 k/in. This is essentially zero for the sake of this analysis. The stiffness cannot be cannot be set to zero as it results in undefined variables within the algorithm

The material properties used for the analysis were those calibrated in the previous chapters. Appendix A documents the entire set of input parameters and includes the input file used for this analysis.

6.1 Prediction Comparisons

In order to get a good picture of the predicted behavior of this girder, it is necessary to break the comparison into two sections; the short-term comparison just after release, and the long-term comparison, which shows the ultimate predicted deflection. This separation is done for two reasons. The first is that the measured camber data exists only up to nine hours after release and so, for long-term comparisons, the AASHTO predictions of camber will be used. The second reason is that if the long-term predictions are included in the comparison, the scaling of the plot is much too large to see the detailed results just after release. All of the plots shown in the following comparison discussion are for the exact same test scenario described above but scaled differently to capture differing levels of detail.

6.1.1 Camber Predictions

Figure 6.2 shows the predicted and actual deflections of the girder out to two days after release.

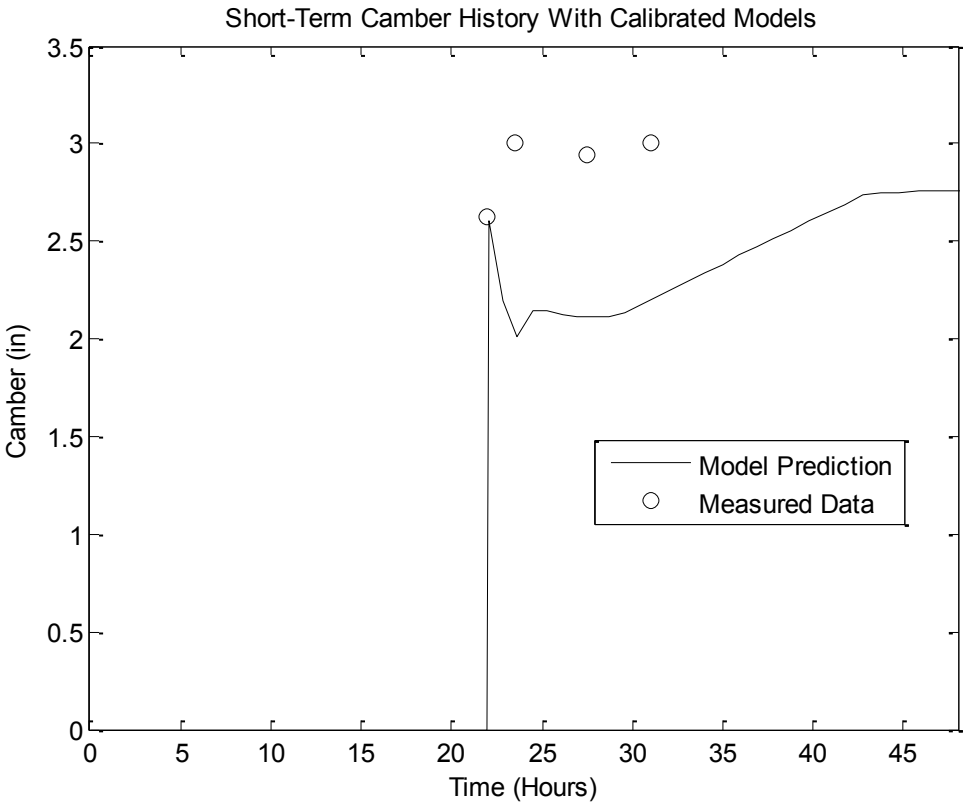

Figure 6.2 Short-Term camber comparison to measured data. (Nguyen, 2013)

The sharp change in camber at a time of approximately 24 hours is caused by the change in support conditions when the girder is moved to its storage location. The predicted and measured release cambers (at 22 hours) are very close but the two solutions then diverge. Table 6.8 below shows the four measured cambers with corresponding times and predicted measurements.

Table 6.8 Comparison of predicted and measured cambers

Time (Hours)	22.00	23.50	27.50	31.00
Measured Camber (in)	2.63	3.00	2.94	3.00
Predicted Camber (in)	2.60	2.01	2.11	2.22
Difference (in)	-0.03	-0.99	-0.88	-0.78

The long-term comparison to the AASHTO prediction is shown in Figure 6.3. The AASHTO prediction was used as a comparison tool in this case for the lack of any measured data.

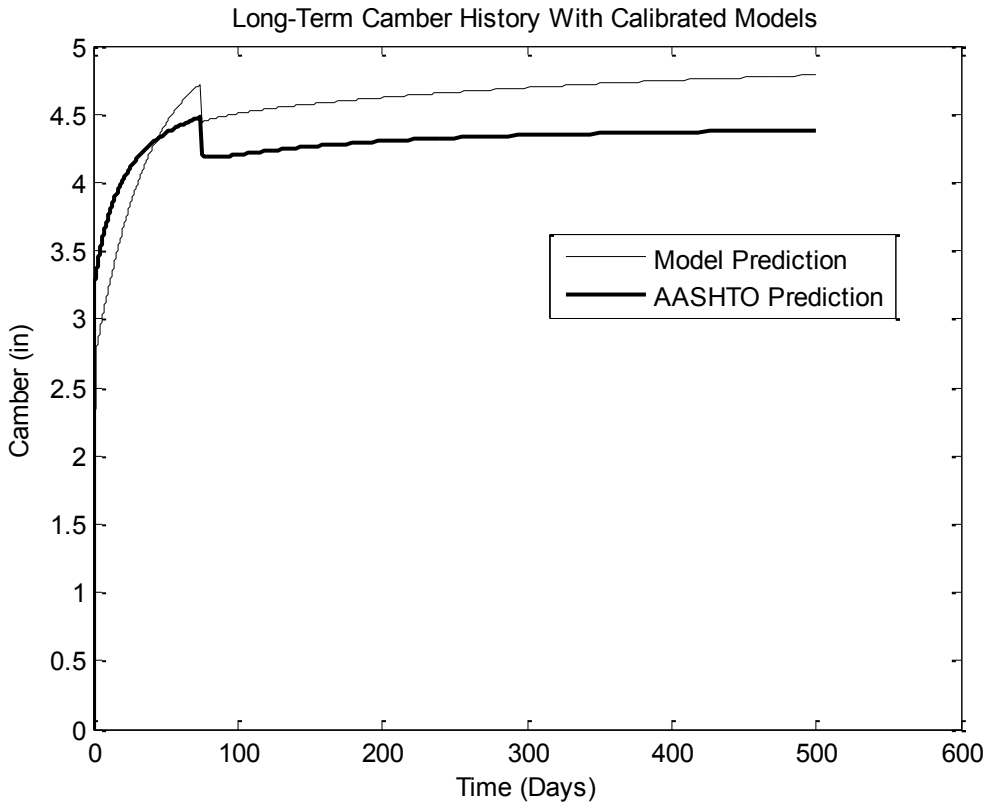

Figure 6.3 Long-term camber comparison to predicted AASHTO cambers

The abrupt change in the camber shown around 75 days is due to the change in support location that occurs when the girder is moved to its site location. In this comparison, the correlation between the new model and the AASHTO model are quite close in the long-term. At 500 days the predictions are 4.61" and 4.38" for the proposed model and the AASHTO prediction respectively. This is a 5% error relative to the AASHTO model.

The reasons for the divergence between measured and predicted short-term cambers just after release are unknown, but the two primary effects that occur at that time, namely creep and thermal effects, that should be reviewed. Figure 6.1 shows that, at release (22 hrs) the girder is

hotter at the top than at the bottom. As it cools to a uniform temperature it will deflect downwards, or lose camber. This drop in camber can be seen in the predicted curve of Figure 6.3. Notice that this reduction in camber reverses at around 28 hours and the camber begins to increase again. This is when much of the cooling has occurred, the thermal component of camber has stabilized, and the concrete creep begins to govern the camber response.

Although this explains why the analysis predicts a camber reduction, it does not explain the disparity between predicted and measured results in the short-term. One possible cause of this error in the prediction is that the creep model does not account correctly for rapid creep that occurs when young concrete is loaded. From Figure 6.3 the long-term creep coefficient is quite accurate, but, because the predicted creep appears to occur more slowly than the measured creep, the model underestimates the camber in the short-term.

Typical creep tests are constant stress tests that start after approximately 14 days of moist curing. Thus they do not reflect well any short-term creep in a girder that is heat-cured for only 16 hours. Because the Kelvin model used here is indirectly calibrated to conventional creep tests, it does not accurately capture the short-term girder creep. This deficiency was also documented by (Barr, Eberhard, Stanton, Khaleghi, & Hsieh, 2000) who studied prestress loss and camber.

In the Kelvin model for creep used here, the dashpot viscosity in the first Kelvin element is the parameter that controls the early age creep rate. In order to investigate this hypothesis, the initial value for this dashpot was modified to see if a better prediction could be obtained. Recall that the value of the dashpot viscosity changes over time, and only the initial value was modified here. In Figure 6.4 and Figure 6.5 this initial viscosity was reduced by factors of 2, 10, and 100 as shown.

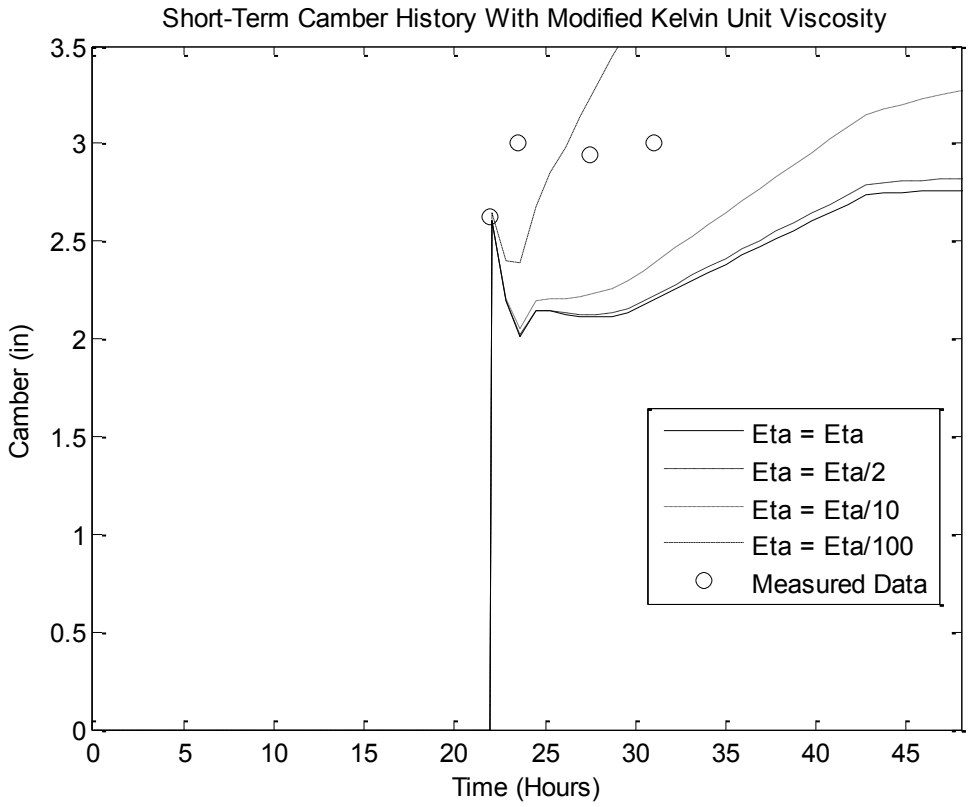

Figure 6.4 Short-term camber predictions with modified Kelvin unit viscosities

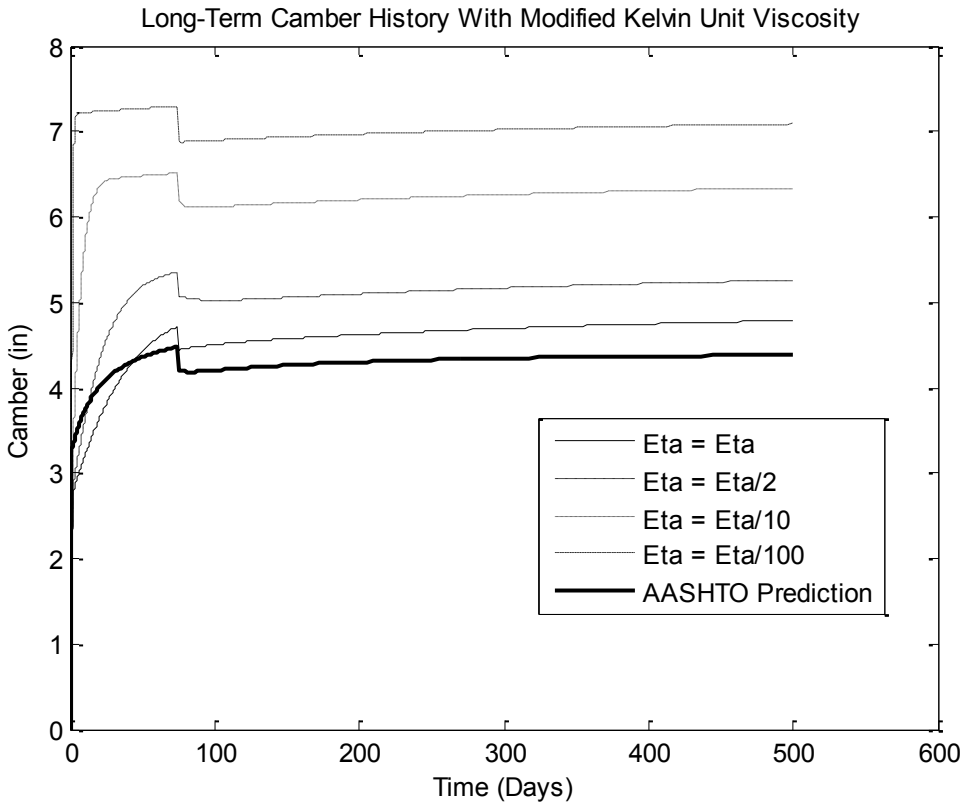

Figure 6.5 Long-term camber predictions with modified Kelvin unit viscosities

From the short-term analysis in Figure 6.4 it can be seen that the predicted camber becomes closer to the measured camber. The creep rate is greatly accelerated and the early age predicted cambers are increased significantly from the previous values. The problem is that when these same reduced viscosity values are used in the long-term comparison, they result in a significant over-prediction of camber. This is due to sensitivity in the interaction of time-dependent model parameters. By reducing the initial value of the viscosity it causes all of the creep to happen very quickly and therefore an over-prediction occurs.

Figure 6.6 shows the creep coefficient curves for each of the 4 scenarios due to a constant unit loading.

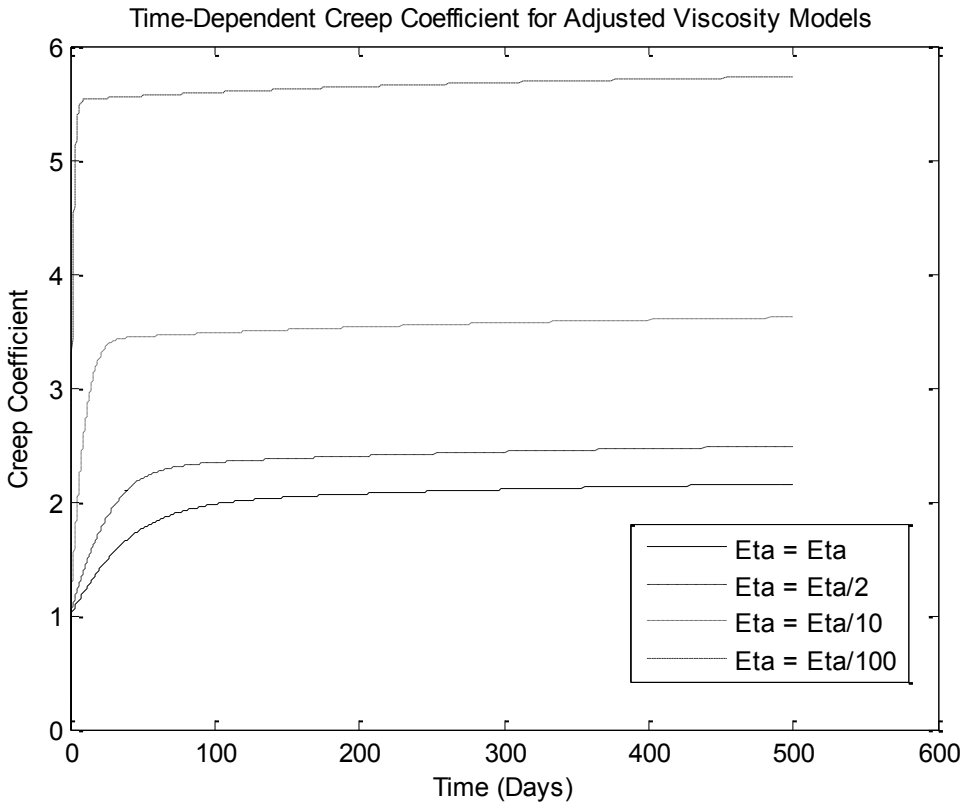

Figure 6.6 Creep coefficient curves for adjusted viscosities

These curves show that the Kelvin model is highly sensitive to adjustment of the viscosities of the Kelvin elements. It also indicates that by changing both the viscosities and stiffnesses of the Kelvin elements, a reasonable prediction for both early age creep and long-term creep coefficients could be obtained.

The outcome of this discussion is that although, the model is versatile and capable of modeling this phenomena, the creep model needs to be calibrated more thoroughly. There are two key problems resulting from the calibration of the creep model that should be remedied.

- The model needs to be calibrated to creep data that includes early loading on heat-cured concrete.
- The results of the modification of the viscosity values indicate that the Kelvin model parameters should be calibrated more carefully such that the creep coefficient at infinite

time is not exaggerated like the one shown above. This finding is largely a consequence of using time-varying model parameters If the springs and dashpots in the Kelvin units had constant properties, the relationship between the ultimate creep coefficient and the spring properties is quite simple, and is given by Equation 4.1. This is not true for units with time-varying parameters, which require more careful calibration.

The current model configuration may be able to satisfy these additional constraints but it may be better to add an additional Kelvin unit to take care of the early creep behavior.

6.1.2 Material Stress Predictions

One of the key features of this algorithm is its ability to explicitly consider the link between the stress response of the prestressing strands and concrete. As the strand relaxes, the concrete stress is also reduced; this changes the creep behavior which in turn affects the strand stress. Figure 6.7 shows the predicted mid-span stress in the strands during fabrication and the first hours after release while Figure 6.8 shows the long-term stress in the strands.

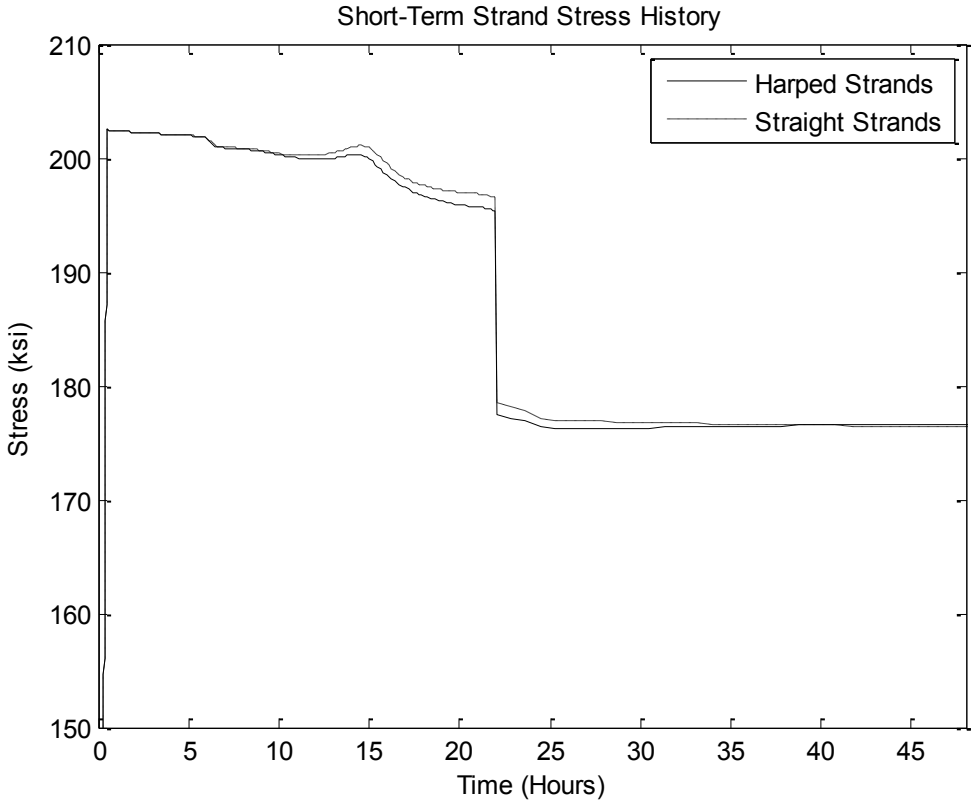

Figure 6.7 Short-term strand stress predictions

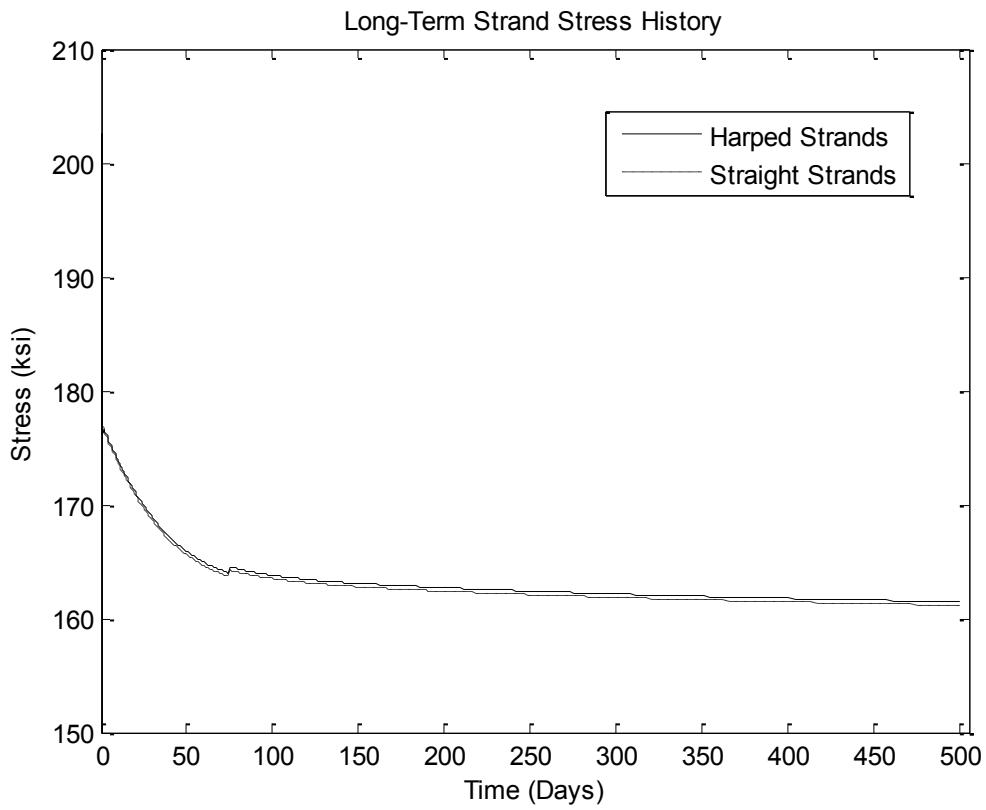

Figure 6.8 Long-term strand stress predictions

The y-axis in these figures has been cut off at 150 ksi so that the window scaling is better for viewing the behavior details during fabrication. At time, $t = 0$, the stress in the strand is 0 and then the jacking occurs over ½ hours.

The predicted strand stress in Figure 6.7 and Figure 6.8 has the following key features:

- After the strand is jacked, the relaxation occurs very slowly and the stress loss is relatively low up to the time of casting.
- Once casting occurs (6 hours) the temperature in the girder rises. This reduces the stress in the strands in two ways. First is the reduction in stress due to thermal expansion of the strand between the fixed abutments. This expansion leads to a reduction in mechanical strain and therefor a reduction in stress. The second effect of elevated temperature is the

accelerated rate of relaxation. These two effects increase the prestress loss beyond that computed using conventional relaxation methods that ignore temperature.

- Once the concrete bonds at 10 hours (4 hours after casting), the prestressing strand is locked to the same strain change as the girder concrete. This leads to an increase in strand stress due to the heating of the girder. As the girder (and strand) increase temperature, the stress relaxes rapidly due to the temperature acceleration effects (the coefficient of thermal expansion is the same for both materials). In order to maintain equilibrium at the nodes, an elastic increase in stress is required and thus the increase in the strand stresses. This increase peaks at 15 hours when the concrete temperature rise plateaus. At this point the relaxation takes over and the stress begins to drop again.
- At release (22 hours) there is a large elastic change in stress. In Table 6.3 the predicted elastic loss is an average of 20 ksi between the two strand types. Using purely elastic analysis with gross section properties, this loss is calculated as 19.5 ksi. The algorithm is at least capable of accurate elastic calculations.
- After release the strand continues to relax at a decreasing rate.

Table 6.3 shows the stress loss in the strands at key points in the history.

Table 6.3 Selected prestress loss values

Event	Bonding	Immediately Before Release	Just After Release	500 days
Harped Strand Loss (ksi)	2.70	7.70	27.2	41.50
Straight Strand Loss (ksi)	2.60	6.50	26.99	41.80

Figure 6.9 and Figure 6.10 show the short-term and long-term stress histories for the girder concrete at the top, bottom, and centroid. Note that compressive stress is negative.

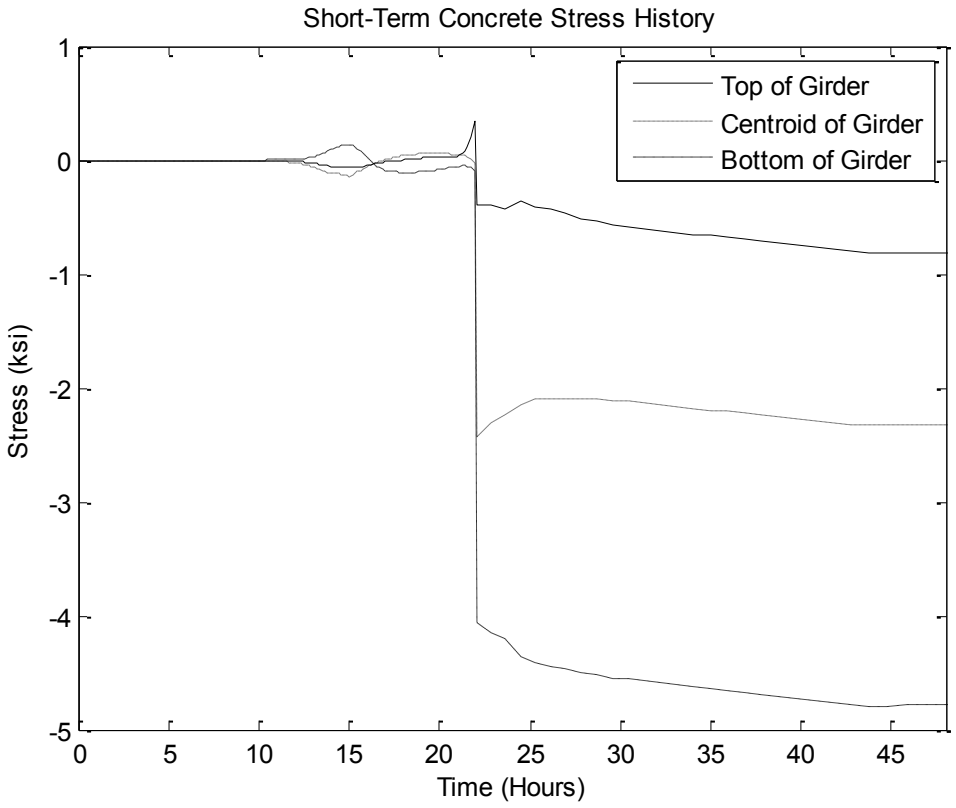

Figure 6.9 Short-term concrete stress predictions

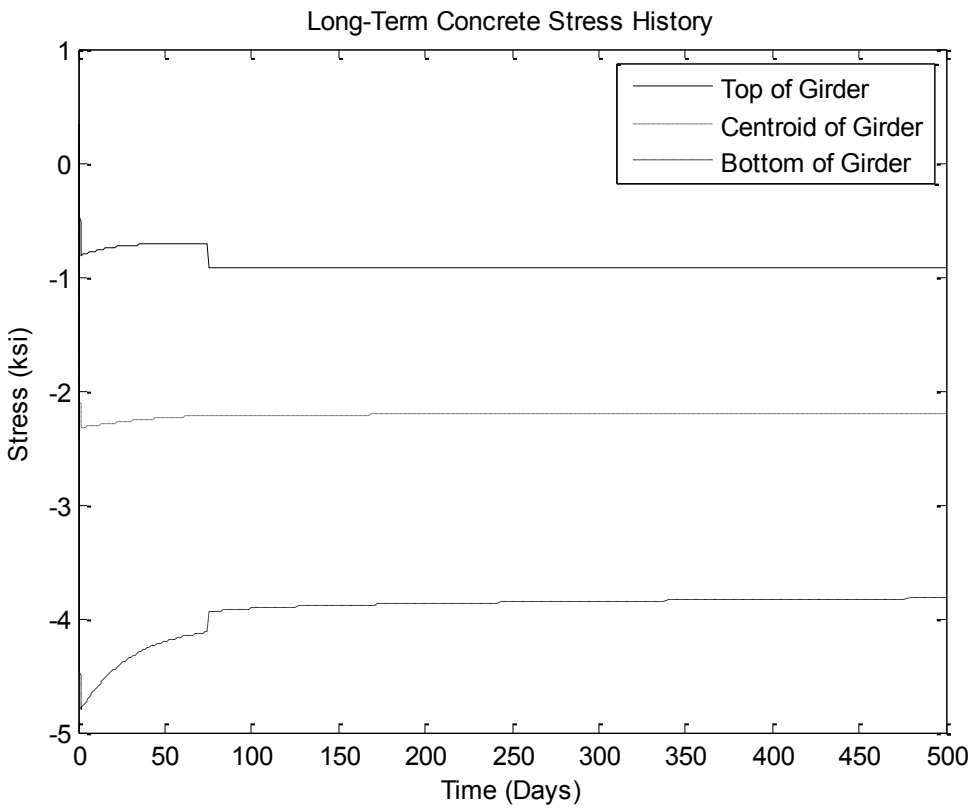

Figure 6.10 Long-term concrete stress predictions

There is no stress in the concrete until it bonds and starts to harden at 10 hours. Immediately after bonding, the stresses in both the top and bottom of the concrete change between tension and compression. This is due to the changing thermal gradient on the girder cross-section. During the bonded, pre-release phase, the total strain is forced to be constant over the height of the girder to prevent deflection. Because the temperature distribution is nonlinear, the thermal strains are also nonlinear, resulting in mechanical strain, and thus stress, nonlinearity to get a constant total strain over the height. This is the reason for the increase in bottom compression stress between 22 and 45 hours. After release, there is a large elastic stress change followed by nonlinear changes in stress caused by the concrete creep and strand relaxation. In the long-term, the compressive stress in all of the concrete decreases. This is due to the loss of prestress and is in agreement with predictions using conventional methods. The reduction in bottom compression

stress at 74 days is due to a change in support conditions to an end supported system. This simulates final condition of the girder before the slab being added.

CHAPTER 7 SUMMARY AND CONCLUSIONS

7.1 Summary

A consistent analysis algorithm has been developed to predict the camber in precast, prestensioned concrete girders. In this algorithm, the girder is analyzed throughout its entire life, from the start of fabrication to the end of its service life, using constitutive models for the materials that include time-dependent behavior. The life-span of the girder is divided into four phases; strand jacking, pre-bonding, post-bonding, and post-release (Chapter 3). In each of these phases the solution is obtained incrementally using a step-by-step algorithm. The necessary calculations include:

- Application of the boundary conditions appropriate to the phase,
- Determination of the increments in axial load and moment along the girder due to the increments in external loads,
- Computation of the changes in axial elongation and curvature at selected locations along the girder,
- Integration of the total axial elongations and curvatures to provide the deflections at the new time.

The curvatures are obtained from the moments by assuming that plane sections remain plane and finding the strain distribution that provides both moment and axial force equilibrium. To do this, the cross-section is divided into horizontal layers. For any trial strain distribution, the axial force and moment are obtained by finding the stress from the trial strain diagram and applying the material constitutive laws, then integrating the stresses over the cross-section. The strain

diagram that satisfies axial force and moment equilibrium is found iteratively using the Newton-Raphson procedure.

The time-dependent constitutive models for both the concrete and prestressing strands are the foundation of the analysis. For the concrete model, a new rheological model was developed using a chain of Kelvin-Voigt units with time-varying parameters. The parameters in the model were then calibrated. In place of measured data, predictions of currently accepted creep models under constant stress were used, because they have already been calibrated against measured data (Chapter 4).

For the prestressing strand, the model proposed by Bazant and Yu (2013) was used. This model accommodates load by time-varying strain and accounts for all of the factors affecting the behavior of prestressed strands. It was optimized to fit measured relaxation data (Chapter 5).

Using these two calibrated models and the geometry of the cross-section, the camber history was predicted and compared to measured girder cambers for the times for which good quality data were available (up to approximately two weeks). For camber comparisons at longer times, the predictions of AASHTO's camber prediction method discussed in Chapter 2 were used in place of measured data (Chapter 6).

7.2 Conclusions

The algorithm developed and explored in this report has the capability to explicitly analyze many of the inter-related factors that affect the camber in precast, prestressed girders that were previously ignored or estimated. Although camber varies significantly with conditions, with this algorithm a more complete understanding of the behavior can be gained. The following conclusions that can be drawn from the development of the global algorithm:

1) The algorithm that was developed in this research provides an effective vehicle through which many of the factors affecting girder camber can be analyzed explicitly. These factors include: temperature history and gradient along the height of the girder, shrinkage gradients, and fabrication effects.
2) The formulation of this algorithm includes the explicit consideration of the interactions between the time-dependent properties of concrete and strand. For example, stress loss in the strands due to relaxation reduces the stress on the concrete and the associated creep strain, and creep of the concrete reduces the strain, and corresponding stress, in the strand. In addition, the algorithm explicitly includes environmental strains due to shrinkage and temperature. The algorithm accounts rationally for these interactions by satisfying equilibrium and strain compatibility on a step-by-step basis.
3) The algorithm was used to predict the camber history for a girder for which short-term measured data were available. The predicted and measured camber histories showed similar trends and values that were similar but not identical. The constitutive model parameters used for this comparison were obtained by calibrating the individual models against time-dependent stress-strain data from material tests.
4) The long-term camber history for the girder was predicted using the AASHTO time-dependent procedure. This was treated as being the measured data. The predictions of the new algorithm were then compared with this long-term "measured" camber history, and gave good agreement.
5) The parts of the model that are subject to the greatest uncertainty, and that lead to the majority of the error, are the environmental loading, especially that due to temperature during fabrication, and the time-dependent constitutive law for the concrete.

6) Some aspects of the behavior during fabrication have a significant influence on the subsequent camber, but are not considered in conventional calculations. Important ones are: the time at which the concrete first bonds to the strand, and the thermal profile in the concrete when the concrete first bonds to the strand and early creep (directly after release.)

In addition to these conclusions from the global algorithm, some conclusions specific to the new creep model for creep are noteworthy.

7) The model can replicate successfully the predictions of the most widely-used creep models in predicting time-varying response to constant stress. For a given stress history and material properties, the various existing models predict a range of strain histories that differ quite significantly. Nonetheless, the new model was able to replicate all of them quite closely once the model parameters had been optimized to achieve that goal. This finding demonstrates the versatility of the model.
8) The model can predict the recovery of creep strains when the stress is reduced, without the need for additional model features.
9) The new model contains many parameters. A comprehensive calibration effort is needed to link them to the commonly used measures of concrete behavior, such as instantaneous Young's Modulus, and ultimate creep coefficient.

7.3 Recommendations for Future Research

Significant work remains to be done before the algorithm can be used in practice. Necessary studies include the following:

1) In order to improve the modeling of these aspects of camber, measured data for calibration is needed. Detailed data on the thermal profile in a girder is uncommon.

2) A much more thorough calibration of the creep model is needed. It is recommended that the Kelvin units be related to specific effects such as basic and drying creep. This would help users to make rational choices for the model parameters.
3) The possibility of creep due to early-age loading should be investigated. Tests could be conducted under circumstances similar to those experienced by girders. In particular, the concrete should be cured at the high temperatures typically used in girder production (up to 180 deg. F) and it should be loaded at a time consistent with the release of prestress in a girder. Such a test program is logistically challenging but the results are needed to improve the profession's understanding and modeling of early-age creep.

The effects of the numerous fabrication effects should be analyzed for their effect on the girder's camber response after release. These factors are analyzed explicitly in this algorithm and can therefore be analyzed for their importance.

4) The model predictions should be compared with measured results for girders for which the long-term cambers are known. Ideally girders would be analyzed from the start of fabrication to well into its service life.

NOTATION

A = area

β = $\frac{K_{Bed}}{L}$, the stiffness per unit length of casting bed

C, D = constants defining aggregate behavior of Kelvin units during a time-step

c = material constant for prestressing strand model

E_c = elastic modulus of concrete

E_e = average stiffness for Kelvin unit over a time-step

E_f = the effective stiffness, given by $E_K + \dot{\eta}$,

E_K = Kelvin unit spring stiffness

E_p = elastic modulus in prestressing strands

ε_{env} = environmental strains including thermal and shrinkage strains were applicable

ε_{mech} = mechanical strain

ε_{Tot} = total strain

$\varepsilon_{Tot,0}$ = total strain at the origin of the cross-section

η = Kelvin unit dashpot viscosity

ΔF = change in applied force that occurs during the time-step

f_{pj} = jacking stress in the strands

f_{pu} = ultimate stress in strands

f_{py} = yield stress in the strands

γ = the ratio of stress relaxation limit to the yield stress in strands

h = material constant for prestressing strand model

I = moment of inertia

K = stiffness

K_{Bed} = total stiffness of the girder casting bed

k = material constant for prestressing strand relaxation

k_B = Boltzmann constant,

L = length

λ = $\sqrt{\frac{\beta}{EA_{Tot}}}$, a stiffness ratio for the girder and bed.

λ_1 = time constant for prestressing strand relaxation

M = moment on the cross-section

M_{ext} = External applied moment on the cross-section

ϕ = curvature of the cross-section

P = axial force on the cross-section

P_{ext} = External applied axial force on the cross-section

P^e = Axial force in an element

ρ = material constant for prestressing strand relaxation

Q = the activation energy,

t = time, either true or fictitious (see Chapter 5, Section 5.1.3)

T = intrinsic time coefficient for Kelvin unit

τ = η/E_f , the intrinsic decay time of the Kelvin unit

T_0 = the reference temperature, 293°K

ΔU_{Tot} = total change in displacement occurring during the time increment

ΔU_{inc} = the increment in displacement change for a given Newton-Raphson iteration

u = nodal displacements

σ = stress

S_n = Simpson's coefficient for a cross-section interface

ξ = true time for prestressing strand

y = vertical location (positive down) from the top of the girder in the cross-section

REFERENCES

ACI Committee 209. (2008). *Guide for Modeling and Calculating Shrinkage and Creep in Hardened Concrete (ACI 209.2R-08).* Farmington Hills, MI: American Concrete Institute.

ACI Committee 435. (1995). Control of Deflection in Concrete Structures (ACI 435R-95). Farmington Hills, MI: American Concrete Institute.

American Association of State Highway and Transportation Officials (AASHTO). (2012). AASHTO LRFD Bridge Design Specifications. *6th edition*. Washington D. C.

Barr, P., Eberhard, M., Stanton, J., Khaleghi, B., & Hsieh, J. (2000). High Performance Concrete in Washington State SR18/SR516 Overcrossing: Final Report on Girder Monitoring. Olympia, Washington: Washington State Transportation Center, report.

Bazant, Z. P., & Baweja, S. (1995). *Creep and Shrinkage Prediction Model for Analysis and Design of Concrete Structures: Model B3.* Farmington Hills: ACI Committee 209.

Bazant, Z. P., & Chern, J.-C. (1984). Rate-Type Concrete Creep Law with Reduced Time. *Journal of Engineering Mechanics*, 329-340.

Bazant, Z. P., & Xi, Y. (1995). Continuous Retardation Spectrum for Solidification Theory of Concrete Creep. *Journal of Engineering Mechanics*, 281-288.

Bazant, Z. P., & Yu, Q. (2012). Relaxation of Prestressing Steel at Varying Strain and Temperature: Viscoplastic Constitutive Relation. *Journal of Engineering Mechanics*, 459-466.

Bazant, Z. P., Hauggaard, A. B., Baweja, S., & Ulm, F.-J. (1997). Microprestress-Solidification Theory for Concrete Creep. I: Aging and Drying. *Journal of Engineering Mechanics*, 1188-1194.

Bazant, Z., & Baweja, S. (1995). Creep and Shrinkage Prediction Model for Analysis and Design of Concrete Structures - Model B3. *Materials and Structures, V. 28*, 357-365, 415-430, 488-495.

(1990). *CEB-fip Model Code 1990. Model Code for Concrete Structures.* London, Great Britain: Thomas Telford Services Ltd.

Gardner, N. (2004). Comparison of Prediction Provisions for Drying Shrinkage and Creep of Normal-Strength Concretes. *Canadian Journal of Civil Engineering*, 767-775.

Hernandez, H. D., & Gamble, W. L. (1975). *Time-Dependent Prestress Losses in Pretensioned Concrete Construction.* Urbana: University of Illinois.

Magura, D. D. (1964). A Study of Stress Relaxation in Prestressing Reinforcement. *PCI Journal*, 13-57.

Muller, H., & Hilsdorf, H. K. (1990). *General Task Group 9.* Paris, France: CEB Comite Euro-Internaional du Beton, Paris France.

Naaman, A. E. (2004). *Prestressed Concrete Analysis and Design.* Ann Arbor: Techno Press 3000.

Nguyen, H. N. (2013). Improving Predictions for Camber in Precast, Prestressed Concrete Bridge Girders. *Masters Thesis*. Seattle, WA: University of Washington.

PCI Industry Handbook Committee. (2010). *PCI Design Handbook - Precast and Prestressed Concrete (7th ed.).* Chicago, Illinois: Precast/Prestressed Concrete Institute.

Rosa, M. (2007). Improving Predictions for Camber in Precast, Prestressed Concrete Bridge Girders. *Masters Thesis*. Seattle, WA: University of Washington.

Stallings, J. a. (2001). Camber and Prestress Losses in High Performance Concrete Bridge Girders. Highway research Center, Harbert Engineering Center, Auburn University in Cooperation with the Federal Highway Administration.

Tadros, M. K., & Al-Omaishi, N. (2003). *NCHRP Report 496 - Prestress Losses in Pretensioned High-Strength Concrete Bridge Girders.* Washington D.C.: National Cooperative Highway Research Program.

Tadros, M. K., Al-Omaishi, N., Seguirant, S., & and Gallt, J. (2003). *NCHRP Report 496 - Prestress Losses in Pretensioned High-Strength Concrete Bridge Girders.* Washington D.C.: National Cooperative Highway Research Program.

Tadros, M. K., Fawzy, F., & Hanna, K. (2011). Precast, Prestressed Girder Camber Variability. *PCI Journal*, 135-154.

Yu, Q., Bazant, Z. P., & Wendner, R. (2012). Improved Algorithm for Efficient and Realistic Creep Analysis of Large Creep-Sensitive Structures. *ACI Structural Journal*, 665-675.

Yue, L. L., & Taerwe, L. (1993). Two-Function Method for the Prediction of Concrete Creep Under Decreasing Stress. *Materials and Structures*, 268-273.

Zia, P., Preston, H., & Scott, N. W. (1979). Estimating Prestress Losses. *Concrete International*, 32-38.

ACKNOWLEDGMENTS

This project was funded by the Daniel Jenny Research Fellowship from the Precast Concrete Institute (PCI). This financial support is gratefully acknowledged.

The help from Quiang Yu is also greatly appreciated. His help in the numerical implementation of the Bazant and Yu's prestressing strand relaxation model was critical to the development of this algorithm.

Hang Nguyet Nguyen's contribution of her collected camber measurements and temperature data were crucial for the validation of this algorithm. She was also a valuable resource for validating the results of the algorithm. Her research also predicts camber and by performing the same analysis and comparing results of the two predictions, the algorithm was de-bugged very efficiently.

APPENDIX A - ALGORITHM INPUT

Control Inputs

Key

- This signifies a cell containing user input
- This signifies a cell automatically generated from previously input values

Analysis Control Parameters

Variable	*Value*	*Meaning*
RelTol	0.00001	- Tolerance on Moment and Axial load error after computing
Nrmethod	0	- 0 = Full Newton-Raphson, 1 - Modified Newton-Raphson
MxIter	500	- Maximum number of Newton-Raphson Iterations
d_delta_Phi	0.0000001	- Change in curvature used to compute stiffness
Delta_eps	0.0001	- Change in strain used to compute stiffness
in	12	- Conversion factor from feet to inches
ConcDens	0.16	- Density of concrete in kcf
Release Maturity (days)	7	- This is the effective concrete maturity at the release of the girder. AASHTO specifies that accelerated curing in the forms is equivalent to 7 days of moist curing.
Pile Analysis	0	- Indicates if a pile analysis only is being run. This turns off all moment
Verbose	1	- The level of indicators describing the code processing. - These are pop-ups that indicate where the code is running at. - A "0" yeilds no indicators and a "5" yeilds maximum number of

Time Control Parameters

Time History Inputs

Event	timstrt (Days)	timend (Days)	Nstps	timstprat	
Jacking	0	0.021	50	1	- Parameters defining the time scale for the jacking process
Pre-Bonding Strand	0.021	0.625	200	1	- Parameters defining the time scale for the pre-bonding analysis of strands only
Bonded, Pre-Release	0.625	0.9167	200	1	- Parameters defining the time scale for the post-bonding, pre-release analysis
Post-Release	0.9167	500	500	150	- Parameters for defining the time scale for the post-release analysis up to the next key event
SlbWght					- Parameters for defining the time scale for the slab weight before hardening analysis
SlbHardened					- Parameters for defining the time scale for the analysis from the time of slab hardening until termination of the analysis

TimInst (Days)	0.001	- This is the time-step size used to represent an instantaneous event

Switches

	Concrete Type				
	1 (girder)*	**2 (slab)***			
ConcOnTim (days)	0.625	0			- Time at which concrete types are hardened and bonded to reinforcing

** From Time History Inputs*

From Time History Inputs

Jack Time (days)	0.021
Release Time (days)	0.9166667
GrdWght Time (days)	0.9166667
SlbWght Time (days)	0

Note: These values are automatically generated and do not need to be input. They are specified separately in case the operator wants to modify how the analysis is completed from the true method.

Girder Anaylsis Locations

	Left End						Midspan						Right End
SctnLoc*	0	0.01	0.02	0.04	0.2	0.4	0.5	0.6	0.8	0.96	0.98	0.99	1

* The location at which section analysis will be completed. Specified as the ratio x Location:Length
This assumes the girder is simply supported.

Nseg 2 - This is the number of intermediate segments between each of the specified locations above.
- This must be and even number

Notes:
- the section locations must be provided anywhere the curvature/moment experiences a sharp change. This includes the following:
  - Support Locations
  - Harping points
  - De-Bonding points
  - Point Loads

Material Property Inputs

Material Properties

Variable ***Value*** ***Meaning***

Concrete (Variable Viscoelastic Model)

Nlink	2
HdExp	1

- Number of Kelvin links to be used in concrete model
- This is the exponent that defines the hardening shape during the pre-release phase. After release the input below controls the time-dependent changes in material constants. (0 = Step, 1 = linear, 2 = parabol, ect.)

		Concrete Type			
	Link Number*	1 (girder)	2 (slab)	3	4
fc_{28} (ksi)	-	11.06			
a	-	3.3			
b	-	0.8821			
Ek (ksi)	1	1007.5			
	2	6492.2			
	3				
	4				
	5				
Ekrat	1	26.639			
	2	3.227			
	3				
	4				
	5				
Ektau (1/tau)	1	136.02			
	2	1.665			
	3				
	4				
	5				
eta (ksi-days)	1	272345			
	2	1029774			
	3				
	4				
	5				
etarat	1	9.332			
	2	6.734			
	3				
	4				
	5				
etatau	1	1058.12			
	2	4.43E-09			
	3				
	4				
	5				

- Concrete Compressive Strength at 28 days
- ACI parameter for determining strength gain with time
- ACI parameter for determining strength gain with time
- Stiffness of Kelvin Spring for concrete
- Ratio of beginning to ending Kelvin stiffness value
- Time constant for the rate of Kelvin stiffness change
- Damper Value of Kelvin unit
- Ratio of beginning to ending Damper values
- Time constant for the rate of Damper value change

*Note that for multiple kelvin links each conrete type needs properties for each link.

ThmCffConc	0.000012

- Coefficient of thermal expansion for concrete (same for all concretes)

Prestressing Strand (Bazant Model)

fpy (ksi)	243	- Yield stress of strands
Ep (ksi)	28500	- Elastic Modulus of steel
gamma	0.55	- Threshold ratio of yield stress for which relaxtion begins
lambda	1000	- Time constant for rate of prestress loss
rho	0.0344	- Empirical constant
c	0.1988	- Empirical constant
k	0.277	- Empirical constant
T0 (°K)	293	- Reference Temperature
QokB	14600	- Temperature constant from Bazant's Paper
TmpConst	1	- Constant added for improved fit to thermal variations
TimAcc	1	- Switch for turing of the affects of temperature on relaxation rate
ThmCffStnd	0.000012	- Thermal coefficient for prestressing strand

Reinforcing Steel (Raynor Steel Model)

Es	29000	- Elastic Modulus
fsy	60	- Yield Stress
fsu	100	- Peak Stress
esh	0.01	- strain at the start of Strain hardening
esu	0.15	- strain at peak stress
n	6	- exponent on strain hardening curve
ThmCffBar	0.000012	- Thermal coefficient for reinforcing bar

Girder Geometry Input

Casting Bed Geometry Input

Casting Bed Arrangment

	Exposed	*Heated*	*Girder**	*Heated*	*Exposed*
Length (ft)	47.5	50	147.5	100	50

* From spcefied length

Total Bed Stiffness 0.001 k/in

Combined Strand Segment Geometry

From Castin Bed Arrangement

Segment	Length (ft)
Exposed	97.5
Heated	150
Encased	147.5

Definition

- The length of strand that is exposed to the outside air temperature.
- The length of strand that is heated by the heating blanket. This may be zero if heated forms are used rather than a blanket
- The length of strand that is encased in concrete. This comes from the girder geometry input.

Cross-Sectional Geometry Input

Girder Geometry

L (ft) 147.5 - Length

Cross-Section Geometry

Girder Geometry (inches)

Trapezoid	b. top	b.bott	h.trap	h.target	conc.type
1	49	49	3	1.0	1
2	49	12	3	1.0	1
3	12	6.125	3	1.0	1
4	6.125	6.125	52.375	1.0	1
5	6.125	12	3	1.0	1
6	12	38.375	4.5	1.0	1
7	38.375	38.375	4.125	1.0	1
8	38.375	36.375	1	1.0	1
9					
10					
11					
13					
14					
15					
16					
17					
18					
19					
20					
	Total Height	74			

Slab Geometry (inches)

Trapezoid	b. top	b.bott	h.trap	h.target	conc.type
1					
2					
3					
4					
5					
6					
	Total Height	0			

Variable	Definition
b.top	- width of the top of trapezoid
b.bott	- width of the bottom of trapezoid
h.trap	- total height of the trapezoid
h.target	- target sublayer height for Simpson's integration purposes
conc.type	- type of concrete that the trapezoid is made of. Corresponds to materials section

Reinforcing Layout (inches)

layer	*nbar*	*ybar*	*areabar*	*barconc*	*barstrt*	*barend*
1	0	1	0	1	0	1
2						
3						
4						
5						
6						
7						
8						
9						
10						

Variable	Definition
nbar	- quantity of bars at that layer
ybar	- distance to the bar from the top of the girder positive is measured downwards from the top of the girder
barconc	- type of concrete that the bar is embedded in corresponding to the column from the material properties section
barstrt	- the beginning location of the bars along the girder expressed as a ratio of
barend	- the ending location of the bars along the girder expressed as a ratio of the

Prestressing Strand Layout

devlen (in) 30 - Development length of strands

layer	*nstnd*	*ystndmid*	*areastnd*	*stndconc*	*fpj*	*hrplft*	*hrprt*	*ystndend*	*dbndlft*	*dbndrt*
1	17	69.4	0.217	1	202.5	0.4	0.6	11.53	0	1
2	40	70.4	0.217	1	202.5	0	1	70.4	0	1
3	2	2	0.217	1	202.5	0	1	2	0	1
4										
5										

* If a value in the table above is not needed to describe the geometry input a "0" rather than leaving it blank

Variable	Definition
nstnd	- quantity of strands at that layer
ystndmid	- distance to the strand from the top of the girder at midspan. Positive is measured downwards from the top of the girder
areastnd	- area of the individual strands
stndconc	- type of concrete that the bar is embedded in corresponding to the column from the material properties section
fpj	- jacking stress of the strand
hrplft	- the harping point of the strand layer at the left end of the girder expressed as a ratio of the length
hrprt	- the harping point of the strand layer at the right end of the girder expressed as a ratio of the length
ystndend	- distance to the strand from the top of the girder at the ends. Positive is measured downwards from the top of the girder
dbndlft	- Debonding location at the left end of the girder expressed as a ratio of the length
dbndrt	- debonding location at the right end of the girder expressed as a ratio fo the length

Applied Loads and Support Condition Input

Support Locations and Times of Relevance

Support #	Left Support Location	Right Support Location	Start Time	End Time
1	0.02	0.98	0	1
2	0.04	0.96	1	74.25
3	0.01	0.99	74.25	1000
4				
5				

Applied Axial Loads and Times of Relevance

Load #	Load (kips)*	Load Location	Start Time	End Time
1				
2				
3				
4				
5				

* - Load is positive if applied to the right and negative to left

Applied Moment Loads and Times of Relevance

Applied Distributed Loads

Load #	Load (kips per inch)*	Start Time	End Time
1			
2			
3			
4			
5			

* - Loads are positive acting downwards. Loads act along entire girder

Applied Transverse Point Loads

Load #	Load (kips)*	Location	Start Time	End Time
1				
2				
3				
4				
5				

* - Loads are positive acting downwards

Thermal Profile Input

Cross Section Thermal Profile

Notes:

- All cells not containing important information must be empty
- Note that temperatures must be provided for each of the key locations selected for each time.
- y locations in the slab should be input as negative values.
- The time stamps correlate with the thermal profile input below. These time steps should be selected with care.

Below are several suggested times at which thermal profiles are advised:

- Initial Jacking REQUIRED!
- Afer casting
- At time of concrete bonding/hardening
- At time of release
- One or two points along the cool down process after girder is removed from form.
- At time of slab casting
- At time of slab hardening
- Ending temperature REQUIRED!

	Time Stamps	0.00	0.2500	0.2708	0.2917	0.3125	0.3333	0.3542	0.3750	0.3958	0.4167	0.4375	0.4583	0.4792	0.5000	0.5208	0.5417
Key Locations	y Location (in)	Temperature °F															
Top of Slab*																	
Top of Girder	0	44	51	52	65	66	67	68	69	71	74	78	81	84	88	92	98
	1	44	51	52	65	66	67	68	69	71	74	78	81	84	88	92	98
	1.8125	44	51	54	67	68	69	70	71	73	76	79	82	85	89	94	100
	6.5	44	51	54	67	68	70	71	72	74	78	81	84	88	92	98	105
	10.5	44	51	55	67	68	69	71	72	74	78	82	85	89	94	99	107
	28	44	51	64	67	67	67	67	67	71	76	81	85	91	96	103	113
	45.5	44	51	64	66	66	66	67	67	69	73	76	80	83	88	92	98
	63	44	51	63	65	66	67	68	69	71	74	78	81	84	88	93	98
	69	44	50	63	64	64	65	66	67	69	71	74	76	79	82	86	90
	72	44	50	61	62	62	62	63	64	64	66	68	70	72	74	77	80
Bottom of Girder	74	44	50	61	62	62	62	63	64	64	66	68	70	72	74	77	80

** If there is no slab in the analysis there can be no temperature infromation given!!!*

Pre-ReleaseThermal Histories

Notes: - All cells not containing important information must be empty

- The temperature history for these strand locations only needs to be defined until the release time
- The temperature history for the exposed strand should have very little fluctuation because it is only exposed to air.
- If there is not a portion of strand that

Time Stamps	0	1								

Strand Locations	Temperature °F									
Exposed Strand	43	43								
Heated Strand Outside Girder	43	43								

Shrinkage Strain Input

Cross Section Thermal Profile

Notes: - All cells not containing important information must be empty
- Note that shrinkage strains must be provided for each of the key locations on the girder noted.
- y locations in the slab should be input as negative values.
- The time stamps correlate with the shrinkage profile input below. These time steps should be selected with care. Below are several suggested times at which shrinkage profiles are advised:
  - Initial Jacking REQUIRED! (should be zero)
  - At time of concrete bonding/hardening (should be zero)
  - At time of release
  - At time of slab casting
  - At time of slab hardening
  - Ending shrinkage REQUIRED!

Time Stamps	0	1000								

Key Locations	y Location (in)	Shrinkage in microstrain									
Top of Slab*											
Top of Girder	0	0	0								
Bottom of Girder	74	0	0								

** If there is no slab in the analysis there can be no temperature infromation given!!!*

APPENDIX B - AXIAL ELEMENT ON ELASTIC BED DERIVATION

This analysis addresses the forces and displacements in an axial element that is supported on a shear-flexible foundation. In the implementation used here, the axial element is the girder form and the shear-flexible foundation is the supporting system. All displacements and forces are horizontal.

In order to outline the derivation used to define the axial girder element that rests on the elastic foundation, it is first necessary to define the geometry of the problem.

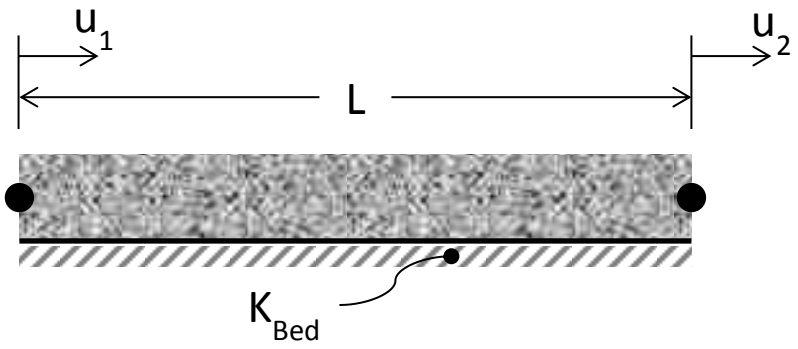

where: K_{Bed} = the total shear stiffness of the foundation over the length of the girder

The next step is to define the distributed stiffness as $\beta = \frac{K_{Bed}}{L}$, where β is the stiffness per unit length.

The flexibility will be solved and then inverted to find the stiffness. First solve the problem for an applied force at node 2 and zero force at node 2.

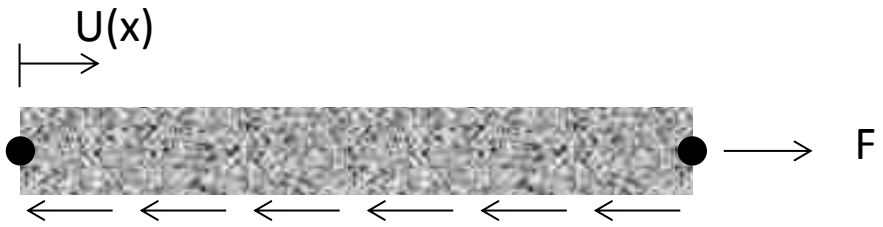

The force equilibrium on an infinitesimally small section can be illustrated as:

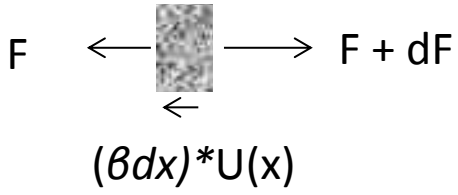

Writing the following relations:

Kinematics: $$\varepsilon = \frac{du}{dx} \quad \text{(B.1)}$$

Constitutive: $$F(x) = EA\varepsilon(x) \quad \text{(B.2)}$$

Equilibrium: $$dF = \beta dx[u(x)] \quad \text{(B.3)}$$

Taking the derivative of Equation B.3 with respect to *x* and substituting with Equation B.2 results in the following differential equation.

$$\frac{d^2F}{dx^2} - \lambda^2 F = 0 \quad \text{(B.4)}$$

where: $\lambda^2 = \frac{\beta}{EA}$

EA = the total cross-sectional stiffness, including contributions from both the concrete and the prestressing strand.

The solution to this differential equation has the general form:

$$F(x) = a\cosh\lambda x + b\sinh\lambda x \quad \text{(B.5)}$$

Applying the boundary conditions, *F(0) = 0* and *F(L) = F* results in:

$$a = 0 \quad \text{(B.6)}$$

$$b = \frac{F}{\sinh \lambda L} \tag{B.7}$$

This results in the force equation along the length of the girder:

$$F(x) = \frac{F}{\sinh \lambda L} \sinh \lambda x \tag{B.8}$$

Now the flexibility matrix can be generated by solving for the displacement due to the applied load. From Equation B.3:

$$u(x) = \frac{1}{\beta} \frac{dF}{dx} \tag{B.9}$$

Using Equation B.8, Equation B.9 can be solved in terms of the applied force, *F*:

$$u(x) = \frac{F}{EA\lambda} \frac{\cosh \lambda x}{\sinh \lambda L} \tag{B.10}$$

The displacements at the nodes can then be solved as:

$$u(0) = \frac{F}{K_{Bed}} \frac{\lambda L}{\sinh \lambda L} \tag{B.11}$$

$$u(L) = \frac{F}{K_{Bed}} \frac{\lambda L}{\tanh \lambda L} \tag{B.12}$$

A similar formulation could be completed for a force applied at node 1. The results would be the reverse of Equations (B.11) and (B.12). This can be used to write the flexibility system as:

$$\begin{Bmatrix} u_1 \\ u_2 \end{Bmatrix} = \frac{\lambda L}{K_{Bed}} \begin{bmatrix} \frac{1}{\tanh \lambda L} & \frac{1}{\sinh \lambda L} \\ \frac{1}{\sinh \lambda L} & \frac{1}{\tanh \lambda L} \end{bmatrix} \begin{Bmatrix} F_1 \\ F_2 \end{Bmatrix} \tag{B.13}$$

This system can be inverted to provide the stiffness formulation needed for this algorithm:

$$\begin{Bmatrix} F_1 \\ F_2 \end{Bmatrix} = \frac{K_{Bed}}{\lambda L} \begin{bmatrix} \frac{1}{\tanh \lambda L} & \frac{-1}{\sinh \lambda L} \\ \frac{-1}{\sinh \lambda L} & \frac{1}{\tanh \lambda L} \end{bmatrix} \begin{Bmatrix} u_1 \\ u_2 \end{Bmatrix} \tag{B.14}$$

where: $K_{Element} = \frac{K_{Bed}}{\lambda L} \begin{bmatrix} \frac{1}{\tanh \lambda L} & \frac{-1}{\sinh \lambda L} \\ \frac{-1}{\sinh \lambda L} & \frac{1}{\tanh \lambda L} \end{bmatrix}$ is the element stiffness matrix.

This provides the elastic element stiffness which can be added to other elements to form the global stiffness matrix as shown in Section 3.4.1. This stiffness is used in the Newton-Raphson iteration scheme but the total strain as a function of location in the girder is needed. This is needed so that an exact force on the cross-section can be developed within the Newton-Raphson iteration. This is done using the formulations of displacement as a function of the applied forces from Equation B.10. For an applied force at node 1 this equation becomes:

$$u(x) = \frac{F_1}{EA\lambda}\frac{\cosh\lambda(L-x)}{\sinh\lambda L} \tag{B.15}$$

Combining Equations B.10 and B.15, the displacement due to general applied forces can be written as:

$$u(x) = \frac{1}{EA\lambda\sinh\lambda L}\langle\cosh\lambda(L-x) \quad \cosh\lambda x\rangle\begin{Bmatrix}F_1\\F_2\end{Bmatrix} \tag{B.16}$$

But in the Newton-Raphson scheme described in Section 3.4.1, the strain is needed in terms of the nodal displacements. This is accomplished by substituting Equation B.14 into B.16:

$$u(x) = \frac{1}{EA\lambda\sinh\lambda L}\langle\cosh\lambda(L-x) \quad \cosh\lambda x\rangle\frac{K_{Bed}}{\lambda L}\begin{bmatrix}\frac{1}{\tanh\lambda L} & \frac{-1}{\sinh\lambda L}\\ \frac{-1}{\sinh\lambda L} & \frac{1}{\tanh\lambda L}\end{bmatrix}\begin{Bmatrix}u_1\\u_2\end{Bmatrix} \tag{B.17}$$

Now the displacement is written as a function of location, *x*, and in terms of the nodal displacements. Total strain can then be determined by deriving with respect to *x*. Taking this derivative and simplifying leads to:

$$\varepsilon_{Tot}(x) = \frac{\lambda}{\sinh\lambda L}[-\sinh[\lambda(L-x)] \quad \sinh\lambda x] * \begin{bmatrix}\frac{1}{\tanh\lambda L} & \frac{-1}{\sinh\lambda L}\\ \frac{-1}{\sinh\lambda L} & \frac{1}{\tanh\lambda L}\end{bmatrix} * \begin{Bmatrix}u_1\\u_2\end{Bmatrix} \tag{B.18}$$